Femtosecond Laser Induced Polyyne Formation

by

Asif Ali Zaidi

A thesis
presented to the University of Waterloo
in fulfillment of the
thesis requirement for the degree of
Doctor of Philosophy
in
Physics

Waterloo, Ontario, Canada, 2010

I hereby declare that I am the sole author of this thesis. This is a true copy of the thesis, including any required final revisions, as accepted by my examiners.

I understand that my thesis may be made electronically available to the public.

Abstract

Polyyne molecules were produced as a result of the femtosecond laser irradiation of liquid acetone $(CH_3)_2CO$ and alkane molecules hexane C_6H_{14} and octane C_8H_{18} using 800 nm, 100 fs duration pulses. These polyynes have been detected as a Raman band in irradiated liquid from 1800 to 2200 cm^{-1}. Polyyne molecules generally detected as a Raman band in SERS experiment are C_8H_2, $C_{10}H_2$, $C_{12}H_2$ and $C_{14}H_2$. Two well established experimental techniques, time of flight mass spectrometry and surface enhanced Raman spectrometry were used to identify positively polyyne formation as a result of femtosecond laser irradiation of acetone and alkane liquids. Small polyynes C_2H_2, C_4H_2, and C_6H_2 were positively detected in the time of flight mass spectrometer TFMS, while longer polyynes from C_6H_2, C_8H_2, $C_{10}H_2$, $C_{12}H_2$ and $C_{14}H_2$ were detected by surface enhanced Raman spectroscopy SERS.

Intensity capping occurs in a liquid due to filamentation, and the resulting intensity in a liquid is $\sim 10^{13}$ W/cm^2 during irradiation. This results in main process of ionization in the larger part of the laser focus as multiphoton ionization MPI. Focal volume increase in a liquid provides a larger volume where ions C^+, C_2^+ and $C^{2+}$are produced to initiate chemical reactions outside the laser focus.

The current work established positively, that the longer polyyne formation does not occur by dehydrogenation of alkane molecules by only breaking the C-H bonds as was previously anticipated. It is proposed in this work that lengthening of polyyne chains occurs due to addition reaction of species of C^+, C_2^+ and C^{2+} to double bonded species themselves produced as a result of the breaking down of the parent molecules in the laser focus. The carbon addition reactions occur outside the laser focus due to the close proximity of molecules in the liquid phase.

Acknowledgments

I would like to express my thanks to Prof. J. H. Sanderson of the Department of Physics and Astronomy at University of Waterloo, who has been my research supervisor. He provided me with many helpful suggestions; In particular, his expertise in mechanical design helped me to develop time of flight mass spectrometer.

I would like to thank my Ph.D. advisory committee Prof. W. K. Liu, Prof. D. Heneke for their guidance during my studies. In particular, I wish to thank Prof. Duley for acting as research supervisor for one year, and for his guidance and helpful discussions during my study period.

I enjoyed insightful discussions with my colleagues and friends, fellow students and postdocs in the ultra-fast laser group: Dr. Fu. Dr. Hu. Good theory discussions with Dr. Paweł Stasiak, Z. Long (Max) and for computer program debugging Dani Xu. I also wish to thank mechanical and electrical laboratory supervisors for their part to develop time of mass spectrometer, In particular electrical workshop supervisor Jacek Szubra for his cooperation to help build new safe electrical system for mass spectrometer.

My uncle, Prof. Masood Zaidi, provided moral and financial support throughout my undergraduate education, thanks uncle. Finally, I would like to express my special gratitude to my wife, Tasneem for her love, support and patience during this study period.

Dedication

In memory of my Late Mother

Bilqees Zaidi

Contents

List of Tables

List of Figures

Chapter 1

Overview

One of the oldest question asked by thinkers is what are the world's basic compositional parts. Possibly the earliest known solution was proposed by Anaximenes of Miltus in the 6th century BC [1], according to his theory four elements were present in the make-up of everything, namely, air, water, earth, and fire. Subsequently, the first atomic theories were developed by ancient Indian philosophers Kanada and P. Katyayana, who believed there were six elements, each element with twenty-four properties. Considering six elements and their combinations and splitting, they explained the world [2]. Democritus proposed that atoms possessed inherent properties such as shape, size, and mass, and other properties like color and taste, resulted from various combinations of atoms (BC 450-370) [3].

In a relatively modern effort John Dalton [4] in 1808, proposed distinguishable atoms for different pure substances. He also proposed the combining properties of atoms, this gave rise to modern chemistry. However, Dalton believed that the atom of an element was indivisible. Later in the 20th century advances by Rutherford in 1911 showed that an atom consists of a positively charged massive center and electrons outside it [5], known as Rutherford's nuclear atom. In 1913, Bohr proposed his atomic model [6] which explained the combining power of an element and predicted the atomic spectra successfully for hydrogen-like atoms. Bohr connected his atomic model to Maxwell's electromagnetic radiation theory. Bohrs' adhoc theory at that time was a good starting point for thinking about the radiation-matter connection and the valency of an element. Chemical bonding (covalent) was explained by Lewis in 1916

[7]. This electron sharing model of bonding and later ionic bonding explained a large domain of chemical formations as we know it today. Also Boltzmann's contribution to Kinetic Theory [8] strongly supported atomic theory. At present, we have a quantum theory of radiation [9] with an associated field particle the photon, this theory explains completely, previously unexplained phenomenon like the black body spectrum.

This thesis is about femtosecond laser irradiation of organic liquids and polyyne formation as a result of irradiation. Irradiated and pure liquids were studied by the time of flight mass spectrometry (TOFMS) and surface enhanced Raman spectrometry (SERS) to identify the polyynes formed in the irradiated liquid. To detect polyynes by TOFMS, a laser ionization study was carried out in detail. A time of flight mass spectrometer was developed with high resolution so that ion peaks with a one atomic mass unit difference are fully resolved. Chapter 3 details the development of the TOFMS. Longer polyyne chains were detected up to $C_{14}H_2$ using SERS. While the study of small polyyne chains and break up of hydrocarbons in the laser focus in vacuum was studied by TOFMS. Combined experimentation employing TOFMS and SERS shed light on the possible mechanism to form longer polyynes than the starting organic liquid.

1.1 Laser-Matter Interaction

Laser light interacting with matter in general can be considered in terms of the electric field interacting with the electrons in atoms or molecules individually if the situation is of the gas phase irradiation. Atoms and molecules are treated by quantum mechanical description, which establishes discrete electronic levels naturally obtained as a solution to the Schrodinger wave equation for atomic and molecular systems. This theory also includes the effects of rotation and vibration of a molecule. Laser radiation is treated in a classical way using Maxwell's electromagnetic theory. This combination constitutes a semi-classical approach to the laser-matter interaction problem.

When an intense laser pulse passes through a material medium, the laser-matter interactions can be highly non-linear and leads to changes both in the medium itself and the transmitted light. This is true even if the excitation frequencies of the target molecule are not in resonance with that of incident light. Several processes can take

place such as ionization due to tunneling TI, multiphoton absorption, over the barrier ionization OBI, multiphoton ionization MPI and multiphoton dissociation MPD, laser initiated material damage, self-focusing and high harmonic generation. All these phenomena constitute a vast topic. In this thesis discussion is mainly about non-resonant laser assisted ionization and dissociation of molecules. The electromagnetic state of matter and the propagation of self-propagating electromagnetic waves can be described classically by Maxwell's equations [11].

Intensity depends on only E_o^2 and the phase angle ϕ has no contribution [13]. This expression gives the estimate of the interacting electric field with the molecules inside the laser focus. Experiments can be planned after knowing material factors such as the ionization potential of the target material.

$$I = \frac{1}{2} c_o \epsilon_o \mathbf{E}_o^2 \tag{1.1}$$

The response of the material medium depends on the light intensity because the polarization $\mathbf{P} = \epsilon_o \chi \mathbf{E}$, can be expanded in higher orders as,

$$P(t) = \chi^{(1)} E(t) + \chi^{(2)} E^2(t) + \chi^{(3)} E^3(t) + - - - - - - - - \tag{1.2}$$

Susceptibilities of different orders [12] indicate processes which can occur in a given material for a known intensity. Linear optical phenomenon at low intensity is described by $\chi^{(1)}$. For higher laser intensity, since properties of the medium change non-linearly due to high electric field associated with the laser intensity all such processes are described by higher order susceptibilities. Linear and the higher order susceptibilities can be calculated exactly by using an interaction Hamiltonian V(t) = - μ . $\mathbf{E}$(t) with the time dependent Schrodinger equation together with perturbation theory. Processes which are likely to occur due to the second order polarization are different than those which occur due to third order polarization. Materials which do not have inversion symmetry such as liquids, gases, amorphous solids and glass $\chi^{(2)}$ vanishes and these materials cannot produce second order non-linear interactions. However these materials produce third order non-linear interactions. For sufficiently large field strengths, the above power series expansion may not converge. This break down will certainly occur if the laser field amplitude becomes comparable to the atomic field strength. Considering the electric field at one Bohr's radius,

$$E_{atomic} = \frac{e/4\pi\epsilon_o}{a_o^2} \tag{1.3}$$

Using E_{atomic}= 6 x 10^{11}V/m, with intensity value I_{atomic}= $\frac{1}{2}c_o\epsilon_o E^2$ gives, I_{atomic} =4 x 10^{20} W/m^2 or 4 x 10^{16} W/cm^2 . This is the starting intensity level for intense field non-linear optics, at this intensity hydrogen atom ionizes efficiently and other nonlinear effects may occur, such as optical damage and self focusing in certain materials.

1.2 Pondromotive Energy.

Considering a free electron in the laser electric field E(t) having mass 'm', charge '- e' according to Newton's law,

$$m\ddot{x}(t) = -eE(t)$$

which leads to the velocity,

$$\dot{x} = v = -(\frac{e}{m})(\frac{E_o}{\omega_o})sin(\omega_o t + \phi)$$

Considering cycle average $\langle sin^2(\omega_o t + \phi)\rangle = \frac{1}{2}$ and $KE = \frac{1}{2}mv^2$, classical electron energy is given by,

$$\langle K.E\rangle = \frac{1}{4}\left(\frac{e^2E_o^2}{m\omega_o^2}\right) = U_p \tag{1.4}$$

Since intensity I α E_o^2 we see that average K.E α I $/\omega_o^2$. The time average of kinetic energy is known as the jitter energy (as it is more commonly associated with the oscillation of the electron about its equilibrium position) or as the ponderomotive energy [13]. This energy can be appreciable. Considering a laser field of wavelength 1.06 μm. One finds by numerical evaluation that the ponderomative energy is equal to 13.6 eV (a typical atomic ionization energy) for $I = 1.3 \times 10^{14}$ W/cm^2.

1.3 Atoms and Molecules in intense laser fields

When a laser pulse of high intensity interacts with atoms or molecules, processes of higher order than single photon absorption or emission become more important. These higher order processes, called multiphoton processes, correspond to absorption or emission of more than one photon. These processes are multiphoton ionization (MPI), multiphoton dissociation (MPD), multiphoton excitation (MPE), and harmonic generation (HG). For multiphoton ionization to occur in atoms or molecules, intensity of at least 10^{10} W/cm^2 is necessary to observe the process for appreciable ionization rate.

Atoms in general have a spherically symmetrical electronic charge distribution around positive nucleus, but molecules in general have linear or other charge distributions, that may influence the ionization rate, as compared to spherically symmetrical atoms. Considering an atom interacting with the laser field, basically the problem can be characterized as the atom being in the influence of the photon's electric field. The Schrodinger equation for this process is [10],

$$i\hbar\frac{\partial}{\partial t}\psi(X,t) = H(t)\psi(X,t) \tag{1.5}$$

where $X = (q_1, q_2, \ldots, q_n)$ denotes coordinates of the n-atomic electrons and $H(t)$: semi classical Hamiltonian of the atom in the presence of the laser field,
where $H_{int}(t)$ is time dependent interaction,

$$H(t) = H_o + H_{int}(t)$$

and with T: kinetic energy and 'V' is potential energy of system.

$$H_o = T + V$$

Time-independent field free Hamiltonian working in the Coulomb gauge $\nabla \cdot \mathbf{A} = 0$,

$$H_o = -\frac{\hbar^2}{2m}\sum_{i=1}^{N}\nabla_{r_i^2}^2 + V$$

Potential energy for multi-electronic system [16],

$$V = -\sum_{i=1}^{N} \frac{2e^2}{(4\pi\epsilon_o)r_i} + \sum_{i<j}^{N} \frac{e^2}{(4\pi\epsilon_o)r_{ij}} \tag{1.6}$$

since the wave length of the incident radiation is much larger than the atomic size the laser electric field, which can be treated as constant over the atomic dimensions according to the dipole approximation. Due to dipole approximation we can now write $A(r,t) = A(t)$ and consideration of a bound charge particle in an electromagnetic field gives interaction part of Hamiltonian as,

$$H(t) = \frac{e}{m}\mathbf{A}\cdot\mathbf{P} + \frac{eN}{2m}\mathbf{A}^2(t) \tag{1.7}$$

Theoretically this problem cannot be solved by perturbation theory because the interaction Hamiltonian (1.7) contains $\mathbf{A}^2$ term which is not small, so perturbation theory breaks down. Now this problem can be treated by the strong field approximation SFA [19]. The ionization rates of the hydrogen atom by the strong field approximation can be calculated after long calculations using hydrognic ground state wave function (E.19). If E_o is the laser electric field than ionization rate 'W' by SFA,

$$W = \frac{\pi}{2}\sqrt{\frac{3E_o}{\pi}}e^{\frac{-2}{3E_o}} \tag{1.8}$$

The ionization rate 'W' is given by WKB approximation as,

$$W = \frac{4}{E_o}\sqrt{\frac{3E_o}{\pi}}e^{\frac{-2}{3E_o}} \tag{1.9}$$

Both formulas (1.8) & (1.9) have the same exponential factor, but the dependence on the laser electric field E_o is different as a coefficient of the exponential factor. SFA ionization rates are better approximations to the experimentally observed data in the range where the ADK theory starts breaking down.

1.4 Ionization

A bound electron is taken out from an atom or a molecule in an ionization process this leaves the rest of atom or molecule as a positively charged ion. Ionization can occur by absorbing a single photon (Resonance ionization) or by absorbing 'n' number of photons (MPI), if 'A' is the irradiated specie in laser irradiation experiments [16].

$$n\hbar\omega + A^q \rightarrow A^{q+1} + e^- \tag{1.10}$$

where 'q' is the charge of the target atomic or molecular system. In studying electron spectra it was found that for intensities $I \ll I_a$ where I_a is the intensity to ionize hydrogen atom, n-photon ionization rates were proportional to I^n as predicted by low order perturbation theory (LOPT), electron spectra in this case is governed by,

$$E_s = (n+s)\hbar\omega - V_o \tag{1.11}$$

where V_o is the ionization potential of an atom or a molecule, n : the number of photons needed for ionization, s : the number of excess photons absorbed.

At higher laser intensities more photons are absorbed than are needed for ionization, this process is called above threshold ionization (ATI). At further high intensities LOPT predictions are not observed and the electron spectrum contains peaks at higher energies [16] than predicted by the theory. However, for understanding of ionization process in laser field and the calculation of ionization rates, useful models are multiphoton ionization (MPI), tunneling ionization (TI) and over the barrier ionization (OBI). It is possible to know the process causing ionization by estimating the value of the Keldysh parameter γ_k [20].

Considering an electron bounded by the coulomb potential in a square well potential with binding energy V_o, and E_e is the energy of the bound electron in the potential well of depth V_o, potential well is along x-axis and its width is 'l'. The incident laser field on interaction modifies the potential barrier in a way that for some time in cycle it is more probable for an electron to tunnel through the barrier figure 1.1.

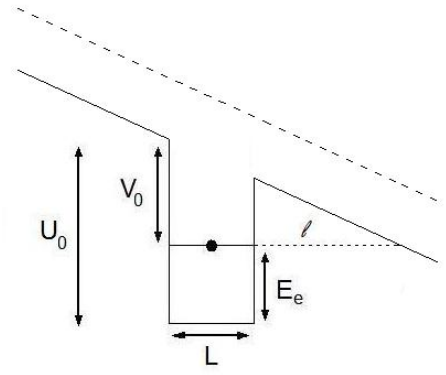

Figure 1.1: Electron bound in a potential well of depth V_o and width 'L'. in the presence of laser the field.

- **E** field of laser interacts with electrons, to rapidly ionize atoms $I \sim 10^{14} - 10^{16}$ W/cm^2.
- **E** field of laser is oscillating field, and electron is bound by a positive potential.
- If the tunneling time t_t is shorter than period of light T_p, laser **E** field is considered static.

$$t_{tunneling} \ll T_{pulse}$$

The potential (modified by laser field) experienced by electron in presence of laser pulse is given by [13],

$$V(x) = U(x) + xeE(t) \tag{1.12}$$

The width of the potential barrier "l" is of instantaneous value $\mathbf{E}(t)$, The value $E_{max}(t) = E_o$. At the peak of the field

$$E(t) = E_o cos(\omega_o t + \phi)$$

Considering the maximum value of the laser field as E_o , the width if the barrier is l, and depth of potential as V_o,

$$l = \frac{V_o}{eE_o}$$

Tunneling time is given by,

$$t_t = \frac{l}{v}$$

Energy conservation gives

$$\frac{1}{2}mv^2 + V(x) = E_e$$

$$v(x) = \sqrt{2\left(V(x) - E_e\right)/m_e}$$

Since V(x) > E_e the velocity of the electron inside the barrier is imaginary, so it violates energy conservation and naturally tends to be out [13]. At the barrier height $V(x) - E_e = V_o$, the electron velocity at the maximum of the barrier is given as $\sqrt{2V_o/m}$. This leads to average electron velocity through the barrier as $\sqrt{V_o/2m}$ assuming that the velocity outside the barrier is zero.

$$t_t = \frac{\sqrt{2mV_o}}{eE_o}$$

Tunneling frequency. $\omega_{tun} = \frac{1}{t_t}$ and in the static field approximation, $\frac{\omega_{tun}}{\omega_o} \gg 1$

$$\omega_{tun} = \frac{eE_o}{\sqrt{2meV_o}}$$

Thus Keldysh parameter γ is defined as a ratio of laser frequency to peak tunneling frequency,

$$\gamma = \frac{\omega_o}{\omega_{tun}}$$

$$\gamma = \sqrt{V_o/2K.E} \tag{1.13}$$

Keldysh parameter is a square root of ratio of ionization potential of a bonded electron (in an atom or a molecule) to the ponderomotive energy imparted by the laser field to the bonded electron, $\gamma \sim 1$ when laser field imparts as much ponderomotive energy as the binding potential V_o . This helps to classify the type of ionization process associated in an ionization process. Considering hydrogen atom in the laser field, and laser intensity is increasing for 800 nm photons, first multiphoton ionization will take place at intensity $\sim 10^{12}$ W/cm^2, on further increasing the intensity to $\sim 10^{14}$ W/cm^2 electron tunneling probability will increase and for further more intense fields $\sim 10^{16}$ W/cm^2 ponderomotive energy KE $> V_o$ than electron will simply move out from the potential barrier classically. Electron moving out classically is known as over the barrier ionization or OTBI. Three processes are classified as,

Over the barrier ionization (OTBI)

$$\gamma \ll 1$$

Tunneling ionization (TI)

$$\gamma \leq 1$$

Multiphoton ionization (MPI)

$$\gamma \gg 1$$

1.4.1 Over the barrier ionization

In this process the laser field strength is large enough to remove electrons away from the atom. This process is expected to become dominant if the peak laser field strength exceeds the atomic electric field strength $E_a = e/a_o^2 = 6 \times 10^9$ V/cm. Fields this large are obtained at high intensities. I_a is the intensity corresponding to the atomic electric field E_a, where $I_a = \frac{1}{2} c_o \epsilon_o E_a^2 = 4 \times 10^{16}$ W/cm^2.

Barrier Suppression Field

Considering a situation when laser and atom interact and the laser intensity is at higher level. The associated electric field can remove electron from atom simply by

field ionization. Laser electric field modifies potential barrier to V(x), considering one dimensional Schrodinger equation,

$$i\hbar\frac{\partial}{\partial t}\psi(x,t) = \left(-\frac{\hbar^2}{2m}\frac{\partial^2}{\partial x^2} + U(x) + xeE(t)\right)\psi(x,t) = 0$$

where

$$E(t) = E_o cos(\omega_o t + \phi)$$

and total modified potential in figure 1.1 is V(x).

$$V(x) = U(x) + xeE(t)$$

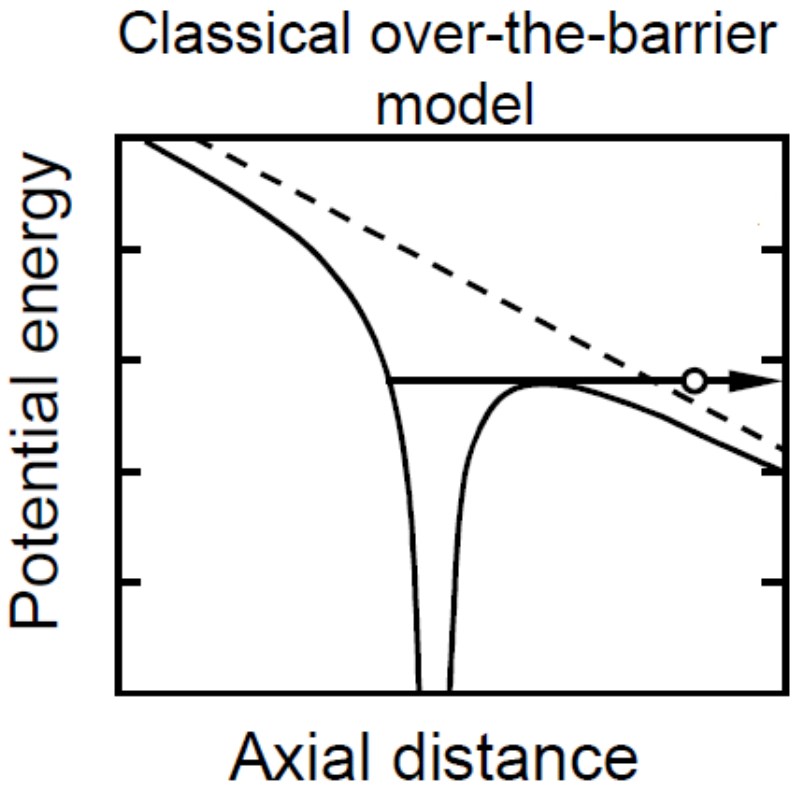

Figure 1.2: Classical over the barrier ionization [21].

Let $U(x) = U(r)$ be the Coulomb potential, $V(r) = U(r) + reE_o$ as field is switched on, V_o is the binding energy of the electron.

$$V_o = \frac{1}{4\pi\epsilon_o}\frac{e^2}{r} + reE_o$$

This can be arranged as,

$$r^2 - \frac{V_o}{eE_o}r + \frac{e^2}{4\pi\epsilon_o eE_o} = 0$$

Using quadratic equation, roots are r_+ and r_-.

$$l = \triangle r = r_+ - r_- = \frac{V_o}{eE_o}\sqrt{1 - \frac{e^3E_o}{\pi\epsilon_o V_o^2}}$$

At max $l = 0$, barrier suppression field is given by,

$$E_o = (4\pi\epsilon_o)\frac{V_o^2}{4e^3} \tag{1.14}$$

As expected the barrier suppression field E_o is related to the ionization potential of the atom or molecule. Calculated electric field value can be used to estimate the laser intensity needed for experimentation with a given molecule using intensity relation (1.1). For our laser system λ = 800 nm; corresponding photon energy E = 1.55 ev: Above formula gives E_o= 2.83 x 10^{10} V/m if $\gamma = 1$ and the intensity will be $\sim 10^{15}$ W/cm^2.

1.4.2 Tunneling Ionization (ADK & MO-ADK)

ADK (Ammosov, Delone, and Krainov)[22] is based on the approximation that the electric field is static. Application of this static field causes decrease in barrier thickness and this increases the quantum mechanical probability of the electron escaping from the potential well figure 1.3. Since there is a difference between an oscillating electric field and a static one, because static field should always build up to a tunneling current, where as oscillating field will not do so. In ADK approximation consideration has been taken into account that this approximation works for low frequency when ionization occurs at a time scale that is smaller compared to the laser period. Thus when $\gamma \simeq 1$ or smaller, the laser field can be treated as quasi static.

Generally the ADK formula has been shown a good approximation to estimate ionization rates for atoms to compare with experimental results. However, there are

discrepancies in molecular ionization rates. Tunneling Ionization rates 'W$_{ADK}$' [22] are given by

$$W_{ADK} = \left(\frac{3e}{\pi}\right)^{\frac{3}{2}} \frac{Z^2}{n^{*9/2}} \left(\frac{4e2^3}{n^{*4}E}\right)^{2n^*-3/2} exp(-\frac{2Z^3}{3n^{*3}E}) \tag{1.15}$$

where 'Z' is atomic number, n^* is related to potential depth $V_o = I_P$, E : electric field of laser; $I = \frac{1}{2}\epsilon_o c_o E_o^2$

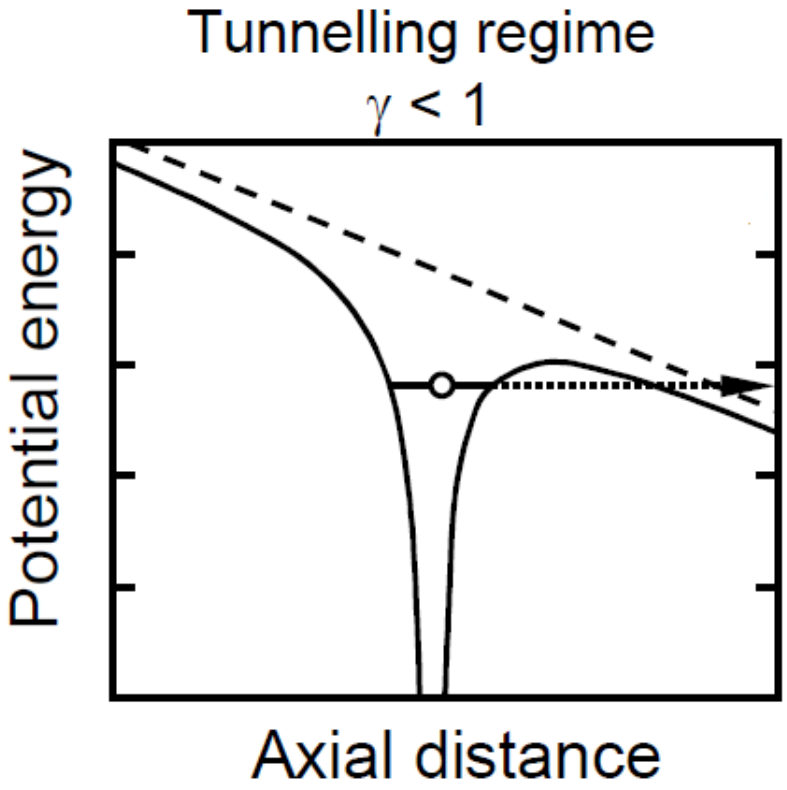

Figure 1.3: Laser field interaction with atomic potential well, figure 1.5 shows distortion in potential generates a thin barrier on one side from where electron can tunnel. Higher the field intensity thinner the barrier, which enhances probability of electron tunneling. [21].

In molecular ADK, or MO-ADK, ionization rates depend on the ionization potential of the atoms. Experimental studies indicate that ionization rates for molecules are in general very similar to the atoms if they have nearly identical binding energies. However, molecules depart from the spherically symmetrical structure of atoms, when this is taken into account in MO-ADK only then discrepancies in ionization rates of pairs with similar ionization potential can be explained.

In MO-ADK, ionization rates of D_2 and O_2 are compared with noble elements Ar and Xe. Pair is D_2:Ar and O_2 :Xe, it was anticipated that the pair will have similar ionization rates but, experimental rates for D_2 are suppressed as compared with Ar. This can be attributed to the alignment of the D_2 molecule along the laser field. In fact, what is important is the extent of alignment of the electronic cloud of the molecule with the laser field. If the molecular electronic cloud alignment is taken into consideration, ionization suppression for some molecules like D_2, can be explained. Saenz [23] has calculated the possible effect of vibrational motion of a molecule, but the impact of vibrational motion on ionization rates is found to be small. In general, it is anticipated that when valence electrons are in the π orbitals, suppression is evident, due to the electronic cloud of the molecules being perpendicular to the molecular axis [24]. MO-ADK provides satisfactory results for ionization of small molecules in intense laser field, this theory can be applied to polyatomic molecules if factors of electronic cloud alignment with laser field are taken into account.

1.4.3 Multiphoton Absorption and Ionization

Multiphoton ionization is a process occurring at high intensity range of (10^{12} to 10^{14}) W/cm^2. In this process an atom or a molecule absorbs more than one photon and leaves the binding potential, such process happen at high intensities when irradiation is carried out by a pulsed laser figure 1.4. In the case of hydrogen atom field ionization takes over near intensity level 10^{16} W/cm^2, this is because for the hydrogen atom ionization potential is 13.6 eV. The type of ionization process talking place can be decided by looking at ionization potential and the intensity of the laser. Multiphoton absorption cross section can be calculated simply by including interaction energy in the atomic Hamiltonian and solving the wave equation by perturbation expansion [25]. Considering the atomic wave function $\psi(\mathbf{r}, t)$ which obeys the time-dependent

Schrodinger equation

$$i\hbar\frac{\partial\psi(\mathbf{r},t)}{\partial t} = H\psi(\mathbf{r},t) \tag{1.16}$$

where the Hamiltonian $H = H_o + \hat{V}(t)$, H_o is the Hamiltonian for a free atom and the interaction energy with the applied optical field, where $\hat{\mu} = -e\hat{r}$. Considering the field as monochromatic one can calculate absorption cross section for one photon , two photon or multiphoton absorption. In our irradiation of organic liquids intensity is capped at about 10^{13}W/cm^2 due to filamentation, resulting the process to be multiphoton ionization.

Multiphoton Absorption

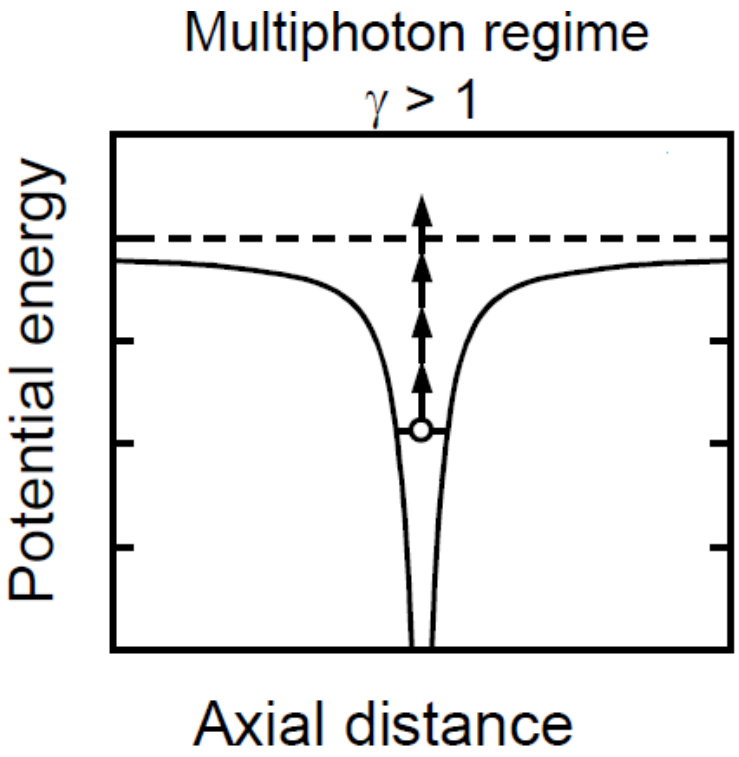

Figure 1.4: Electron in ground state of hydrogen atom absorbs several photons in a high intensity multiphoton absorption and atom ionizes [21].

1.5 Molecular ionization & dissociation in Laser field

Experiments on laser molecular ionization and dissociation on diatomic and poly-atomic molecules indicate that generally processes can be classified in the following groups considering units A and B are atomic [26],

1. Dissociation

   $n\hbar\omega + AB \longrightarrow A + B$

2. Ionization

   $n\hbar\omega + AB \longrightarrow AB^{+} + e^{-}$

3. Dissociative ionization

   $n\hbar\omega + AB \longrightarrow A + B^{+} + e^{-}$

4. Coulomb explosion

   $n\hbar\omega + AB \longrightarrow AB^{+} + e^{-}$

   $n\hbar\omega + AB^{+} \longrightarrow A^{+} + B^{+} + e^{-}$

Molecular ionization and subsequent dissociation in an intense laser field (I $\geq 10^{14}$ W/cm^2) can be understood by a phenomenological model. This model considers dissociation in the long wavelength limit, i.e. laser E-field is static. In a simplified way one can consider a rising pulse incident on a diatomic molecule having two positive nuclei, providing a double well potential for a bound electron figure 1.5. Laser field interacts with this system, causing changes in the neutral molecular potential surfaces. At equilibrium distance Coulomb energy is given by,

$$E_e = \frac{Q_1 Q_2}{R_e}$$

where Q_1 and Q_2 are atomic ion charges, and atomic units are used in writing Coulomb energy formula. R_e: equilibrium internuclear separation of neutral molecule

At each ionization stage electronic polarizability of molecule will change each ionization causes tighter hold on the remaining electrons. It looks intuitively that for subsequent ionization of molecule there will be not much change in ionic internuclear distance or at a distance "R_c" stabilization occurs before eventual dissociation. Posthumus phenomenological model [27] helps to calculate molecular relaxation distance "R_c" for different diatom's. In laser field, double-well potential energy curve is given by,

$$U = -\left(\frac{Q_1}{\left|x - \frac{R_c}{2}\right|} + \frac{Q_2}{\left|x + \frac{R_c}{2}\right|}\right) - eE_o x \tag{1.17}$$

E_o: the laser electric field amplitude

R_c: molecular relaxation distance

Electronic energy level in the double well at "R_c" can be approximated as,

$$V_e = \frac{\left(-V_1 - \frac{Q_1}{R_c}\right) + \left(-V_2 - \frac{Q_2}{R_c}\right)}{2} \tag{1.18}$$

where, V_1 and V_2 are known ionization potentials of atomic ions. In this way, using known atomic ionization potential, molecular relaxation distance "R_c" can be calculated in a good approximation with respect to experimental results on molecules like N_2, O_2, Cl_2, I_2, and CO. If model is extended to triatomic or polyatomic molecules one can imagine multi-well system, generating same potential changes probably in more approximate fashion, because as molecular chain increases energy distribution in different vibrational modes of molecules, is likely to have some impact on dissociation dynamics.

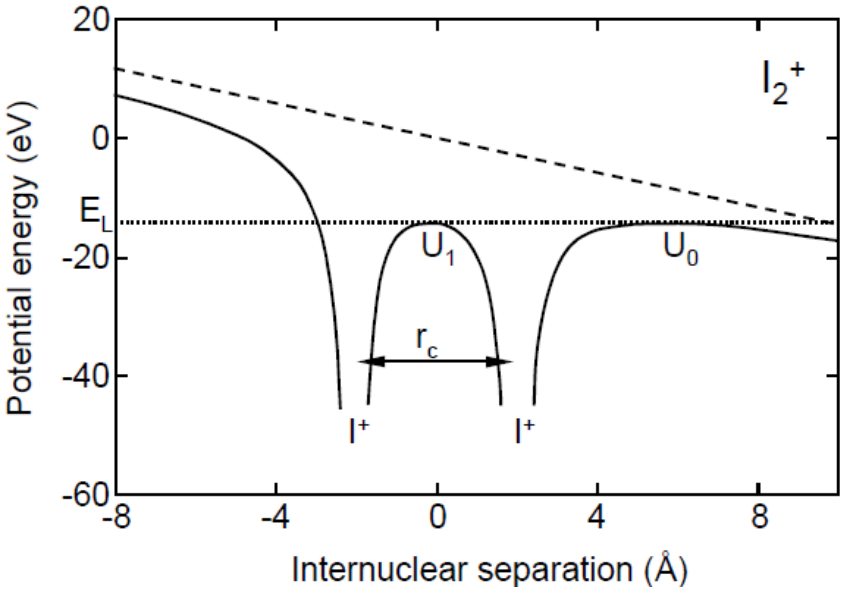

Figure 1.5: Molecular ion I_2^+ in intense laser field. Laser field is represented by negative slope straight line (dashed) and potential energy of the outer most electron is represented by sold double well potential plotted by sold curve. (From Posthumus *et al* 1995.) [27].

Process of molecular dissociation and appearance intensities can be explained by considering molecular potential diagram at different internuclear distances. At an internuclear separation of 5 a.u the energy level is well above the central potential barrier.

- An intensity of $5\times$ 3 10^{13} W/ cm^2 is required before the outer barrier is suppressed to the energy level of the electron figure 1.6.
- When inter nuclear distance 'R' increases the electronic energy level, E_L, rises and secondly, the electric field, now acts over a longer distance. Field is now more effective in lowering the outer potential barrier.
- At 7.5 a.u and beyond, the central barrier rises above the energy level of the electron. Now electron localization; this lowers the appearance intensity even further. Due to this localization, the electron level in the well on the left will be raised by a sufficiently strong electric field up to the top of the central

barrier. This is indicated by the vertical arrows in figure 1.6. At this stage less intensity of 1.2×10^{13} W/cm^{2}is needed to ionize the molecule.

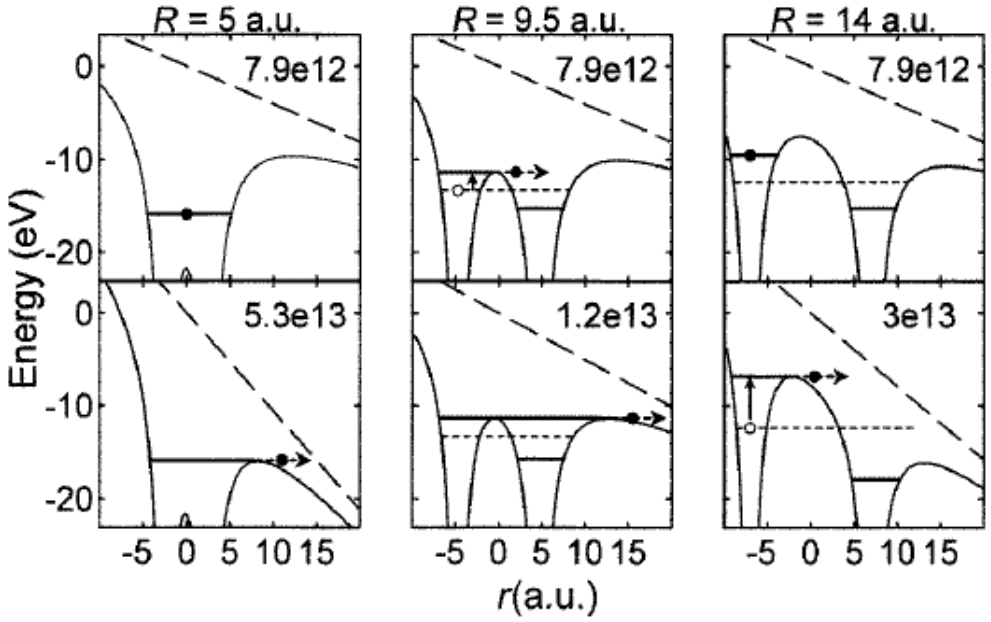

Figure 1.6: I_2^+ in intense laser field. Molecular potential interacting with laser field has been plotted at three internuclear separations. Appearance intensity is the lowest for internuclear distance of 9.5 a.u. [28].

Above internuclear distance of 10 a.u the central barrier, which now rises above the outer barrier, becomes the obstacle to ionization and since the level of the inner barrier increases as a function of "R" , and the appearance intensity as well. All dissociation channels have dip in appearance intensity at critical distance R_c. This happens because the enhanced ionization is closely related to the process of electron localization.

1.6 Polyynes

Polyynes are linear carbon chain molecules with acetylene as their basic unit, or they are hydrogen capped carbon chains C_nH_2 with n $\geq$ 2 and even, C_2H_2 is a monomer. In polyynes carbon atoms have sp hybridization. This leads to chains with alternating triple bonds figure 1.7. This alternating triple bonds makes them interesting due to creating alternating zones of high and low electronic charge densities. The zone of high electron charge density is more likely to be attacked by positively charged atomic or molecular species, therefore polyynes are expected to be more chemically active in similar conditions in comparison with their alkanes counterparts. Due to triple bonds present in carbon which enable polyynes to be a better conductors, polyynes can have technological applications of nano-wires. polyynes are rigid and stable with linear organic liquids such as octane and hexane at room temperature.

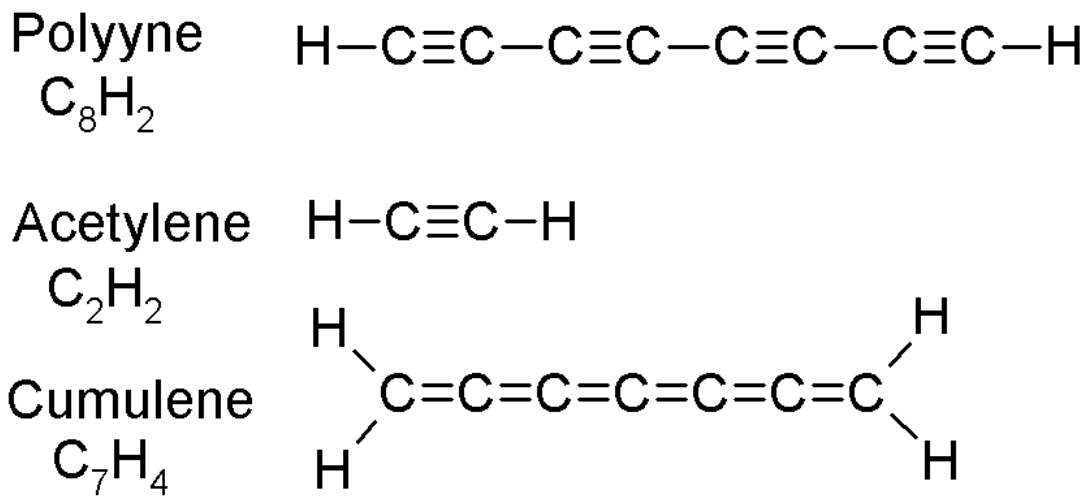

Figure 1.7: Simple hydrogen capped polyyne molecule C_8H_2 of size 1 nm, acetylene C_2H_2 is a monomer of polyyne.

Polyyne molecules in this study are only hydrogen capped but linear polyyne molecules exist with heavy carbon groups attached instead of hydrogen, as an example two benzene molecules can be attached capping polyyne molecules. Attachment of heavier groups of molecules alters vibrational frequency of polyyne and also may have an impact on the chain stability figure 1.8.

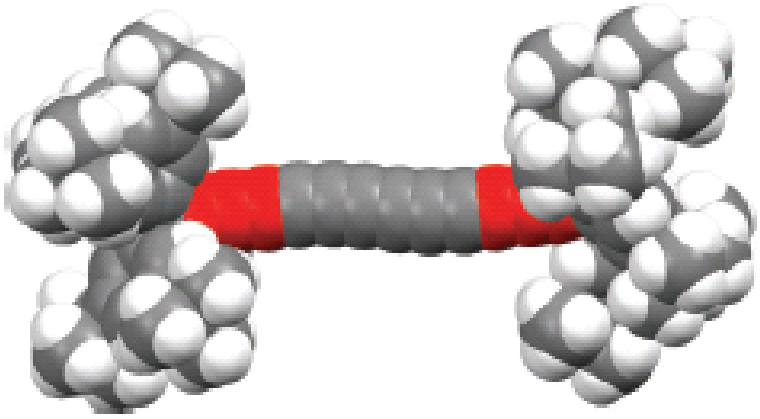

Figure 1.8: Polyyne molecules capped by massive molecular groups [29].

1.6.1 Significance of polyynes

Polynnes are more wide spread in nature than originally was thought, such as metabolites of plants, fungi and marine organisms. Moreover the biological activity of naturally occurring polyynes are known to antibiotic, antiseptic and even as anticancer has been recognized now [30]. Presence of polyynes has been found in interstellar medium where hydrogen exists in small quantity [31]. Polyynes are precursor to fullerenes and single layer nano-tubes SLNs', this by itself constitutes a very active modern research field [32].

Due to triple bonds present in carbon which enable polyynes to be a better conductors, polyynes can have technological applications of nano-wires, which can be used as connectors in nano electronics [33]. Polyyne nano wire C_{10} H_2 has Young's modulus 40 times than diamond, this appears to be the strongest known material in linear dimension [34]. Another device application that has been currently being investigated by resonance Raman and HPLC techniques for the formation of the nano coaxial cable by inserting a polyyne into a carbon nanotube figure 1.9.

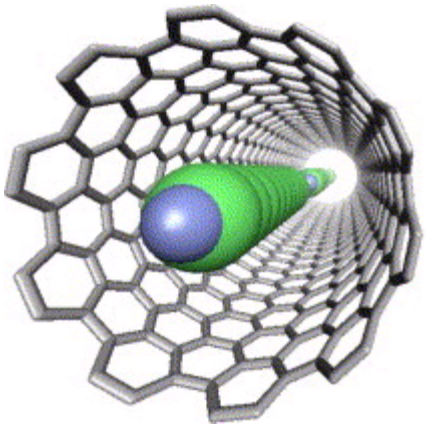

Figure 1.9: Nano-coaxial cable using C_{10} H_2 and single wall carbon nanotube [33].

1.7 Polyyne formation methods

Polyyne formation in larger amounts is only possible by prolong electric arcing. The best liquids for rapid polyyne formation appears to be hydrocarbons. The polyynes accumulate linearly with arcing time into organic liquid. This is also true for the submerged arc, where the graphite electrode provides the precursor molecules required for the formation of polyynes. It has also been shown that there is no direct formation of polyynes by pyrolysis at the focus of nanosecond laser pulses in hydrocarbon liquids even at pulse energies in excess of 300 mJ [36, 35].

1.7.1 Nanosecond laser irradiation

Polyynes have been initially generated by the laser ablation of suspended graphite [36, 44, 37, 35]. In these experiments, polyyne molecules do not originate from decomposition of the solvent but by the ablation of suspended particles. linear hydrogen-capped polyynes (C_nH_2: n = 10, 12, 14, and 16) were formed in benzene and toluene, while those of n = 8, 10, 12, and 14 were produced in hexane. The formation rates of polyynes increased with increasing particle concentration from 0.5 to 4 mg/ml. The formation rates of polyynes decreased with increasing wavelength of the Nd:YAG laser. Experimental arrangment is shown in figure 1.10.

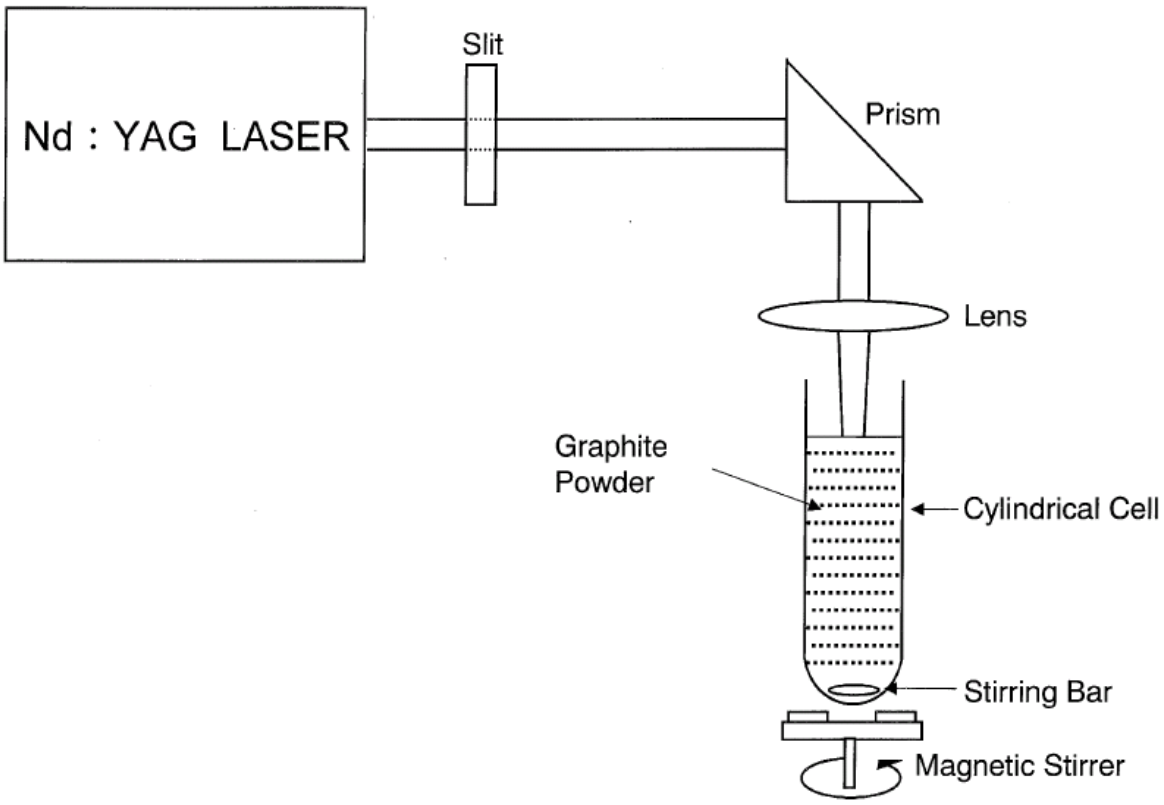

Figure 1.10: Polyyne formation using nanosecond laser on graphite suspension in hexane or benzene [39].

1.7.2 Femtosecond laser irradiation and polyyne formation.

However femtosecond laser irradiation of frozen acetone generates polyynes. Our group has generated polyynes by direct irradiation of liquid acetone [40], and also by direct irradiation of octane [41]. Recently in 2010 polyynes have been generated by Sato *et al* [42] by irradiating hexane with 100 fs, 800 nm pulses. They detected polyynes by using HPLC and nano second resonance Raman spectroscopy. Same results were observed in our hexane irradiation experiment figure 1.11. However polyyne formation by femtosecond laser irradiation of 100 fs 300 μJ pulses show capping in polyyne chain at $C_{14}H_2$ in case of both hexane and octane irradiation. Irradiated liquid in general is a complex mixture of polyynes, cumulenes and other organics as a result of break up of the original molecule in laser focus.

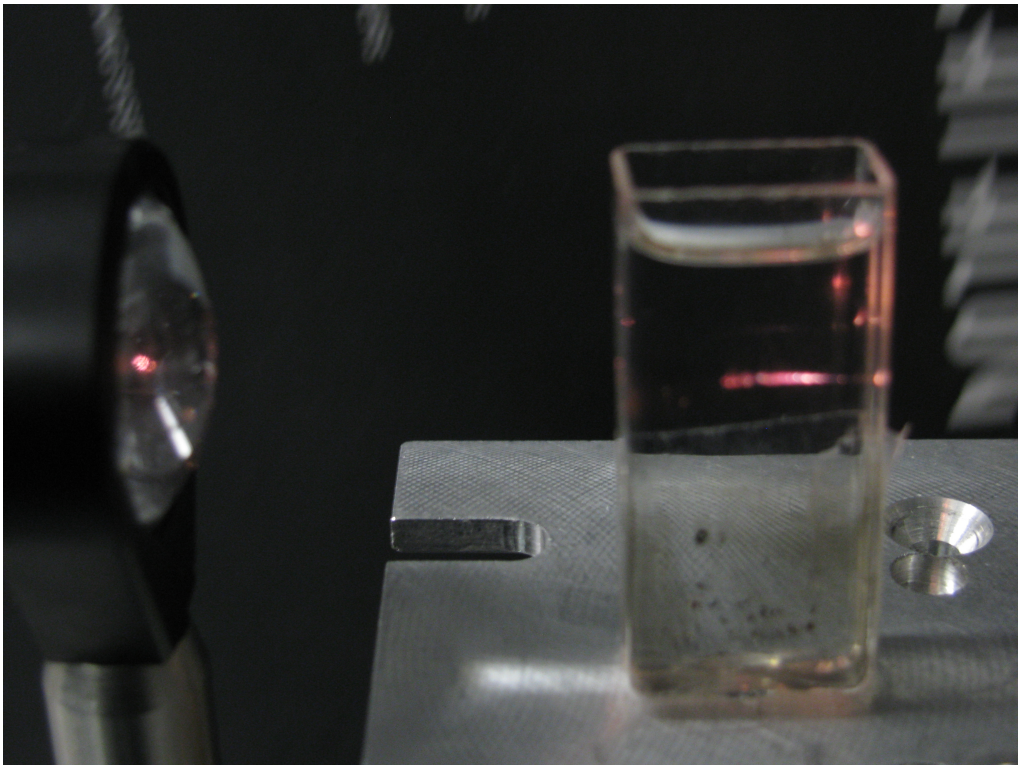

Figure 1.11: Femtosecond laser irradiation of hexane by 100 fs, 800 nm laser puses with intensity of $\sim 10^{15}$ W/cm^2.

1.7.3 Polyyne detection and characterization

Theoretical calculations performed by Kurti et al [43] has shown Raman bands of both polyyne and cumulene carbon chains usually occur around 2000 cm^{-1}. Tabata *et al* [45] has observed experimentally polyyne bands to occur between 1800 to 2200 cm^{-1}range. Polyyne formation in alkane liquids and acetone occurs due to the addition of C^+ or C_2^+ or other charged carbon species interacting with double bonded species produced by laser focus. This interaction is facilitated by multiple collisions in the liquid medium. Irradiated liquid is a mixture of original liquid, polyynes and cumulenes.

In this study small polyynes are detected by time of flight mass spectrometer TOFMS, based on duel stage extraction system. Femtosecond laser was used for ionization of the sample and ions are collected by MCP detector. TOFMS shows

complete range of small polyyne formation.

To detect longer carbon back bone polyynes from C_6H_2 to $C_{14}H_2$ surface enhanced Raman SERS has been used. 0.1M solution was used with ratio 1:5, containing 50 nm silver nano particles. Good signal enhancement was observed when CW laser of 488 nm was focused on the surface interface two media.

1.8 Raman Spectroscopy

The Raman effect can be observed by illuminating a material sample by a laser in the visible spectrum and observing the scattered light in the direction perpendicular to the original laser beam figure 1.13. In general, the scattered light contains frequencies different from the original frequency ω_o. The overall spectrum contains three components figure 1.14,

- Light scattered at same frequency 'ω_o' this is due to the elastic scattering from the material also known as Raleigh Scattering. This component is the most intense.
- Stokes Lines: light scattered with frequency lower than original frequency i.e $(\omega_o - \omega) = \omega_s$
- Anti-stokes Lines with frequency more than incident source frequency i.e. $\omega_a = (\omega_o + \omega)$.
- Similar to infrared spectroscopy (IR) Raman spectroscopy also provides information about vibrational frequencies of the molecule. In some situations where the nature of the molecular bond is covalent Raman effect is more important. In general for vibrational spectral study both methods IR and Raman effect complement each other.

Normal Raman

In normal Raman Spectroscopy, the exciting frequency 'ω_o' is chosen such that its energy is far below the first electronic excited state. Only a small amount of sample is required in Raman spectral study because focused laser beam size is usually about 2 mm. This is an advantage over the IR spectral study where relatively larger sample is needed. Raman spectra can be obtained by placing sample in a glass container suspended in water because both glass and water have no effect on Raman spectra of the sample, while IR is strongly absorbed by both glass and water.

Raman spectrum of liquids and solid samples can be obtained by the Renishaw Raman spectrometer figure 1.12, with a wave filter and Argon ion CW laser operating at 488 nm. Standard sample of silicon is run before using the actual sample for adjustment. Liquid sample is placed in 5 ml glass bottle and the laser light is focused on the surface. A computerized spectrometer control and data acquisition is used for this experiment. Data can be saved to a data file that can be easily imported into a spreadsheet program for further analysis. The data files consists of a column of wavelengths and a column of signal intensities. Such a data plot is shown figure 1.15.

Resonance Raman Spectroscopy.

In resonance Raman (RR) spectroscopy, scattering occurs when the exciting frequency ω_o is chosen such that its energy coincides with an electronic excited state. Using this effect, it is possible to enhance vibrations of a particular group in a molecule. This mode is more useful in vibrational studies of larger molecules. Due to the resonance effect intensities of the Raman band increase by a factor of 10^3 to 10^5 compared to normal Raman intensities.

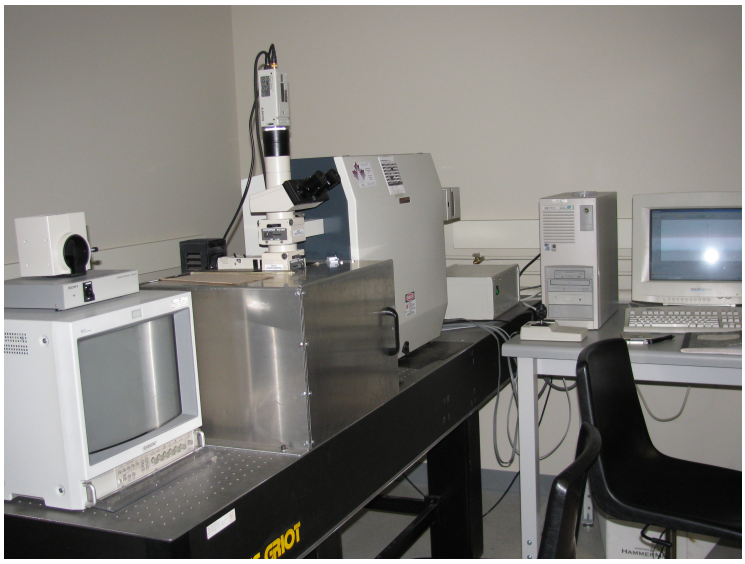

Figure 1.12: The Renishaw Raman spectrometer with a wave filter and Argon ion CW laser operating at 488 nm provided by wave filter. This laboratory is at the electrical engineering department of University of Waterloo.

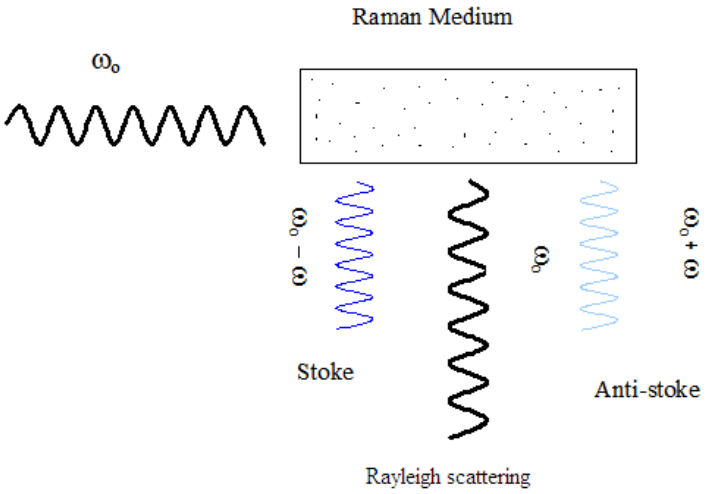

Figure 1.13: Raman scattering observed perpendicular to incidence. Anti-stoke component is less intense, for practical purposes stokes lines are measured.

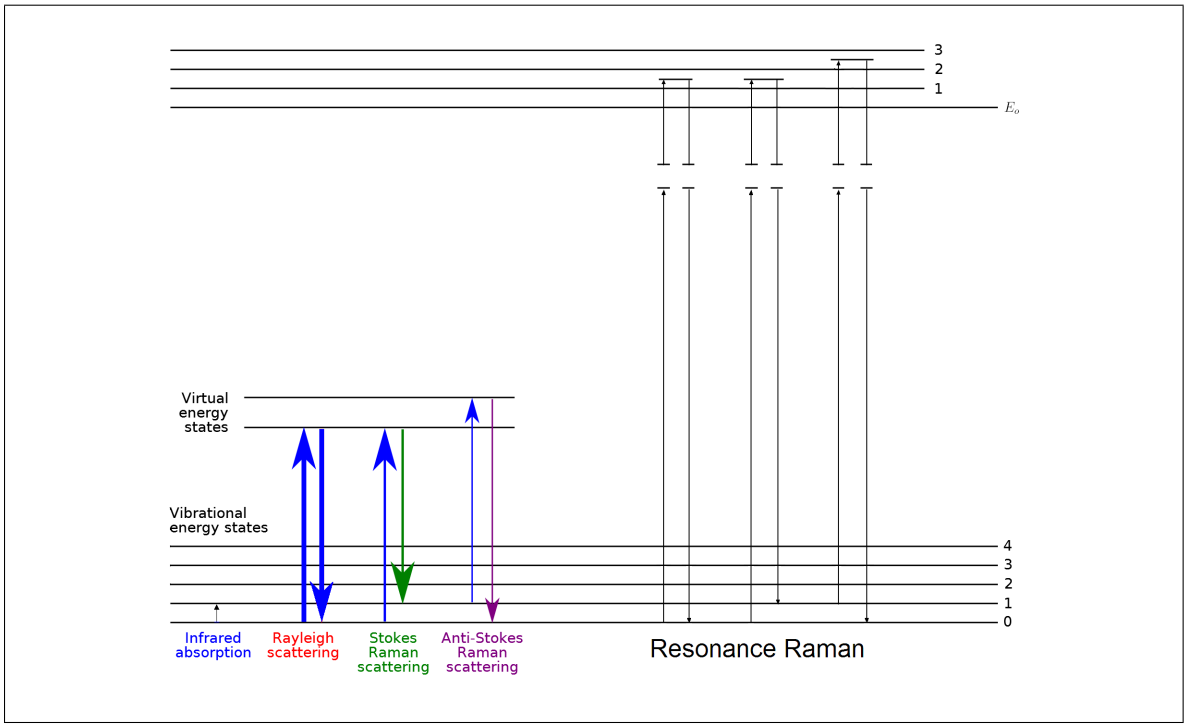

Figure 1.14: Energy level diagram showing Stokes and anti Stokes lines. Stokes lines are used in Raman experimental studies because of higher intensity.

The intensity of Stokes lines is higher than anti-stokes lines figure 1.14 because at room temperature more molecules are likely to be in the ground state. The Boltzmann's factor $exp(-\frac{\hbar\omega}{KT})$ determines the occupation at absolute temperature 'T'. Stokes lines are therefore used to observed spectrum. In Raman spectroscopy vibrational frequency shift is measured figure 1.13 with respect to original incident laser frequency ω_o. Raman scattering is very weak $\sim 10^{-5}$, therefore laser excitation is needed. Raman Scattering can be explained by considering the electric field 'E' of the incident radiation as equation (1.6) without a phase factor.

$$E(t) = E_o cos(\omega_o t) \tag{1.19}$$

E_o: Amplitude: ω_o: Laser frequency.

Considering the simple case of a diatomic molecule irradiated by the 'CW' laser of frequency ω_o, in a visible range the induced electric dipole moment 'P' will be $P = \alpha E$, where α is the molecular polarizability,

If the molecule is vibrating then in terms of normal modes, for small vibrations [46],

$$\alpha = \alpha_o + \sum_{\omega} \left(\frac{\partial \chi}{\partial Q_\omega} \right)_o Q_\omega \tag{1.20}$$

where Q_ω is the normal mode with frequency ω. In the case of one degree of freedom with frequency 'ω',

$$Q_\omega = A_\omega cos(\omega t) \tag{1.21}$$

Using equations (1.19), (1.20) & (1.21), the dipole moment is given by,

$$P(t) = \alpha_o E_o cos(\omega_o t) + \frac{1}{2} \left(\frac{\partial \alpha}{\partial Q_\omega} \right)_o A_\omega E_o \left[cos(\omega_o - \omega)t + cos(\omega_o + \omega)t \right] \tag{1.22}$$

- The above expression (1.22) indicates first term is an oscillating dipole radiating at the source frequency 'ω_o' this represents elastic Raleigh scattering.
- If $\left(\frac{\partial\alpha}{\partial Q_\omega}\right) = 0$, the vibration is not Raman active.
- In the second term Stokes lines figure 1.14 corresponds to $\omega_s = (\omega_o - \omega)$ and anti-Stokes corresponds to $\omega_a = (\omega_o + \omega)$.

1.8.1 Surface Enhanced Raman Spectroscopy (SERS)

When molecules are adsorbed on a certain appropriately prepared metal surface, these adsorbed molecules show enhanced Raman signal by 10^5- 10^6 times stronger than that of the non-adsorbed same molecular species. This enhancement is very important since the Raman effect is a feeble effect. Due to this considerable enhancement a small amount of sample is needed and a standard laboratory set up is capable of trace analysis with high accuracy.

The Raman spectra is obtained in visible or near infrared region. In Raman study, the choice of the substrate surface is important, The surface material choice is made with respect to an adsorbed molecule and laser wavelength used. Usually rough metallic surfaces can be used, for organic molecules silver or gold nano-suspension works very well. SERS enhancement may be understood by considering molecular polarizability P = α E, enhancement is generated by two factors, 'E' the electromagnetic factor and α the molecular polarizability factor.

When the laser electric field is near adsorbed molecule on a nono-silver surface, the electric field interaction with the metal surface generates surface plasmon on the metal surface [46]. This increases molecular polarization 'P' of molecules having π bonds. Since intensity of Raman scattering is directly proportional to the square of the induced dipole moment, output signal is enhanced by a factor of $\sim 10^5$.

The plot figure 1.15 below shows SERS spectra of both irradiated and pure octane. The experiment was performed to see if polyynes are present in the irradiated octane sample after two hours of 100 fs laser irradiation with the wavelength of 800 nm and energy of 300 μJ. For enhancement, nano-silver solution was used and a CW argon ion laser of wavelength 488 nm was focused on the boundary separating two media to

get the best possible signal. SERS spectra obtained shows polyyn presence at a well defined interval of 1800 to 2200 cm^{-1}.

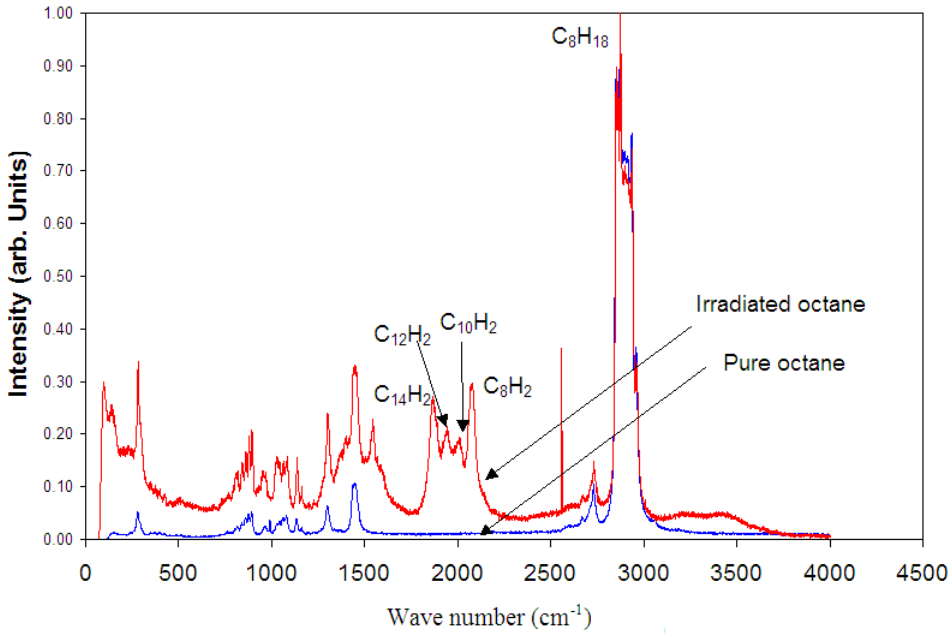

Figure 1.15: Comparison of a pure and irradiated octane's normalized SERS spectra. Irradiated octane spectra shows presence of Polyynes, when nano-silver solution was used for enhancement.

SERS spectra of non-polar chain molecules containing multiple chain elements like C - C, C = C and C ≡ C, is helpful in detection of small amounts of species having long chain double and triple non-polar bonds like polyyne molecules [25] in irradiated alkanes. Polyynes contain conjugated triple bonds i.e. between two carbon atoms one sigma σ and two π bonds. Sigma bond charge density is localized between two bonded atoms, but charges belonging to π bonds are not localized. In a good approximation π electrons can be effectively considered delocalized over the length of the conjugated polymer. This increases both the linear and non linear optical response of conjugated polymers, in our experiment on polyynes. When polyynes are attached onto a nano-silver surface in the presence of the laser field surface plasmon generated on the nano-silver surface further helps in the optical response and adsorbed polyynes

are clearly visible in SERS spectra. Irradiated octane NR spectra figure 1.16 shows no evidence of polyynes because silver nano-particles were not added.

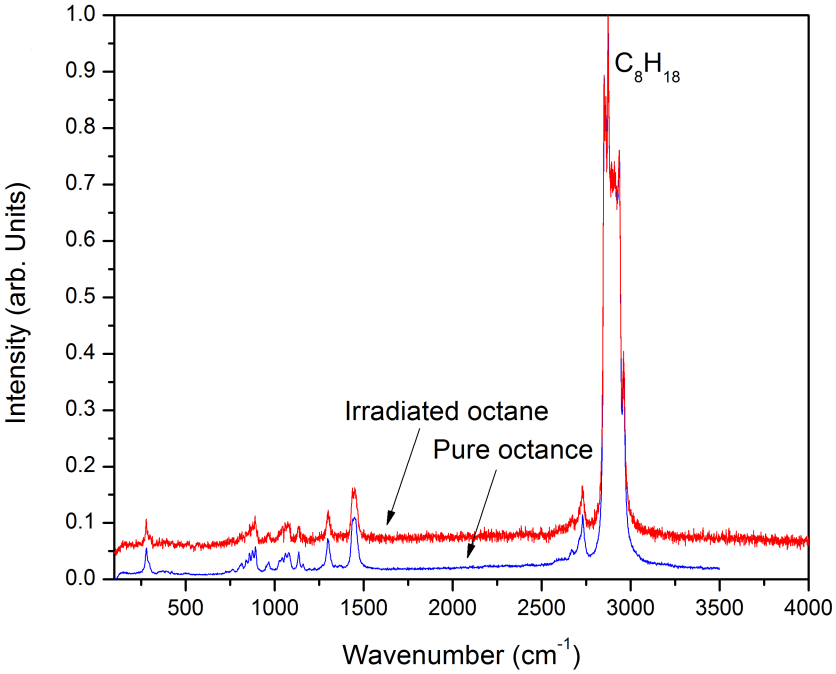

Figure 1.16: Comparison of pure octane and irradiated octane (with 800 nm 100 fs pulses at 300 μJ). Normal Raman spectra without surface enhancement both spectra appear the same.

Chapter 2

Experimental research review on pulsed laser ionization and detection of atomic and molecular species

2.1 Introduction

Pulsed lasers provide high peak power sufficient to match the order of atomic electric field. Laser ionization experiments performed by pulsed lasers range typically from an intensity of 10^9 W/cm^2 to 10^{16} W/cm^2, with pulse width varying from several nanoseconds to few femtoseconds. In a laser-matter interaction experiment, the laser electric field interacts with the bound electrons in an atom or a molecule causing ionization. For mass spectrometry, this is a desirable result both in the case of a spherically symmetric atom or a polyatomic molecule. Ionization can occur via over the barrier ionization (OBI), ADK tunneling mechanism, or multiphoton ionization (MPI). The mechanism of ionization has been classified by the Keldysh Parameter γ [20]. On the material side, the ionization and dissociation problem has been studied extensively from simple atoms in the gaseous phase to polyatomic molecules. Some of these molecules are large enough to touch the size of nano-molecular range, for example, octane, aromatics, polyynes and more complex molecular species.

2.2 Initial experimental investigations of ionization modes in the laser fields

The early experiments on laser ionization used nanosecond or pecosecond laser pulses and noble gas elements as a target to study single or multiple ionization of the target atom. L'Huillier *et al* (1983) measured the ionization rate of xenon using a 1064 nm wavelength laser [47] with a pulse width of 50 ps. She concluded that at high intensities, multiple ionization was a sequential process, and at low intensities, non-sequential. *Sequential ionization* implies that, during the laser pulse, electrons are removed in a step-wise manner while *non-sequential ionization* means more than one electron is removed simultaneously.

$Xe + n\hbar\omega \rightarrow Xe^{+} + e^{-}$

$Xe^{+} + n\hbar\omega \rightarrow Xe^{++} + e^{-}$

Non-sequential ionization leads to the following state in a single step, ('n' is the number of photons absorbed).

$Xe + n\hbar\omega \rightarrow Xe^{++} + 2e^{+}$

Codling *et al* (1987) devised an experiment using hydrogen iodide (HI), which has the same electron number in the outer shell as Xe [48]. The molecule was multiply ionized by a 600 nm laser pulse, with the pulse width of 600 fs. The highest stage of ionization observed was HI^{6+}. It was thought that if ionization happens sequentially, then in the HI case, the emitted proton energy should be substantially less than in comparison with non-sequential ionization. The protons were observed to have a maximum kinetic energy of around 21 eV, hence Codling *et al* (1987) concluded that the ionization mechanism was sequential for hydrogen iodide. In the case of non-sequential ionization, emitted proton energy due to Coulomb repulsion should be 42 eV as indicated by the potential curve diagram figure 2.1. Lambropoulos (1985) and Codling *et al* (1987) showed that an atom or a molecule is not instantly affected by the peak electric field of the laser pulse [49], but the ionization rates depend on the temporal pulse profile instead. Augst *et al* (1989) studied multiple ionization of noble gases, at that time peak pulse power improved considerably. It was found that a classical field ionization model figure 1.4 successfully predicted the appearance intensities of specific charge states [50].

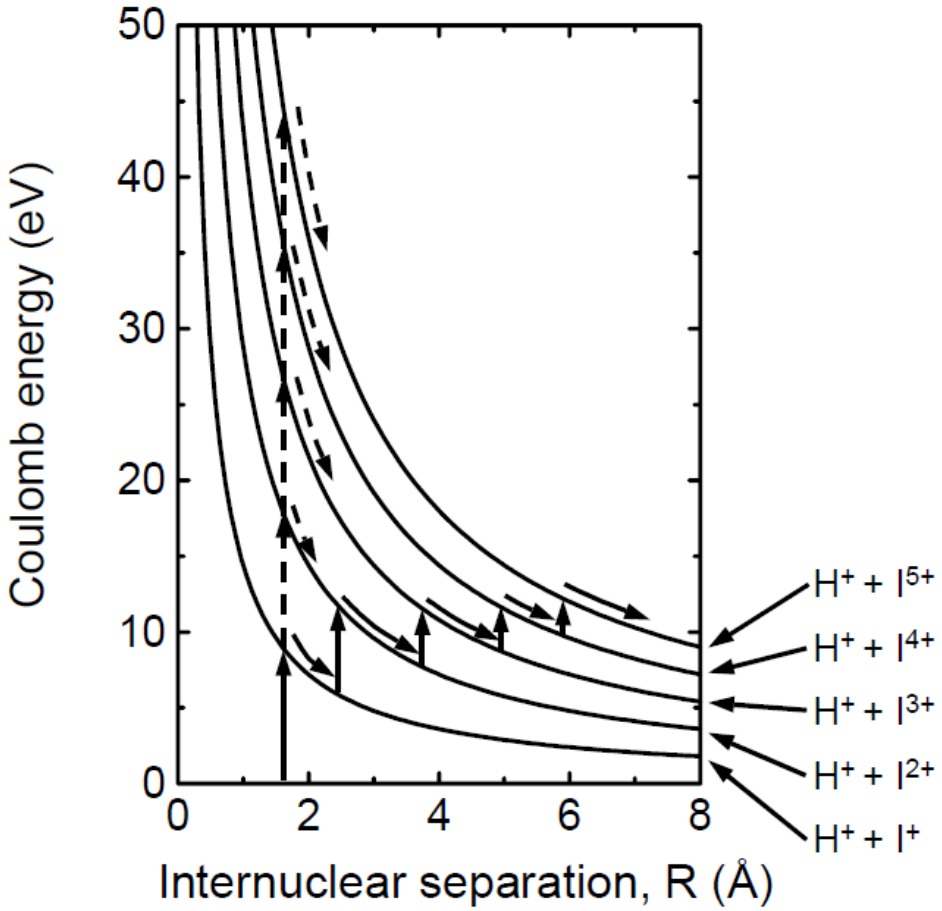

Figure 2.1: Potential curves for HI molecule. Solid lines represent sequential ionization and dashed arrows represent non-sequential ionization. [48].

The ionization mechanism was approximated using the over the barrier method. As the laser field increases in strength, the electron can escape over the potential barrier directly into the continuum. Later multiple ionization experiments with simple molecules by Frasinski *et al* (1987) (N_2) and Codling *et al* (1987) (HI) indicated that molecular ionization is somewhat different than atomic ionization. Further they observed that the polarization of the laser pulse also has an impact on the ionization rates [51]. Non-sequential ionization of Xe and Kr studied with 200 fs femtosecond laser pulses by Larochelle, A. Talabpur and S. L. Chin in 1997 indicated large enhancement in the probability of double ionization of both Xe and Kr. Their findings indicated that the probability of non-sequential ionization of any charge state is a

linear combination of the tunneling probability of the previous charge state [52].

McKenna *et al* (2006) studied ionization and dissociation of the N_2 molecule in intense 55 and 220 fs, linear and circularly polarized, 790 nm laser pulses [53]. They tried to study the mechanisms underlying multielectron dissociative ionization (MEDI) of molecules in intense laser-fields. Their paper mainly tried to explain observed kinetic energy release (KER) through fragmentation is persistently lower than that given simply by Coulomb explosion (CE) at mean internuclear separation R_e. The proposed model generally considers dissociation at an increased critical internuclear distance R_c where $R_c > R_e$. It is explained by electron localization quantum mechanically [54] or classically [27]. The dependence of ionization rates on the molecular structure and symmetry along the polarization direction means that investigating the effect of molecular orientation with the field is important. Tong *et al 2002* [24] adapted the ADK tunneling model [22] to take into account the molecular orbital symmetry and reproduced well the experimental ionization rates for N_2, F_2, D_2 and O_2. They observed that the angular direction of the laser polarization with respect to the orbital axis is critical. A similar dependence on the symmetry of the highest-occupied molecular orbital (HOMO) was proposed by Muth-Böhm *et al* [55]. They argued that since the HOMO has different geometrical orientation in space it may affect the ionization rates. Studies of single ionization on N_2 molecule showed no dependence on polarization, indicating a lack of alignment of the neutral molecule. However, double ionization showed an enhancement in the linear N_2^{2+} signal resulting from a combination of both the alignment of the N_2^+ ion coupled with a higher ionization rate for the E-field acting along the molecular axis. Theoretically calculated KER values are generally found to be in reasonable agreement with the measurement. Higher charge states N^{4+} and N^{5+} are believed to be produced at much longer bond lengths as anticipated earlier.

Recently Gaire *et al* (2009) investigated ionization and dissociation dynamics of the singly charged ions of N_2^+, CO^+, NO^+, and O_2^+ [56]. In contrast to most earlier studies on MEDI that used neutral molecules as precursor targets, they begin with the singly charged molecular ions themselves in the form of an ion-beam target. This choice avoids differences in molecular geometry due to the outer most bonding orbitals, as H_2^+ is different than H_2. In their experiment the molecular ion targets are exposed to ultra short 40 fs to 7 fs intense 790 nm laser pulses at intensity of 7×10^{15} W/cm^2. They distinguished between *direct* and *indirect ionization* with direct being the ionization at

equilibrium distance R_e (nuclei can be treated as frozen) and indirect at $R_c > R_e$. Other possible mechanisms for MEDI is that molecules can stretch only on the dissociation curve and then ionize to different levels at $R_e < R < R_c$. In summary, more channels at 40 fs pulse duration are observed compared to 7 fs pulses at the same intensity. Comparing dissociation between different molecules, it appears all molecules display structure in their KER distributions. Finally, in multiple ionization the molecules lose this structure in KER and start to resemble one another more closely in both angle and KER shape. Overall they found that the 7 fs data are also consistent with the stair step mechanism used to explain the 40 fs data. Whereas for 40 fs the molecules stretch more between ionization steps, for 7 fs the molecules do not have this opportunity. In the limit of very long pulses $\sim$ 100 fs, it is expected that the stretching between steps will reach 'R' values close to 'R_c'. Whereas in the limit of very short pulses $\sim$ 3 fs, processes driven by electron re-scattering ionization will become more direct, occurring near the equilibrium distance $R = R_e$. They concluded that while for dissociation the KER and angular distributions are unique to a specific molecular ion, for the higher ionization channels the spectra of all molecular ions under study start to resemble one another, the molecular ions seems to lose their identity.

Wu *et al* (2010) did experimentation on O_2 to study double and triple ionization of the oxygen molecule very recently [57]. The kinetic energy releases (KER) and the angular distributions were obtained through coincidentally measuring the ionic fragments of doubly or triply charged parent ions. Based on these measurements, they concluded that multiple ionization occurs through stair step process under the current experimental conditions. During the time interval between two ionization events, the internuclear distance is stretched by the assistance of the laser field. The longer the pulse duration is, the longer the internuclear distance stretches. The stretch of the internuclear distance results in the decrease of the measured KER's. The angular distributions are influenced by both the laser intensity and the pulse duration. Long pulses cause dynamic alignment of the neutral molecules before ionization. Most importantly, they observed that when the laser intensity is 2.5×10^{14} W/cm^2 and the pulse duration is 8 fs, the alignment effect can be neglected.

2.3 Ionization and detection of molecules

Laser based ionization and detection of species depends on two major factors, namely the type of incident pulse and the nature of the target (atom or a complex molecule). However, it is highly desirable to achieve uniform ionization whether the target is an atom or a complex molecule. Studies have been done by several authors on small and large molecules to achieve this end, such as Smith *et al 1998* [58], Ledingham *et al 1997* [67], Castillejo *et al 1999* [60]. and Itakura *et al 2001* [61]. In their observation the most important experimental fact was that after laser excitation, molecules have often been found to rapidly dissociate with respect to the parent ion formation. It was concluded that this is due to the dissociative excited states having lifetimes shorter than the laser pulse widths. This often results in extensive fragmentation, yielding small or nonexistent parent ions. This situation leads to ambiguous chemical identification for molecular species. When a molecule absorbs one or two photons, it can reach a dissociative state. To defeat this dissociative state, an appropriate pulse width and wavelength combination is needed. To study this problem the following review identifies three basic factors involved in molecular ionization requiring to form intact molecular ions scaling from diatomic to the nano-molecular range.

The electric field from a focused picosecond or femtosecond pulsed laser is very intense and may match the molecular Coulomb field experienced by the valence electrons. Under such conditions the ionization of the molecules can take place through a field ionization (tunneling ionization) mechanism which competes with the multiphoton absorption-ionization processes. A qualitative criterion for the kind of mechanism involved is provided by the adiabatic parameter γ , defined by Keldysh [20]:

$$\gamma = \left(V_o/1.87 \times 10^{-19} I\lambda^2\right)^{1/2} \tag{2.1}$$

where V_o is the ionization potential expressed in eV, 'I' is the laser intensity in W/ cm^2 and λ is the laser wavelength in nm. When $\gamma << 1$ field ionization prevails, while for $\gamma >> 1$, multiphoton ionization is the main mechanism. Recently this criterion has been reconsidered and a more pragmatic definition of tunneling ionization is thought to be $\gamma < 0.5$ [62]. These values are in the intermediate regime and although it is felt that multiphoton ionization is the dominant mechanism, the field ionization mechanism

cannot be excluded, at least for the higher laser intensities. A comprehensive review of field ionization has been carried out by Codling and Frasinski [63] with particular reference to the dissociative ionization of small molecules in intense laser fields.

Multiphoton absorption by molecules can lead to fragmentation by two distinct mechanisms [64]. First, the molecule can absorb a number of photons resonantly or non-resonantly to reach a dissociative state below the ionization level. If the laser pulse length is longer than the lifetime of the state then the molecule fragments to form neutral daughter species. Depending on the laser intensity, these fragments may absorb further photons within the initial laser pulse to ionize or further fragment. This process is known as dissociation followed by ionization (DI) or *ladder switching*. If the pulse is very much shorter than the lifetime of the dissociative state then the up-pumping rate may be so high that the ionization level is reached. The manifold of ion states can absorb further photons and fragment. Alternatively, the molecule can be pumped via a series of levels to some highly excited state of the molecule which then fragments to ions. These two variants result in ionization followed by dissociation (ID) or ladder climbing. Many molecules fragment by ID alone (e.g. the aromatics) [65] while others, e.g. the nitro compounds and the organometallic molecules, fragment by the DI route. Often the two mechanisms compete, with *ladder climbing* becoming more dominant as the pulse width decreases. It is also possible that ladder switching can occur from the ionic manifold of states if the lifetimes of these states are shorter than the pulse width. In this case both the ion and neutral fragments can absorb further photons. For analytical purposes, DI fragmentation is often of little use since it causes loss of the parent ion. The following sections sheds more light on the most important factors in obtaining intact parent ion. The pulse width dependence, wavelength dependence and the intensity dependence.

2.4 Pulse width dependence

Irradiation of NO_2 with laser pulses from the nanosecond to 300 fs range shows that the femtosecond irradiation reveals the most information. As the pulse width decreases NO_2^+ peak grows.

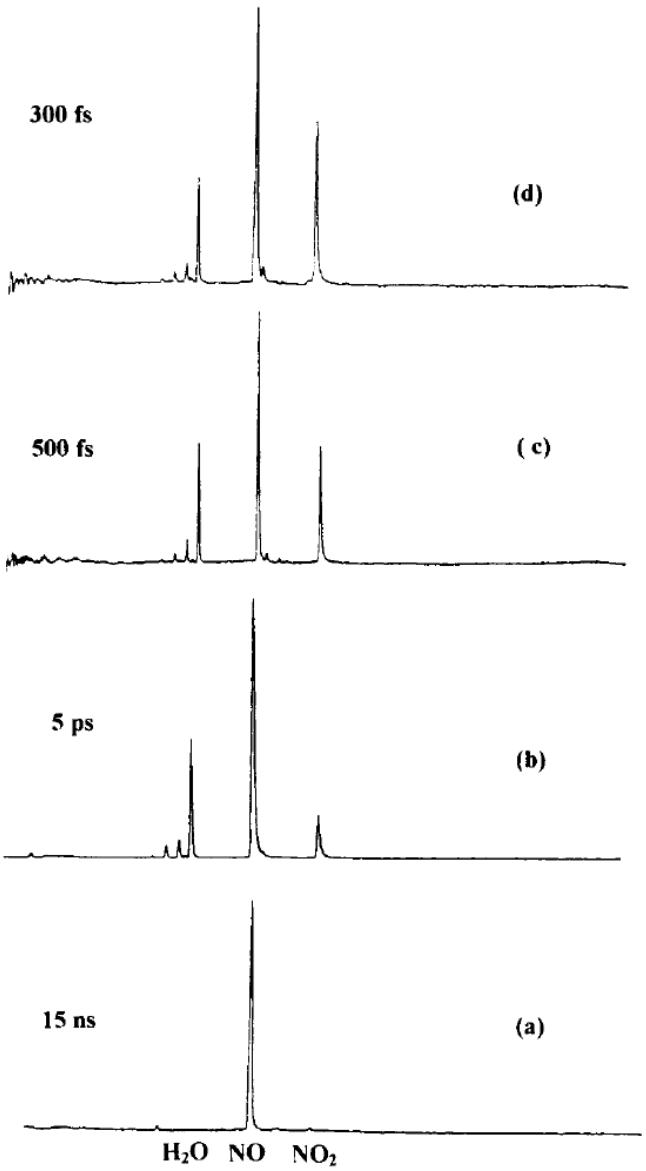

Figure 2.2: Pulse width dependence on ion signal of NO_2 molecule. [66]

To observe intact parent ion formation, experiments were done first on small molecules, using different pulse widths, wavelengths and intensity ranges. Experiments done on NO_2 irradiation indicated the differences in fragmentation due to pulse width. In figure 2.2 the incident laser wavelength used was 248 nm and the laser intensity was $\sim 10^{11}$ W/cm^2. To explore pulse width dependence, Ledingham *et al* covered a broad range of pulse widths from 15 nano-second to 300 femto-second. These experiments [66] indicate that the nanosecond pulses only produce a clear peak for the NO molecule, while the parent ion peak is of the background level. As the pulse width decreases peaks for H_2O, and NO_2 becomes taller. The pulses below 1 ps show the most clear parent ion signal.

Although these initial experiments were done on small molecules, later experimentation by Ledingham group [67] showed that taller parent ion peaks are obtained easily in the case of middle weight aromatic organic compounds when pulse width of 50 fs is used. Later 50 fs pulse width found to be useful for fairly large molecules like CuOEP and NiOEP with molecular mass of 600 amu figure 2.7. Ledingham group concluded that 50 fs duration pulse width is the best choice to perform laser based ionization and detection experiments or trace analysis.

2.5 Wavelength dependence.

Experiments performed by different groups indicated that at a given intensity and pulse width, more molecular ion production is observed by 800 nm wavelength than 400 nm wavelength pulses. This point was investigated by Castillejo *et al* [60] and Dewitt *et al* [68] by subjecting aromatic hydrocarbons to both wavelengths. They found the selection of an 800 nm wavelength is more appropriate for taller parent ion peak formation in middle weight molecules. In figure 2.3, the spectra of benzene and cyclohexane irradiated with 800 and 400 nm pulses indicate benzene has less fragmentation and more parent ion formation at 800 nm. Although cyclohexane fragments much more than benzene but the spectrum at 800 nm has taller parent ion peak. This lead to the conclusion that fragmentation is less at wavelength of 800 nm.

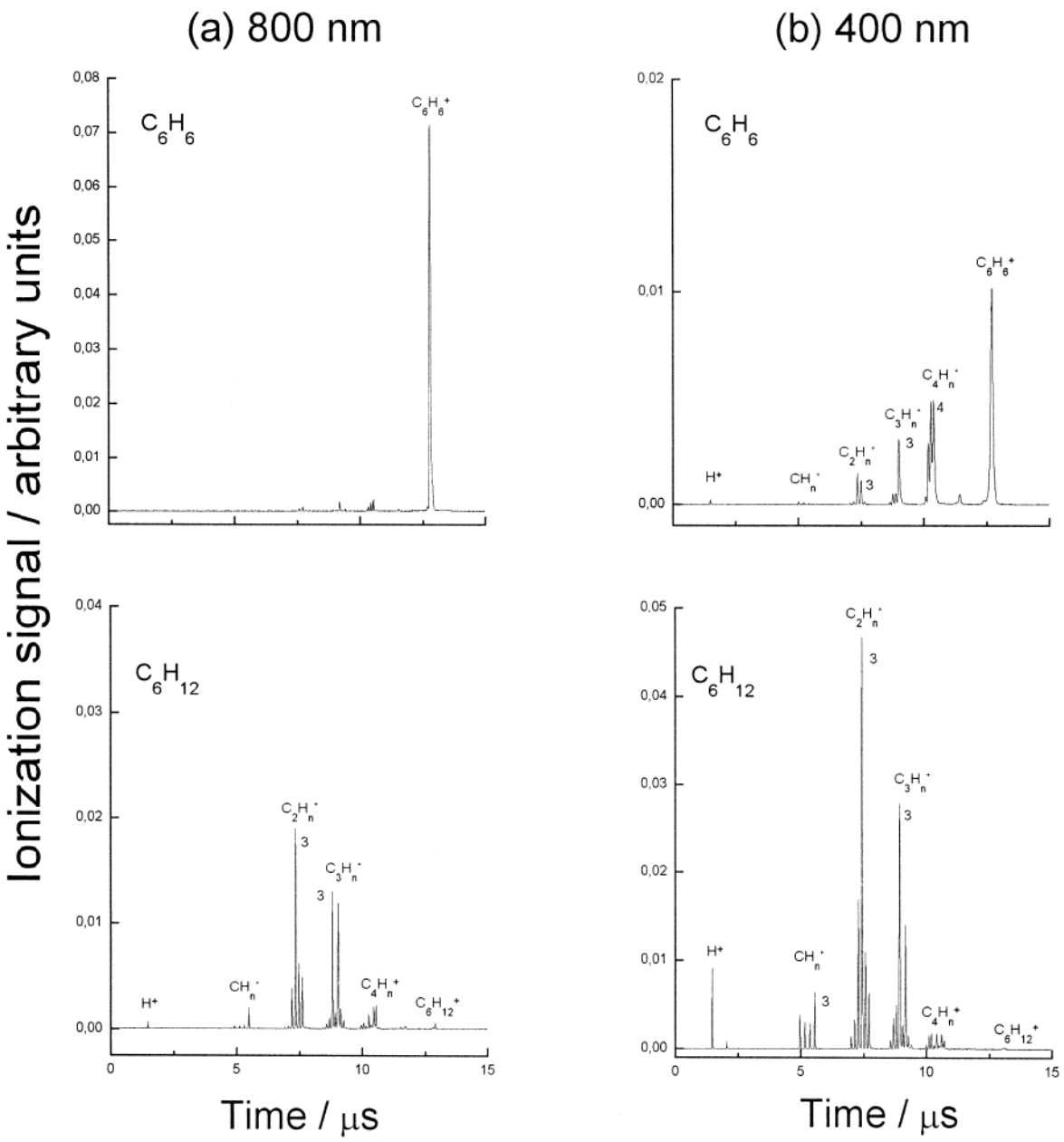

Figure 2.3: Spectra of benzene and cyclohexane irradiated with 800 and 400 nm. [60].

2.6 Intensity dependence

The ion yield plotted as a function of intensity at two different wavelengths 750 nm and 375 nm was investigated by Smith *at el* [69]. In their experiments the pulse width of 50 - 90 fs was maintained.

The intersection of the 750 and 375 nm curves represents an equal probability of the parent molecular ion production for the different wavelengths. This corresponds to an optimum operating intensity of about 10^{13} W/cm^2. Wavelength independence characterizes a more flexible and general analytical approach. A degree of saturation of the ionization signal is apparent in figure 2.4 at the higher laser intensities. This can be seen as a reduction in the rate of change of ion yield as the beam intensity increases. It is also clear that the gradient of the 750 nm curves are steeper than those of the 375 nm which suggests that up to the first ionization potential the absorption process proceeds via a multiphoton model.

With the increase in intensity at 750 nm the appearance of multiply charged molecular ions has been observed in the ion spectrum and this was accompanied by less dissociation as observed at 400 nm. Whether infrared at 800 nm has less dissociative effect than UV at 400 nm, has been studied extensively by the Glasgow group, this is in agreement with studies by Dewitt *et al* [68]

For analytical purposes, a degree of wavelength independence has been identified. For laser intensities approaching 10^{14} W/cm^2, the molecular ion yield has been found to be similar for both 750 and 375 nm as shown in figure 2.4. Moreover, at intensities approaching ion yield saturation, it is evident that parent molecular ion detection is obtained for the three molecules, benzene, toluene and naphthalene. This points to a possible quantitative procedure for molecular detection. At intensity level 10^{14}- 10^{15} W/cm^2 similar results are obtained for subpicosecond pulses.

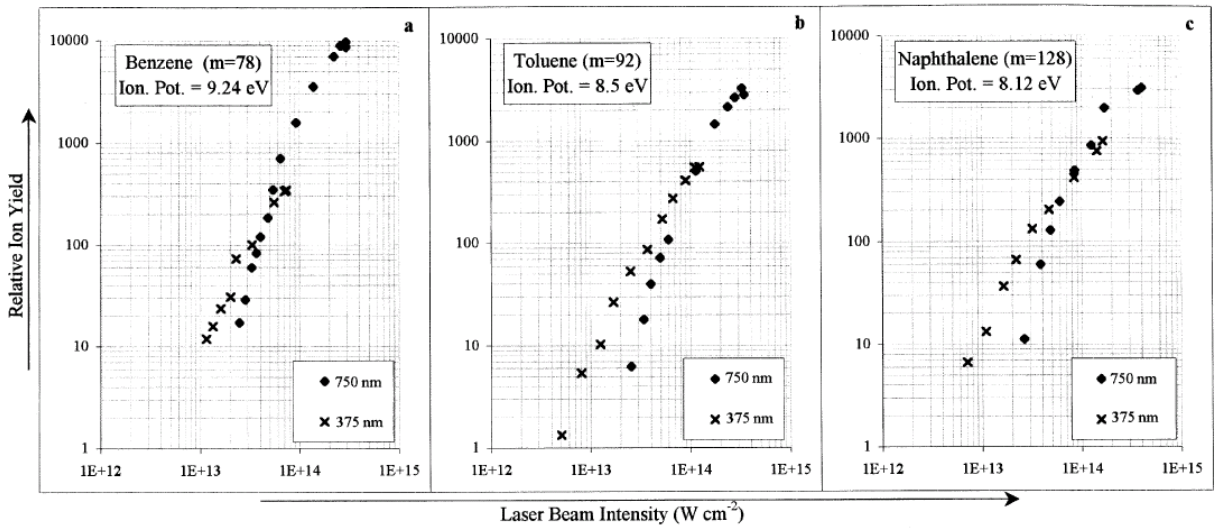

Figure 2.4: Intensity dependence of benzene, toluene and naphthalene at 750 nm and 375 nm. [69]

2.7 Uniform molecular ionization.

Fang *et al* [70]discussed in detail *uniform molecular analysis using femtosecond laser mass spectrometry.* Their central idea was to form large parent ion peaks using a suitable combination of pulse width, wavelength and intensity . It is highly desirable to obtain large parent ion peak for different atoms and molecules having varying ionization potential. It was shown by the Glasgow group, that a combination of the 50 fs pulse width, 800 nm wavelength and 10^{15} W/cm^2 intensity generates large parent ion peaks relative to the rest of the spectrum in most small and middle weight molecules. Their study range includes almost all types of inorganics, some small linear chain organics, and cyclo-organic compounds like benzene , toluene, anthracene etc. They showed that objective of dominant parent ion peak can help to detect small quantities of substances by laser irradiation. In their view, the procedure and mechanism of ion production plays a key role in analytical ability. The following table summarizes the notable work of many groups and their study parameters to obtain distinct parent ion peaks.

	Wavelength (nm)	Width	Intensity (W/cm^2)	Products[a]	
				Parent ions	Fragment ions[b]
Zandee *et al.*[c]	~390	5 ns	$\sim 10^9$		$C_2H_k^+$ (0.3)
					$C_3H_j^+$ (0.2)
					$C_4H_i^+$ (0.2)
					C^+ (0.2)
Bosel *et al.*[d]	259	5 ns	3×10^8		C^+ (0.4)
					$C_2H_k^+$ (0.2)
					$C_3H_j^+$ (0.2)
	504	5 ns	5×10^9		C^+ (0.5)
					$C_2H_k^+$ (0.2)
Bhardwaj *et al.*[e]	532	35 ps	4×10^{13}		C^+ (0.3)
					$C_3H_j^+$ (0.2)
					$C_2H_k^+$ (0.2)
DeWitt *et al.*[f]	780	170 fs	3.8×10^{13}	$C_6H_6^+$ (1.0)	
Castillejo *et al.*[g]	800	200 fs	1×10^{13}	$C_6H_6^+$ (1.0)	
	400		1.2×10^{12}	$C_6H_6^+$ (0.4)	$C_4H_i^+$ (0.4)
Castillejo *et al.*[h]	800	50 fs	2×10^{14}	$C_6H_6^+$ (0.2)	C^+ (0.2)
					$C_3H_j^+$ (0.2)
Talebpour *et al.*[i]	800	200 fs	$<5\times10^{14}$	$C_6H_6^+$ (0.9)	$C_4H_j^+$
					$C_3H_j^+$
Smith *et al.*[j]	750	50 fs	3×10^{14}	$C_6H_6^+$ (0.5)	
				$C_6H_6^{2+}$ (0.3)	
	375	90 fs	1×10^{14}	$C_6H_6^+$ (0.6)	$C_4H_j^+$ (0.2)
Ledingham *et al.*[k]	790	50 fs	2×10^{15}	$C_6H_6^+$ (0.7)	
				$C_6H_6^{2+}$ (0.2)	
Shimizu *et al.*[l]	800	120 fs	1×10^{17}		C^+, C^{2+}

Figure 2.5: Comparison of the previous studies on benzene in intense laser fields indicating 800 nm, and 50 fs and intensity $\sim 10^{14}$ W/cm^2 is a good choice for this mass range to obtain tall parent ion peak [61].

In the laser matter interaction problem, the experimentalist has a choice of pulse width, pulse energy and incident wavelength. Above considerations show that wavelength independence can be achieved by using an intensity interval of 10^{13} to 10^{15} W/cm^2. However, IR wavelength of 800 nm is more suitable because it causes less fragmentation. Moreover, it seemed resonable to choose femtosecond pulse width. Further study by experimental groups indicate best choice is 50 fs pulses X. fang *et al* 1999 [70]. Experiments with 800 nm and 50 fs pulses produce large parent ion peaks and a doubly charged halfway peak of the parent ion.

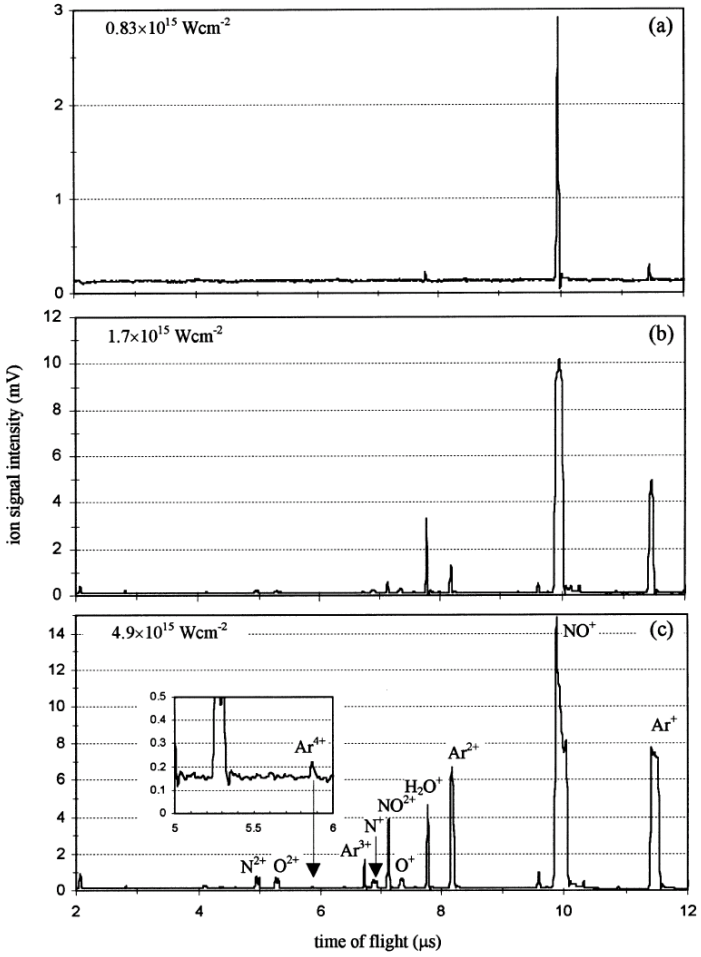

Figure 2.6: TOF spectra of NO at different intensities, at the pulse width of 50 fs.[70] .

For uniform molecular analysis to be attainable for small and sufficiently large polyatomic molecules, one needs to consider another parameter that is variation in ionization potential of different molecules. A combination of laser parameters which lead to uniform ionization of different types of molecules can be a good standard to quantify laser ionization problem. Figures 2.5 and 2.6 show that ionization of small to relatively large molecules of different ionization potential ionize in a standard way by 800 nm, 50 fs pulses of intensity 10^{15} W/cm^2. This set of wavelength, pulse width, and pulse energy has been defined as *uniform laser ionization standard* by Ledingham group [59].

2.8 Ionization of large molecules.

Hollingsworth *et al* used CuOEP figure 2.7 to obtain large parent ion peak for the study perspective of uniform molecular analysis to be attainable for sufficiently large polyatomic molecules [71]. A combination of laser parameters which lead to the uniform ionization of different types of molecules can be a good standard to quantify the laser ionization problem. Figures 2.5 and 2.6 show ionization of small to relatively large molecules of different ionization potential ionize in a standard way by 800 nm, 50 fs pulses of irradiance 10^{15} W/cm^2. This set of wavelength, pulse width, seems to hold for sufficiently large molecules with one or multiple ring structures.

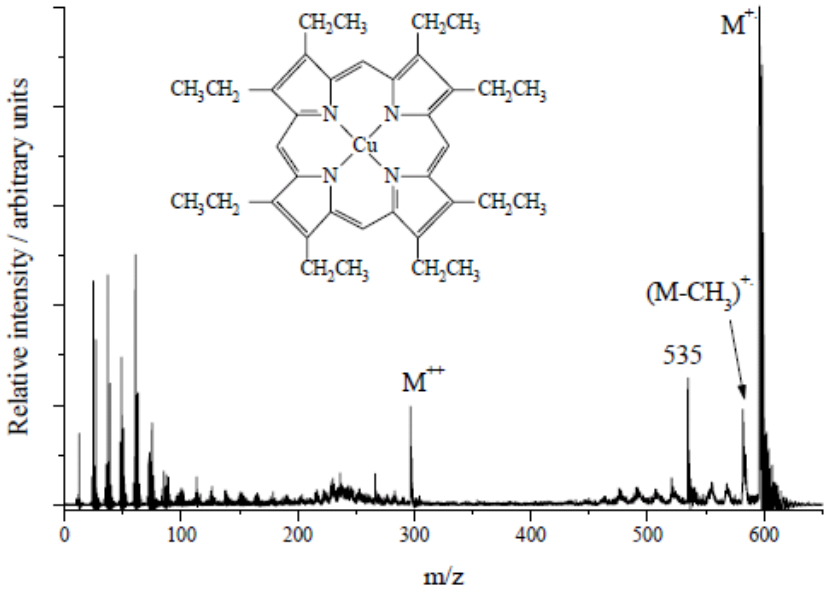

Figure 2.7: Large molecular ion peak forms for a large organic molecule of mass 600 amu. This spectrum was taken at 750 nm and pulse width of 50 fs by A. Hollingsworth *et al* [71].

A strong molecular ion peak is observed in the femtosecond photo ionization mass spectra for both nickel and copper octaethylporphyrin at this laser wavelength figure 2.7. The molecular ion signals are the base peaks in the spectra for both molecules. Fragmentation, due to successive methyl group loss, is markedly more prominent with increasing laser pulse duration, as can be seen from the picosecond mass spectrum in figure 2.8. No significant parent ion signal has been observed at 750 nm using pulses

of nanosecond duration. The femtosecond ionization mass spectra of both CuOEP and NiOEP also exhibit peaks due to the doubly charged molecular ions, present at half the mass-to-charge ratio of the corresponding singly charged molecular ion. Also present are doubly charged fragment ions.

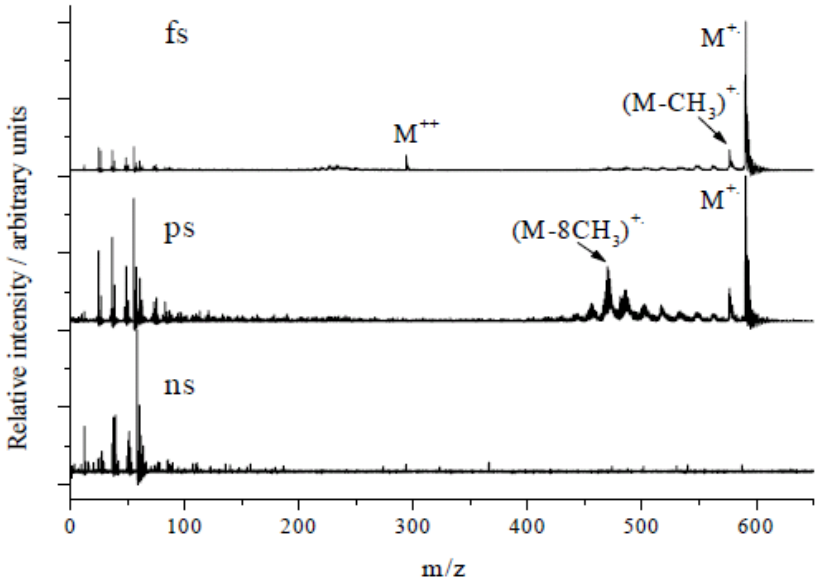

Figure 2.8: Comparison of pulse width in three regimes ns, ps, fs, is plotted on the same scale using wavelength of 750 nm, by A. Hollingsworth *et al* 1997 [71].

A comparison of three pulse widths in figure 2.8 by Hollingsworth *et al* shows that the best possible choice is femtosecond pulses. In the appropriate intensity interval of 10^{13} to 10^{15} W/cm^2, cause the least fragmentation and ladder climbing happens which is represented in the TOF spectra as a large parent ion peak and a half way doubly charged ion peak.

A somewhat different prospective than usual prospective on molecular ionization of the very large molecules has been given by Lezius *et al 1999 in* their paper *'Nonadiabatic Multielectron Dynamics in Strong Field Molecular Ionization.'* This article identifies three main contributing factors for the ionization of the large molecules; the wavelength, intensity and the molecular size. Since the paper has taken pulse width in femtosecond as given, so impact of pulse width variation has not been taken as a factor [72]. However, this article points out an important idea for the case of larger

molecules, one cannot consider usual laser field interaction as, an interaction with a single molecular valence electron only. For large molecules of the size considered in their ionization experiment like, hexatriene (0.72 nm), all trans-decatetraene (1.35 nm) and β-carotene (3.2 nm) it was considered more appropriate to view all delocalized electrons over a molecule as capable of absorbing energy from the laser field. In this view, the real mechanism which explains ionization rates for very large molecules is non-adiabatic multielectron (NME) dynamics. The experimental evidence supporting this idea is the observed spectrum, at intensity of 10^{13} W/cm^2, kinetic energy release in the fragments is beyond that expected for simple photochemical bond cleavage in polyatomic molecules.

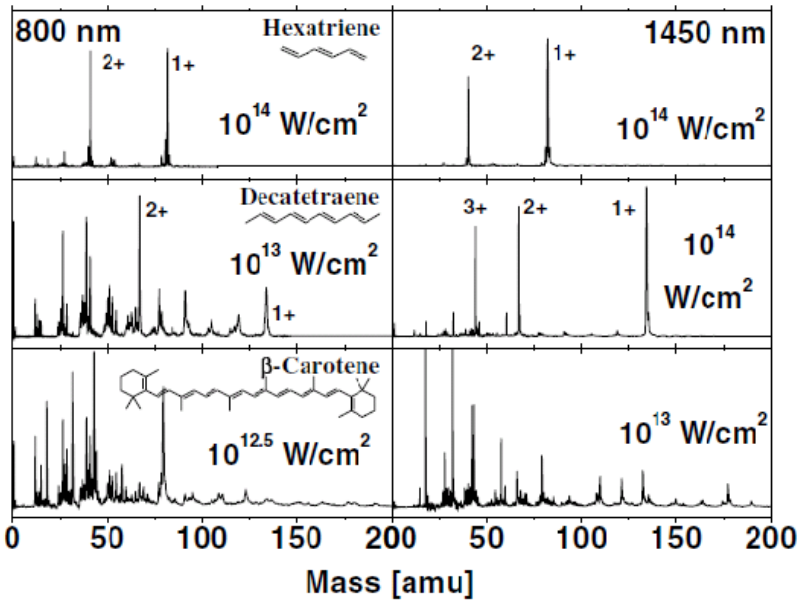

Figure 2.9: Mass spectra of hexatriene, decatetraene, and β-carotene at 40 fs. Spectra shows that 1450 nm wavelength is more suitable with respect to less dissociation Lezius *et al 1999*. [72].

Hexatriene (0.72 nm) shows little fragmentation of several charge states of the parent molecule figure 2.9, a characteristic of tunnel ionization. Longer decatetraene (1.35 nm) shows a similar result at 1450 nm but its fragmentation patterns vary with wavelength, exhibiting a transition to very extensive fragmentation by 800 nm. Much longer β-carotene (3.5 nm) shows extensive fragmentation at all wavelengths studied.

2.9 Empirical Model to Calculate Molecular Ionization Potential

This Part is adapted from an article that was published in J. Phys. B: At. Mol. Opt. Phys., 39:3769-3779, 2006, produced in collaboration with J. P. Brichta, Wing-Ki Liu, Alexandre Trottier and Joseph H. Sanderson.

This model enables one to calculate molecular first ionization potential for molecules by knowing the ground state energy of the individual constituent atoms. Molecules contain atoms at a distance $r - R_i$ where R_i is the position of ith molecules. This model considers electron distributed equally over all atoms of the molecules, one can consider this as a fractional charge distribution model, as an example for molecule ABC charge distribution will be considered 1/3 on each atom. Model works well for small molecules [27, 73, 74].

Potential of a molecule 'ABC' in external electric field is given by

$$V(\mathbf{r}) = -\left(\sum_{i=1}^{3} \frac{Q_i}{\mathbf{r}-R_i}\right) - \mathbf{E}\cdot\mathbf{r}$$

Potential for a free molecule

$$V(\mathbf{r}) = -\left(\sum_{i=1}^{3} \frac{Q_i}{\mathbf{r}-R_i}\right)$$

Energy of a molecule containing 'n' atoms is given by

$$E_n = -\frac{1}{n}\sum_{i=1}^{n}\left(I_i + \sum_{j=1, j\neq 2}^{n} Q_j\right) \tag{2.2}$$

where I_i is the ionization potential of the i-th atom. Ionization energy calculation for diatom's.

$$V_o = \frac{1}{2}\left[\sum_{i=1}^{2}\left(\frac{1}{2}I_i + \sum_{i=1}^{2}\frac{1}{2}\frac{Q_j}{R_{ij}}\right)\right] \tag{2.3}$$

Consider homonuclear diatom's of the first group of periodic table.

$$R_{21} = R_{12} \text{ and } I_1 = I_2 = I$$

$$V_o = -\tfrac{1}{2}\left(I + \tfrac{27.2}{R}\right) \quad \text{eV}$$

Molecule	V_o (Ionization potential) calculated	Accepted	% diff
Homonuclear Diatom's			
H_2	-16.39	-15.43	6.1
Li_2	-6.21	-5.112	21.5
Na_2	-5.79	-4.90	18.2
K_2	-4.76	4.062	17.2
O_2	-12.75	-12.07	5.63
N_2	-13.740	-15.58	11.81
Heteronuclear Diatom's			
CO	-12.57	-14.01	10.28
NO	-13.30	-13.78	.03
Triatomics			
CO_2	-11.54	-13.78	16.3
OCS	-12.43	-11.17	11.2

Although this establishes a good workable model to calculate ionization energy of diatomic or triatomic molecules but accuracy of calculated value does not seem to fall in some obvious trend.

2.10 Conclusion

Small inorganic molecules, where molecules are not highly polar, molecular ionization standard holds well. This standard also holds good for middle weight cyclo-organics like benzene and its derivatives, but there has not been much study on long linear chain molecules to establish large parent ion peak by Ledinghams' group or other investigators. The above considerations also shows that for higher molecular weight molecules, ionization process is more complicated and the current standard of uniform molecular ionization faces difficulty as indicated in the spectra of figure 2.9. It seems as the molecular weight and complexity increases, use of the longer wavelengths can produce lesser dissociation. One can conclude that this standard may further be enhanced by considering longer IR wavelengths at first stage (say 1000 nm with pulses as short as 10 fs with an intensity of 10^{16} W/cm^2). It would be interesting to see if the saturation point in the figure 2.4 changes and if the range of molecular uniform ionization can be extended to include a wider range of molecular species.

Chapter 3

Design of Time of Flight Mass Spectrometer

Laser-matter interaction experiments are conducted in high vacuum, this allows charged species to fly to detector freely in few microseconds after ionization in source region. Charged ions fly to detector placed at appropriate length according to square root law. This time of flight mass spectrometer(TOFMS) is based on Wiley-McLaren duel stage extraction system [75]. Duel stage extraction in linear TOFMS allows one to place detector at space focus plane, and space focus plane can be moved arbitrarily using ratios of applied voltages on source and extraction region. This allows designing TOFMS for desired resolution and dimensions. This time of flight spectrometer contains four main regions, source region, acceleration region, drift region and MCP Detector. All this is in contained stainless steel casing which can hold high vacuum up to 10^{-20} T, casing is connected with a Turbo pump and a backing pump.

3.0.1 Source Region

Laser beam is focused by a concave mirror of focal length 5 cm, located inside TOFMS. Beam focus is exactly in the center of the source region. Molecules ionize in the laser focal volume and soon after ionization electric field acts and moves ions along the axis of TOFMS towards acceleration region. However ions spend some time 't' in the source region. Assuming if only component of velocity is along TOFMS axis ions should move classically along the TOFMS axis.

3.0.2 Acceleration Region

A high negative acceleration voltage is applied in the kilo-volt range to accelerate ions to high kinetic energies, ions spend time t_2 in this region. Dimension wise this is the smallest region of the instrument but allows control of focusing by controlling the ion kinetic energy substantially by changing the applied voltage.

3.0.3 Drift Region

This region allows ions to move freely towards the detector in a straight line along the TOF axis in time t_3. This is the largest region and determines the linear dimensions of the equipment. The acceleration plate and the detector at the other end bound this region. The drift tube is made up of stainless steel of diameter 1.54 cm. Ions cross this region with velocities inversely proportional to the square root of their masses. The whole instrument (all three regions) are in a long stainless steel casing which is connected to high vacuum turbo pump to create a vacuum up to 10^{-9} Torr.

3.1 Single Stage Extraction

A single stage instrument contains a small source region and a drift region. Ions fly form the source to the detector in the simplest terms spending approximately no time in the source region $t_s = 0$. The kinetic energy gained by ions after formation is due to the applied voltage. Considering m, mass of ion, q, charge of ion, t, flight time, d, flight distance and V, the applied voltage,

$$\frac{mv^2}{2} = qV \tag{3.1}$$

The time of flight is given by,

$$t = \sqrt{\frac{m}{q}}(\frac{1}{2V})^{1/2}d \tag{3.2}$$

This implies,

$$t \propto \sqrt{\frac{m}{q}} \tag{3.3}$$

The time of flight is proportional to the square root of the ratio of the mass to charge known as square root law. $k = (\frac{1}{2V})^{1/2}d$, depends on the geometrical factors i.e. dimensions of the instrument and the applied fields. The energy gained by ions after formation is due to the applied voltage V.

The source region is much smaller than the drift region, but still finite, therefore for a more accurate estimate of time of flight for a single stage extraction system [76] one must consider time t_s spent in the source region. The time spent in the source region using equation (3.1) and $E = V/d$ and using $d = s$.

$$v = (\frac{2qEs}{m})^{1/2} \tag{3.4}$$

Rearranging and integrating over the source region depth,

$$\int_0^{t_s} dt = \left(\frac{m}{2qE}\right)^{1/2} \int_0^{s_o} s^{-1/2} ds$$

denoting the source length as s_o.

$$t_s = \sqrt{\frac{m}{q}} \left(\frac{1}{2Es_o}\right)^{+\frac{1}{2}} 2s_o, \tag{3.5}$$

Above equation (3.5) gives correct time of flight taking into account the depth of the source region. Total flight time is given by, where t_d is the time spent in the drift region and t_o is the time delay due to detector response time. considering fast detector respose $t_o \sim 0$ therefore,

$$t = t_s + t_d + t_o$$

$$t = \left(\frac{m}{2qEs_o}\right)^{1/2} (2s_o + d)$$

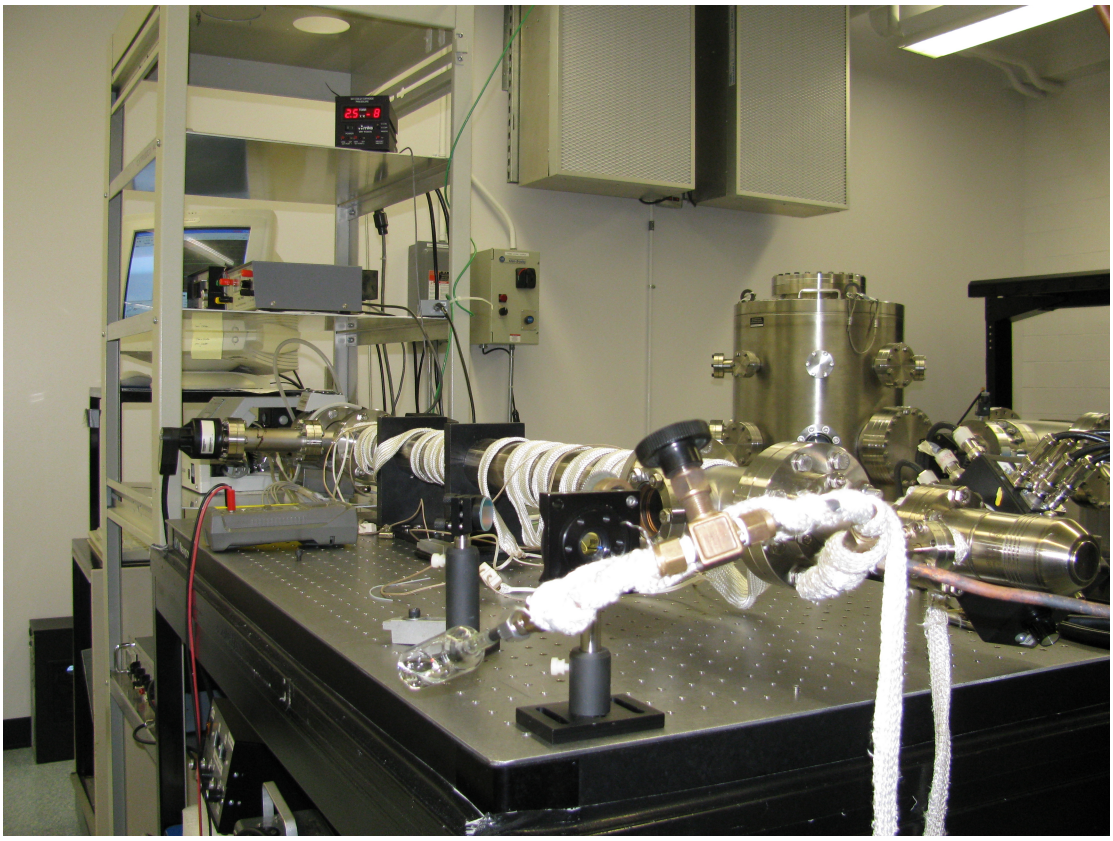

Figure 3.1: Time of Flight Mass Spectrometer at ultra-fast laboratory. This TOFMS is based on Wiely-Mclaren duel stage extraction system. TOFMS is kept at high vacuum $\sim 10^{-9}$T, working pressure is $\sim 10^{-7}$T.

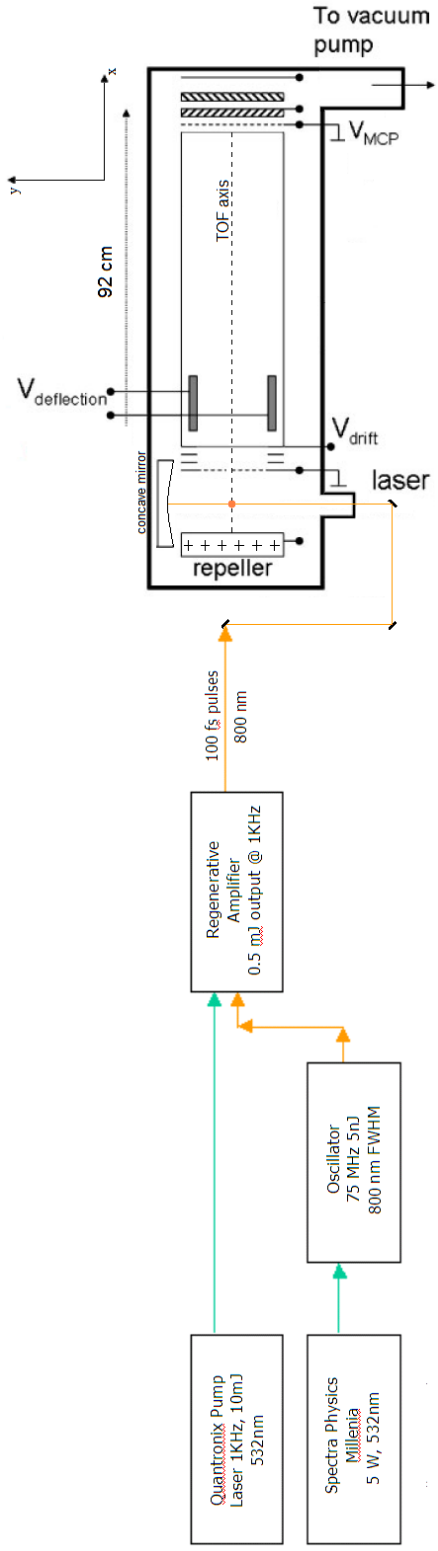

Figure 3.2: TOF-Laser system in laser laboratory.

3.2 Dual Stage Extraction and space focusing

The laser beam is focused in the center of source region, ionization occurs in a small focal volume of radius of few micrometers as in figure 3.2. The extraction field is 10^7 V/s, where 's' is the source region depth and 'V' is the applied voltage. Ions can form at slightly different locations within the source region. Considering ions formed at 's_o' at laser focus center and at slightly offset back and forward locations at $s_o - \Delta s_o$ and $s_o + \Delta s_o$. Ions produced at earlier position spend more time in source-extraction field hence gain more energy from field comparing with ions produced at s_o or $s_o + \Delta s_o$. All ions catch up with each other at distance 'd' from the laser focus is defined as the space focus plane. The location of this plane is at a point at which ions have spent an equal time in extraction and the drift region. Wiley-McLearen [76, 75] design used the acceleration region to move the space focus plane to the desired length by adjusting the source and acceleration fields as dictated by the mass resolution requirements. Mass resolution is directly proportional to flight time, and so after calculating the total flight length the space focus plane can be located at the detector. In TOF design acceleration field $E_1 \gg E_o$, the field in the source region; therefore an ion spends a very short time in the acceleration region.

Time spent in the source region, by ions formed at the focus,

$$t_o = \sqrt{\frac{m}{2qE_o}} \left(2s_o^{1/2}\right) \tag{3.6}$$

Ions formed at the TOF axis at a distance 'Δs_o' away from the focus;

$$t_1 = \sqrt{\frac{m}{2qE_o}} 2(s_o + \Delta s_o)^{1/2}$$

$$\Delta t_o = t_1 - t_o = \sqrt{\frac{m}{2qE_o}} 2 \left[(s_o + \Delta s_o)^{1/2} - s_o^{1/2}\right]$$

$$\Delta t_o \approx \left(\frac{m}{2qE_o}\right)^{1/2} \frac{\Delta s_o}{s_o^{1/2}} \tag{3.7}$$

Time taken by ion to travel through the drift region after forming at s_o,

$$t_d = \left(\frac{m}{2qE_o}\right)^{1/2} \left[\frac{1}{\left(s_o + \frac{E_1}{E_o}\right)}\right] d \tag{3.8}$$

Let

$$\sigma = s_o + \left(\frac{E_1}{E_o}\right) s_1 \tag{3.9}$$

$$\Delta t_d = \left(\frac{m}{2qE_o}\right)^{1/2} \left[\frac{1}{(\sigma + \Delta s_o)^{1/2}} - \frac{1}{\sigma^{1/2}}\right] d \tag{3.10}$$

Expanding and simplifying;

$$\Delta t_d = \left(\frac{m}{2qE_o}\right)^{1/2} (\frac{\Delta s_o}{2\sigma^{3/2}}) d \tag{3.11}$$

From equations (3.10) and (3.11)

$$\Delta t_d = \Delta t_o$$

$$d = \frac{2\left(s_o + \frac{E_1}{E_o} s_1\right)^{3/2}}{s_o^{1/2}} \tag{3.12}$$

The location of the space focus plane depends on the ratio of fields E_1/E_o and this ratio can be changed to suit the physical and the resolution requirements. Increasing the ratio (E_1/E_o) pushes the space focus plane towards the detector. To estimate the distance of the space focus plane in a duel extraction system one has to consider the total time difference Δt of an ion formed at location s_o and $s_o + \Delta s_o$, this is the sum of the time differences in all three regions.

$$\Delta t = \Delta t_o + \Delta t_1 + \Delta t_d \tag{3.13}$$

Δt_o and Δt_d are given by equations (3.7) and (3.11) respectively. Only the time spent in the acceleration region is now needed, since

$$v = \left(\frac{2qEs}{m}\right)^{1/2}$$

In the acceleration region an ion enters with velocity v_i and leaves with velocity v_f

$$v_i = \left(\frac{2q}{m}\right)^{1/2} (E_o s_o)^{1/2}$$

$$v_f = \left(\frac{2q}{m}\right)^{1/2} (E_o s_o + E_1 s_1)^{1/2}$$

$$t_1 = \left(\frac{m}{2qE_o}\right)^{1/2} \left(\frac{2s_1}{\sigma^{1/2} + s_o^{1/2}}\right) \tag{3.14}$$

where σ is defined as in equation (3.9), the difference in time spent by an ion formed at 's_o' and one formed at $s_o + \Delta s_o$ is given by

$$\Delta t_1 = 2s_1 \left(\frac{m}{2qE_o}\right)^{1/2} \left[\frac{1}{(\sigma + \Delta s_o)^{1/2} + (s_o + \Delta s_o)^{1/2}} - \frac{1}{\left(\sigma^{1/2} + s_o^{1/2}\right)}\right]$$

Expanding $(\sigma + \Delta s_o)^{1/2}$ to the first order

$$(\sigma + \Delta s_o)^{1/2} = \sigma^{1/2} \left(1 + \frac{\Delta s_o}{\sigma}\right)^{1/2} = \sigma^{1/2} \left(1 + \frac{1}{2}\frac{\Delta s_o}{\sigma} + \ldots\right) = \left(\sigma^{1/2} + \frac{1}{2}\frac{\Delta s_o}{\sigma} + \ldots\right)$$

and $\frac{1}{2\sigma^{1/2}} \ll \frac{1}{2s_o^{1/2}}$ when $E_1 \gg E_0$

$$\Delta t_1 = -\left(\frac{m}{2qE_o}\right)^{1/2} \left[\frac{\Delta s_o}{s_o^{1/2}\left(\sigma^{1/2} + s_o^{1/2}\right)}\right] s_1 \tag{3.15}$$

$$\Delta t = \left(\frac{m}{2qE_o}\right)^{1/2} \left[\frac{1}{s_o^{1/2}} - \frac{s_1}{s_o^{1/2}\left(\sigma^{1/2} + s_o^{1/2}\right)} - \frac{d}{2\sigma^{3/2}}\right] \Delta s_o$$

At space focus point $\frac{\Delta t}{\Delta s_o} = 0$

$$d = \frac{2\sigma^{3/2}}{s_o^{1/2}} \left(1 - \frac{s_1}{\left(\sigma^{1/2} + s_o^{1/2}\right)^2}\right) \tag{3.16}$$

Design of a time of flight instrument requires selecting d, s_o, s_1 and the voltages. When d is known, knowing s_o, s_1 and the desired resolution the flight tube length can be calculated. For the above equation (3.16) a MATLAB program (Appendix. A) gives different choices of designs based on mass resolution requirements figure 3.3.

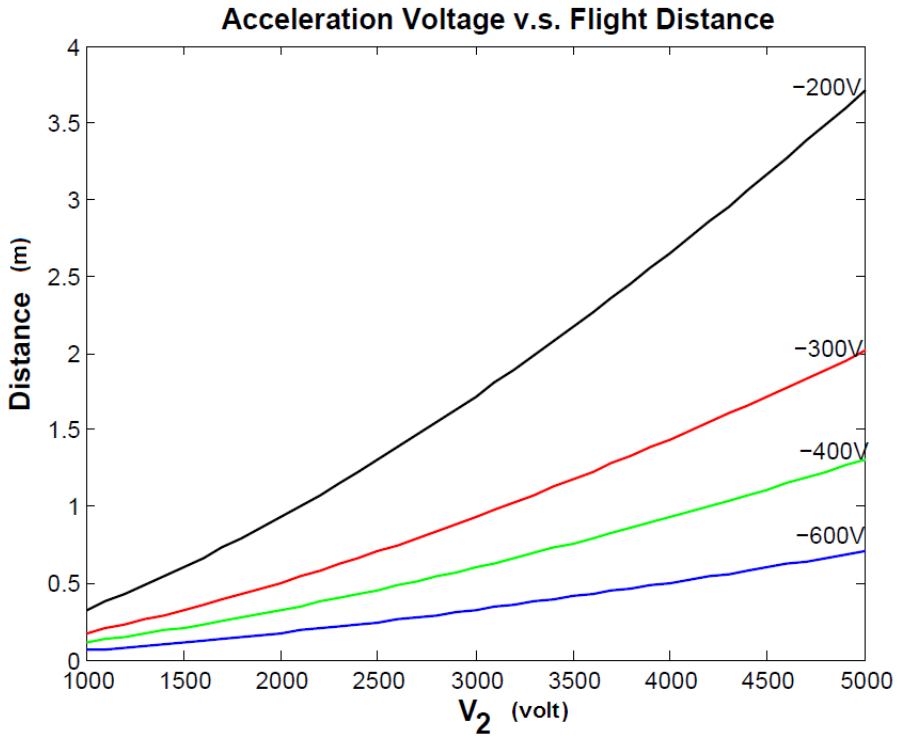

Figure 3.3: Flight distance as a function of the acceleration voltage, in this plot along a given curve voltage at the source region is constant.

3.3 Time of flight in duel Stage extraction

The time of flight includes the sum of the time $'t'$ in all three regions and can be calculated by considering a charged particle moving in an electric field. This calculation includes particles having velocity components only along the TOF axis, particles having components off axis will be lost for longer flight tubes. In the gas phase at a laboratory temperature of about 25^{o}C molecular speeds has a Maxwell-Boltzmann's distribution. For a molecule of mass m, velocity v_o, and the absolute temperature 'T'

Maxwell's distribution of molecular speeds is given by,

$$f\left(v_o\right) = 4\pi \left(\frac{m}{2kT}\right)^{3/2} v_o^2 \exp\left(\frac{-mv_o^2}{2kt}\right) \tag{3.17}$$

For a singly charged carbon ion figure 3.4, energy due to thermal motions in the gas phase at 25^{o}C is of the order of 10^{-16} J, this is much less in comparison with the energy gained by a carbon ion if accelerated at 3000 V. Moreover as Maxwell's distribution indicates if the mass of the ion increases random speeds are slower and even less effective for higher charge states. However for more precise measurements the inclusion of this initial random velocity v_o is necessary.

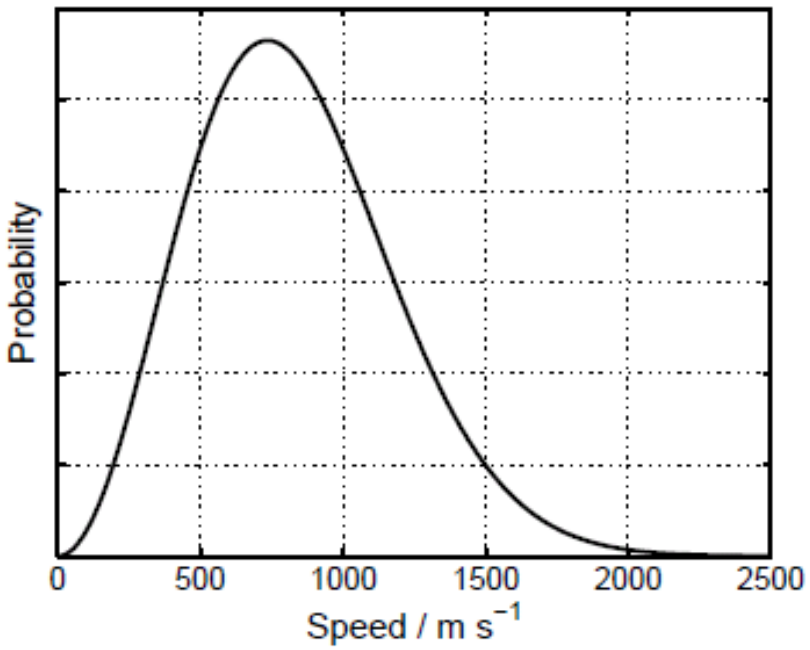

Figure 3.4: Maxwell's distribution of velocities for carbon ion at 25^{o}C. [74].

3.3.1 Initial Kinetic Energy Distributions.

Ions are generally formed with some initial kinetic energy and this initial velocity component can be in any direction. The total kinetic energy is given by,

$$K.E = eV + \frac{1}{2}mv_o^2$$

where $U_o = \frac{1}{2}mv_o^2$ is the initial kinetic energy.

The initial kinetic energy is due to the ion's initial component of velocity along the time-of- flight axis. An ion with energy $eV + U_o$ arrives at the detector sooner than one with no initial kinetic energy, resulting in tailing of the mass spectral peak toward the low-mass side. Considering the velocity component U_o along the time-of-flight axis to be directed toward the detector, it is also possible (particularly when ions are formed in the gas phase) that initial velocities for some ions will be directed away from the source exit. In the initial stages of acceleration, these ions turn around and exit the source with the same energy as those initially moving in the forward direction [76]. These ions exit the source at a later time, known as the turn-around time. Arriving at the detector somewhat later, they may contribute to a small amount of tailing on the high-mass side of the mass-spectral peak.

The turn around time contributes to a constant peak width, its effects are reduced by longer flight distances and longer flight times. The effects of initial kinetic energy spread are in general reduced by higher accelerating voltages, that is by selecting applied voltage $eV \gg U_o$.

3.3.2 Time of flight Equation for a duel stage extraction system.

A time of flight equation can be set up by simple classical charge particle moving in 'E' field , particle with mass m , charge q, depth of the source and acceleration region s_o and $s_1$while fields in the source and the acceleration regions are E_o and E_1 respectively. Ions start to move towards detector crossing source, acceleration and the drift regions in times t_1, t_2, t_3 figure 3.5,

$$s = x_o + v_o t + \frac{1}{2}at^2.$$

With $x_o = 0$ at laser focus; time of flight in first region is t_1,

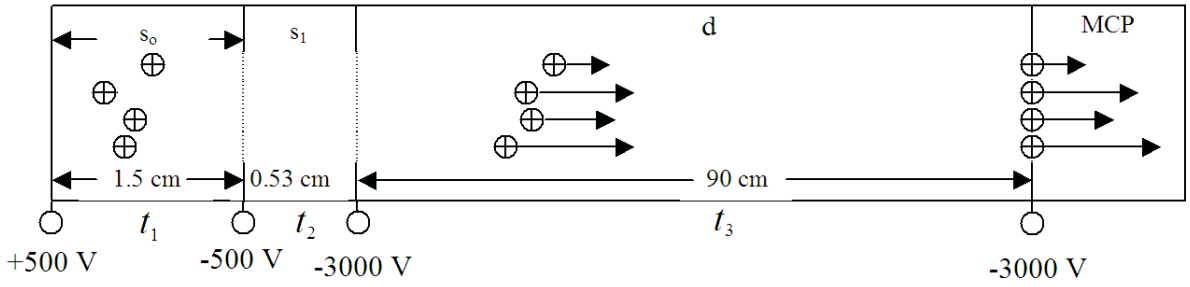

Figure 3.5: Typical internal workings:Space focusing by duel stage extraction system [75].

$$t_1 = -\frac{2}{a}v_o \pm \sqrt{\left(\frac{2}{a}v_o\right)^2 + \left(\frac{8s_o}{a}\right)},$$

substituting value of accelerating in electric field $a = \left(\frac{qE_o}{m}\right)$,

$$t_1 = \left(\frac{m}{qE_o}\right)\left(-v_o \pm \sqrt{v_o^2 + \frac{2qE_o}{m}s_o}\right),$$

and velocity of ion at the end of first region is v_1,

$$v_1 = \pm\sqrt{v_0^2 + \frac{2qE_o}{m}s_o},$$

thus velocity of an ion at the end of second region is

$$v_2 = \sqrt{v_1^2 + 2a_2s_2}$$

$$v_2 = \sqrt{v_o^2 + \left(\frac{2q}{m}\right)(E_os_o + E_1s_1)}$$

The time spent by ions in acceleration region,

$$t_2 = \frac{\left(v_o^2 \frac{m}{q} + 2\left(E_o s_o + E_1 s_1\right)\right)^{1/2} - \left(v_o^2 \frac{m}{q} + 2E_o s_o\right)^{1/2}}{E_1} \tag{3.18}$$

The time spent in crossing the drift region,

$$t_3 = \frac{d}{v_2} = \frac{d}{\sqrt{v_o^2 + \left(\frac{2q}{m}\right)\left(E_o s_o + E_1 s_1\right)}}$$

Total time of flight t is given by adding times in three regions as,

$$t = t_1 + t_2 + t_3$$

$$t = \frac{v_1 - v_o}{a_1} + \frac{v_2 - v_1}{a_2} + \frac{d}{v_3}$$

Substituting values

$$t = k\sqrt{\frac{m}{q}} \tag{3.19}$$

where

$$\begin{aligned} k = & \frac{\left(v_o^2 \frac{m}{q} + 2E_o s_o\right)^{1/2} - v_o\left(\frac{m}{q}\right)^{1/2}}{E_o} \\ & + \frac{\left(v_o^2 \frac{m}{q} + 2\left(E_o s_o + E_1 s_1\right)\right)^{1/2} - \left(v_o^2 \frac{m}{q} + 2E_o s_o\right)^{1/2}}{E_1} \\ & + d\left(\frac{q}{m}\right)^{1/2}\left(v_o^2 + \frac{2q}{m}\left(E_o s_o + E_1 s_1\right)\right)^{-1/2} \end{aligned}$$

From Equation (3.19) we note,

$$t \propto \sqrt{\frac{m}{q}}$$

The time of flight of ions is directly proportional to the square root of their charge

to mass ratio, all other parameters basically provide a multiplying factor which can change with respect to the geometrical factors of the design such as selection of the voltages and lengths of regions, source s_1, acceleration region s_2 and the drift region d. This indicates that an experimental plot of $\sqrt{\frac{m}{q}}$ and time t along the TOF axis should be a straight line, ideally points on the line representing individual ions ought to fit very closely.

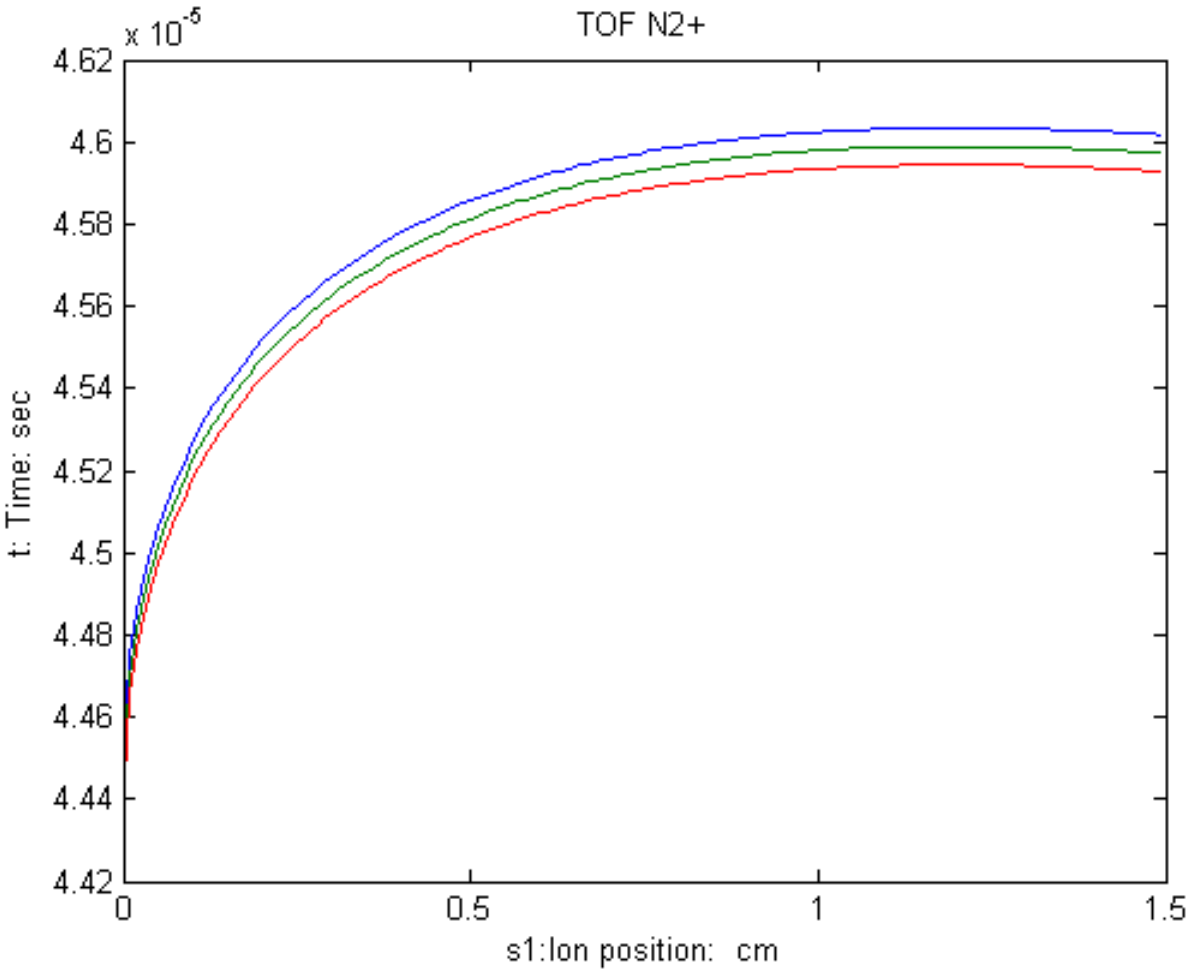

Figure 3.6: The time of flight as a function of ion position in the source region. Plot shows graph leveling off after the sharp rise show tendency expected by Wiley-MacLarens' design.

3.4 Mass Resolution

Mass resolution is defined as

$$R = \frac{m}{\Delta m} \tag{3.20}$$

For time of flight mass spectrometer in which ions accelerate to constant energy, considering

$$t = \left(\frac{m}{2qv}\right)^{\frac{1}{2}} d \tag{3.21}$$

Taking time derivative of 'm' and using equation (3.21)

$$R = \frac{m}{\Delta m} = \frac{t}{2\Delta t} \tag{3.22}$$

$\Delta t \rightarrow$ Full width at half maximum (FWHM)

Equation (3.22) implies mass resolution depends upon time resolution [76]. Therefore it must also depend on laser pulse width, detector response, recorder bandwidths, digitizing rates, as well as the initial kinetic energy distribution and ion decay due to fragmentation. A program in MATLAB generates different straight lines for the plot of resolution verses acceleration voltage (Appendix. A).

3.4.1 Fragmentation & Mass Resolution

The ionization process causes increase in internal energy of a molecule by absorbing extra photons in laser focus may result in increasing rot- vibrational energy. This increased energy manifests as vibration of different modes and molecule can go into dissociation mode depending on type of excitation. Basically fragmentation can occur any time during the flight path, longer the flight path more chances of fragmentation. Moreover longer pulses cause more fragmentation then shorter pulses. Fragmentation also depends on the type of bonds and the size of molecule. Fragmentation affects mass peaks hence affect the mass resolution.

Prompt Fragmentation occurs within the ionization zone. Flight time in this case obeys the square root law. If many parent ions fragment this way than it results in loss in parent ion concentration. Sufficiently longer pulse many cause this fragmen-

tation product but not impacting much TOF spectra . **Metastable fragmentation** occurs in the source while the ions are being accelerated by the field. This impacts most the mass resolution. Fragmentation occurring at this time produces ions that arrive the detector at times in between the molecular ion and its fragments. This causes tailing of the mass peak towards the lower mass side and also contributes to baseline noise. **Post Source fragmentation** occurs in the drift region, the fragments have the same velocities as the molecular ion, but this also causes loss in molecular ion concentration. Some loss of fragment ions occurs if fragments have velocity components at an angle to TOF axis, this can cause more loss of ions if the flight tube is longer.

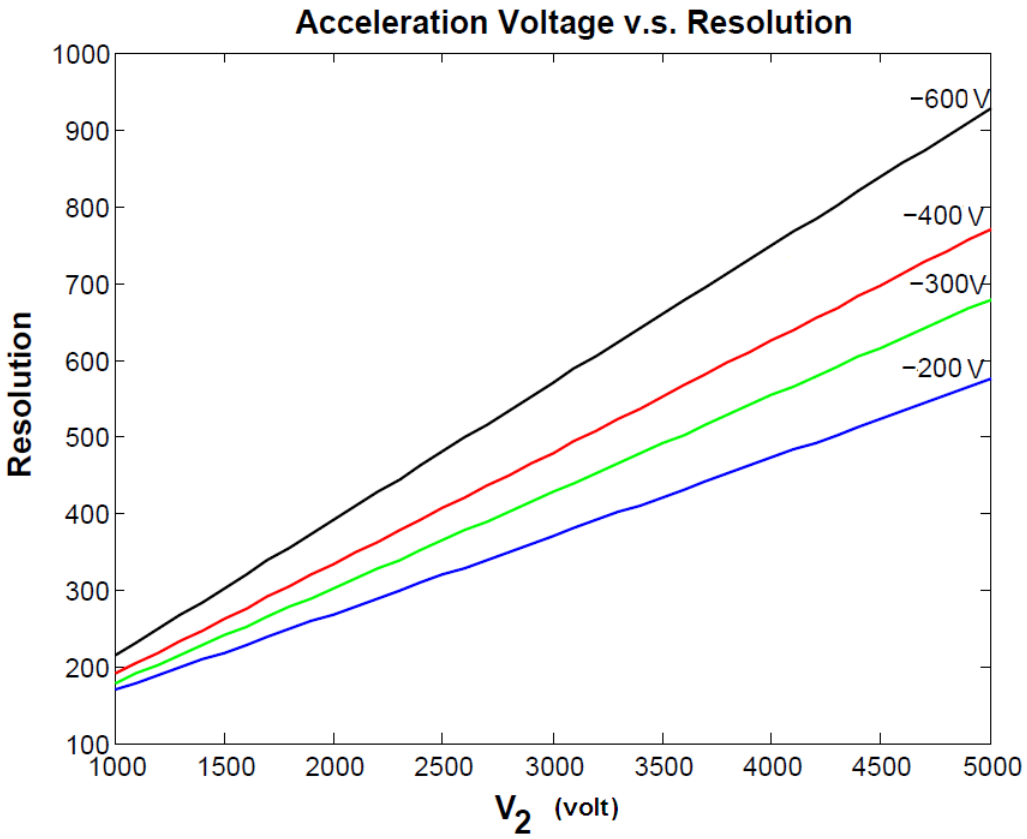

Figure 3.7: Mass resolution as a function of the acceleration voltage has been plotted for keeping voltage at the source constant. One single line represents a constant source voltage.

3.4.2 Calibration of Mass Spectrometer

Mass spectrum can be calibrated by measuring the time of flight of two known masses H^+ and another heavier mass involved in the experimentation.

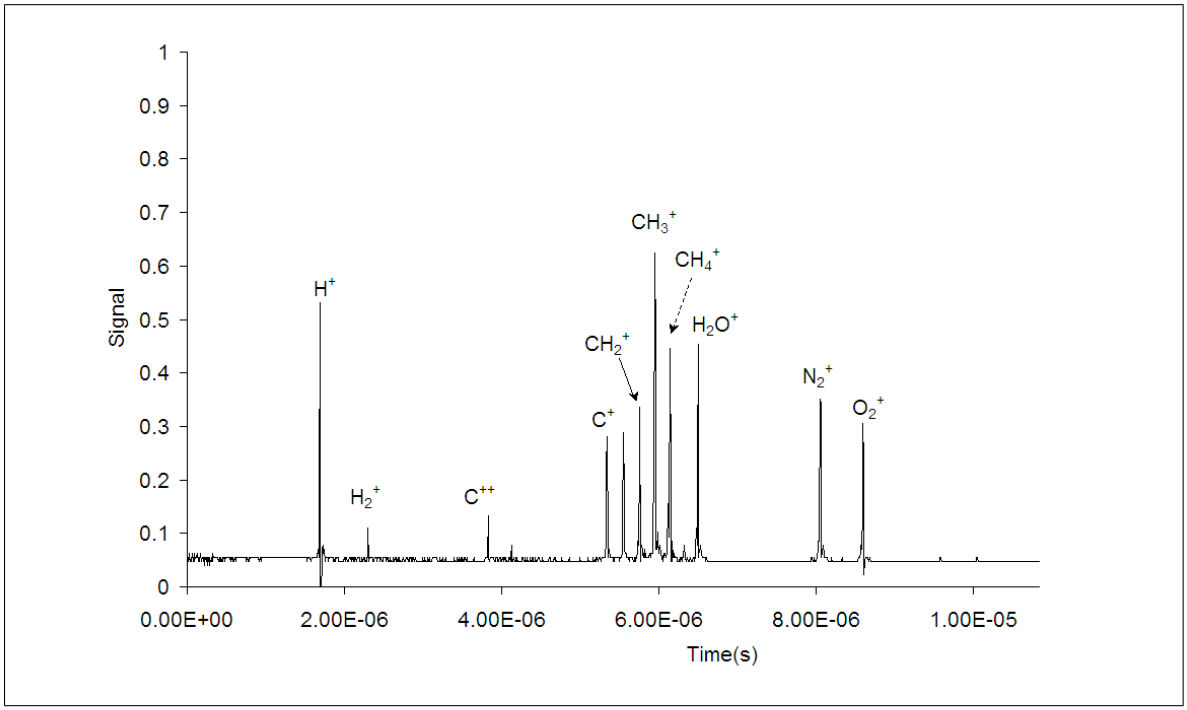

Figure 3.8: Mass spectrum of Air and Methane for calibration. All charged species in CH_4 group have peaks separated by one atomic mass unit. this spectrum is taken on conditions unusually kept for acquiring data on experimental samples in vapor phase. All molecular ion peaks are sharp and identified.

Ion identification is possible as the total time of flight is proportional to sqrt(m/q). Time of flight of the lightest and heaviest ion is plotted against sqrt(m/q). All peaks fit to this straight line exactly figure 3.9, on the line y = mx + c, where 'y' is sqrt(m/q) and 'm' is the slope of line, variable 'x' is time 't', and 'c' is the y-intercept. Once the constants are determined, the $\frac{m}{q}$ of any ion can be determined and corresponding peak position can be identified. This spectrometer is clearly distinguishing mass peaks 1 amu apart as shown by air-methane spectrum figure 3.8. To calibrate, spectrometer ions used were H_2^+, O_2^+, H_2O^+, and CH_4^+. In this case the slope is 6.3 x 10^6 and the 'y' intercept is - 0.1346.

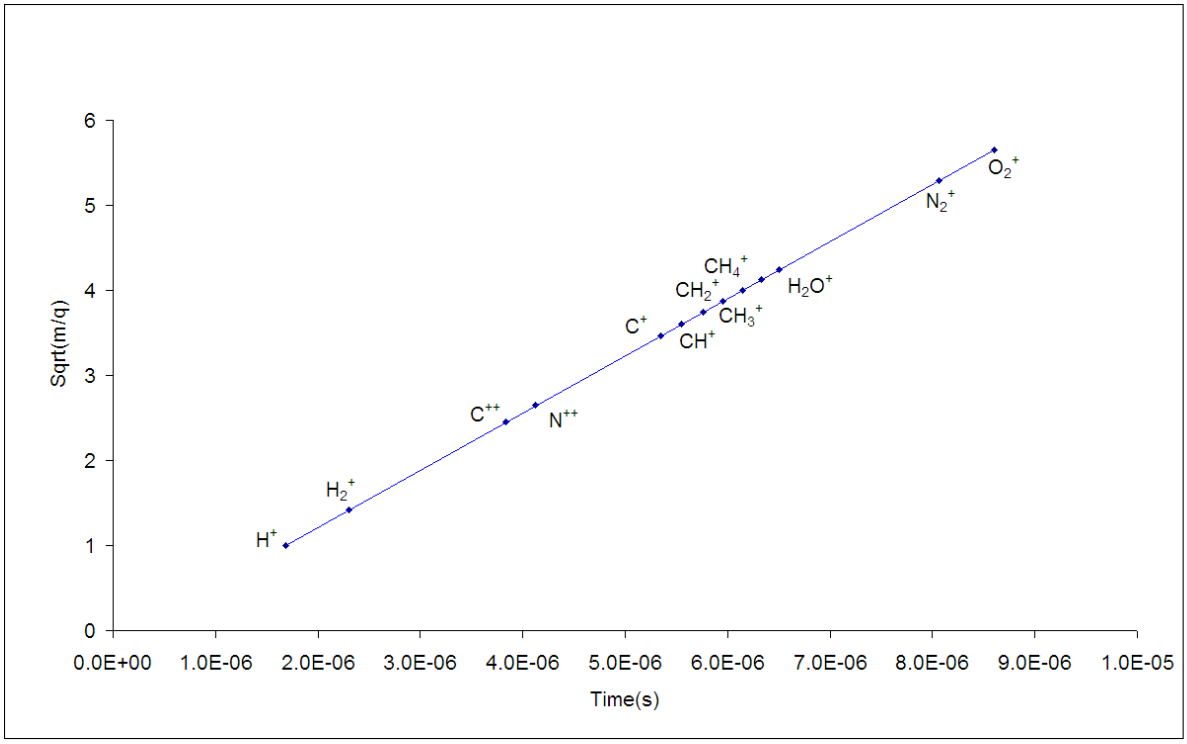

Figure 3.9: Plot of sqrt(m/q) as a function of time. This is an excellent fit to all anticipated species present in mass spectrometer for Air-CH_4 spectrum. Two molecular ions heaviest and lightest generate a line that fits all other charged species very well including C^{++}.

3.4.3 Microchannel Plate Detector

Two micro channel plates in chevron configuration, with conducting circular stainless steel shims, are placed in a ceramic container constitutes a detector figure 3.10. The front end of the detector fits on one end of the drift tube 96.6 cm away from the source region. It is tightly held by two screws on a flight tube. A voltage is applied for biasing through electrode strip so that across both channel plates the voltage is 2500 V. The biasing voltage should be applied carefully, first thousand volts application can be in steps of 200 V and waiting time between voltage increase can be one minute, after 1500 V mark voltage steps can be 100 V and waiting time of about 2 minutes is suitable for safety. The voltages applied V_1, V_2, V_3 are such that the voltage across each MCP should not exceed 1200 V. details of the electrical circuit for the detector are given in Appendix D.

A micro channel plate, 'MCP', contains an array of small glass tubes about 1 mm fused together to form a thin disc. When an ion hits at an angle on the wall of the MCP tube, it generates electrons which on colliding with the MCP tube wall again generate more electrons, causing an electron avalanche, enough for detecting single ion. Two MCP connected in chevron configuration generate a high gain of 10^6. The MCP plates were purchased from Photonis USA, part number G10-25SE/DT/6/E/A, with channel diameter 10 μm, plate thickness of 0.86 mm, disc diameter 25 mm, engineering grade, resistance $\sim$ 200 MΩ. The output of the MCP is fed in an amplifier and then in a computer containing gage scope cards to acquire data.

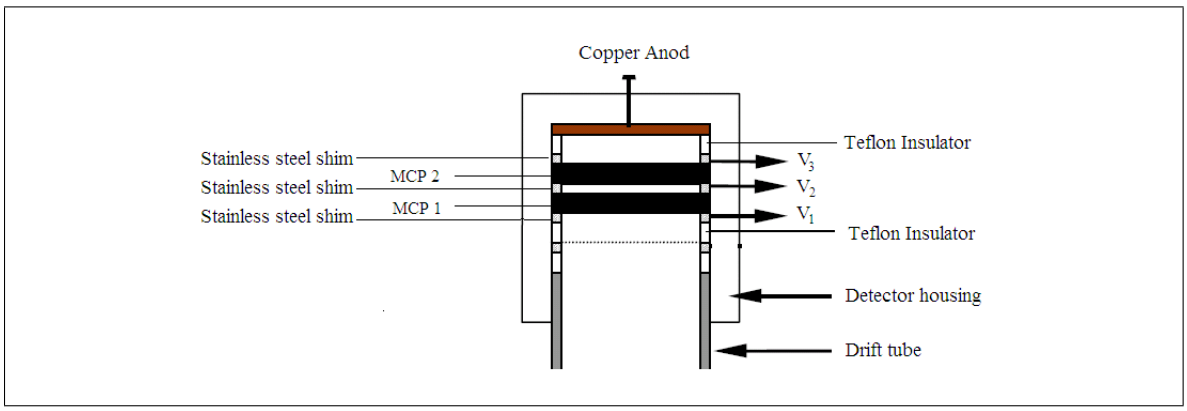

Figure 3.10: Detector mounted on the drift tube. Detector housing is made of teflon, Two MCPs' are used in chevron configuration. [21].

3.5 Mechanical Design

The source region with the acceleration region are attached to one end (the source end) on a stainless steel drift tube of dia 2.54 cm. The detector is connected on the other end of the drift tube 96.6 cm away. This inner mounted drift tube is covered by stainless steel casing 124 cm long and of outer dia 6.32 cm. The Basic design consideration was to have an instrument easy to repair whenever problem occurs, with this respect it was considered important that instrument should have opening from both source and detector ends. According to this consideration outer casing of this TOF has three sections figure 3.11. The source casing contains the source and acceleration regions and a laser inlet window, on the back side of the source region

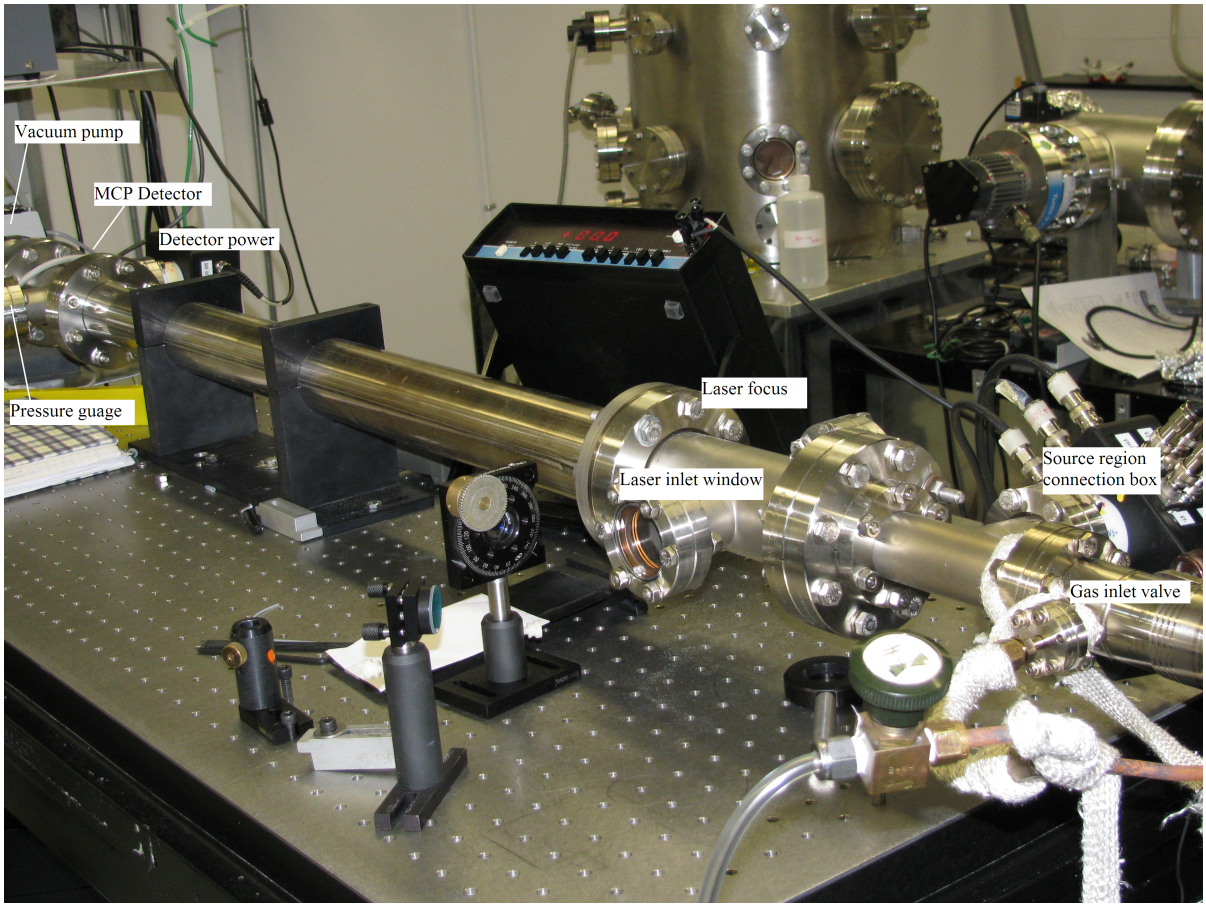

Figure 3.11: TOFMS design allows opening from two sides, the detector and the source region. Source and detector power supply are separate units.

casing a leak valve is connected by a flange. The source side casing also contains a feed through to power the source region. The source section casing is connected by a flange to the central casing 88.5 cm long basically covering the drift tube. The central section is further connected (The detector end) with the help of a flange to another third casing part containing a pressure gage attached by a flange. This outer third casing also provides cover to the detector region. On one side of detector side casing a feed through is connected by a flange for the detector electronics and the other side of this casing is connected with a pressure gage. All three outer casing parts are made up of stainless steel capable of holding a high vacuum of 10^{-20} T.

3.5.1 Vacuum system

High vacuum of 10^{-9} T is maintained at all the time and during experiment an operation vacuum of 10^{-7} to 10^{-6} Torr can be maintained by adjusting the vapor inlet valve near source region.

The inner flight tube of diameter 1", from one end near leak valve close to source region and the other end nearly a meter away detector is mounted on drift tube. All this is in a stainless steel casing of diameter as in figure 3.11. This is connected with a flange of 2.74" on both sides. This enables two flange connection to both source input side laser window end and on the other detector end, where pressure measuring cold Gage is attached. The whole system, is 1.24 m long, is to be kept in vacuum. A turbo molecular pump (Pfeiffer Vacuum, TMU07P, 50 L/s) mounted on detector end of TOF. This pump is further attached to a backing pump.

3.6 Electrical Design

In this TOFMS source electronics is near the source region, connected through a feed-through to the outside power supplies figure 3.12. A high voltage of 3000 V is supplied to the acceleration region, with a variable backing plate and middle plate voltages so that experiments can be performed with different source conditions. All voltages on any plate can be monitored any time by using an external VTVM. The source side wiring's are done with insulation coated copper wires and for extra protection wires are covered with teflon tubing given the high voltages involved.

The detector side electronics is close to the detector and can be reached by opening one flange. All the connections are on a feed through with all wiring's covered by teflon tubes. This side is connected to detector power supply maximum 3000 V to michrochannel plates in a distributed fashion. From this side one pin connection goes to pre-amplifier carrying output signals to be amplified. Various components and detailed connections of both the source and the detector side electronics are given in Appendix C and Appendix D.

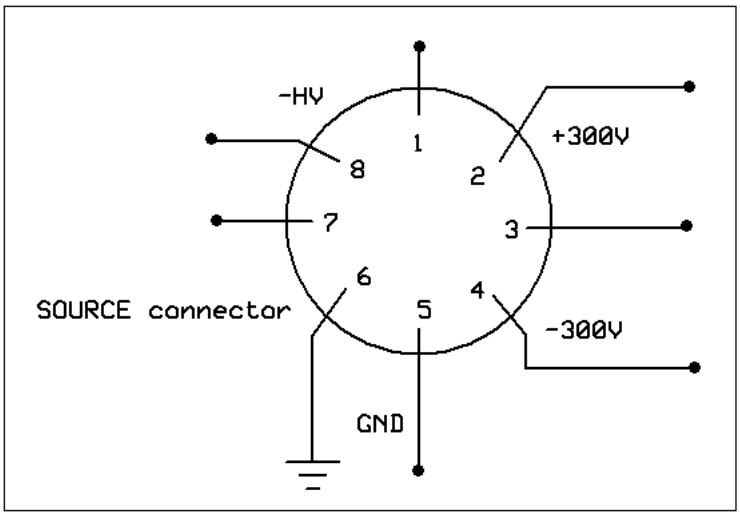

Figure 3.12: Feed-through connections for the source region.

3.6.1 Ion Deflectors

The flight path in this TOMS is about 1.0 meter. This can result in a considerable loss of ions. One inherent factor is the initial speed distribution; this lets us collect ions born only along the TOF axis. An ion deflector consisting of four plates, two plates in pair (parallel to each other) has been placed at the starting position of the drift tube. Physically opposite side plates are given voltages of opposite polarity in a controlled fashion. Each pair of plates is 4 cm long and 0.5 cm wide with rounded corners. Each plate can be given up to 300 V of either polarity to control ions. The ion deflectors are separated from flight tube by Teflon spacers to avoid any adverse electrical effects. Ion deflectors powered by a separate power supply, can float with respect to drift tube voltage.

The ion deflectors help if ions have slight deflections and deflectors improve spectra overall when proper setting is done. First a spectrum can be taken as it is and then it is improved by adjusting out laser input mirror, after proper voltage is applied to the ion deflectors at a suitable combination (can slightly vary depending on experimental conditions) gives best spectrum on computer screen. Laser beam and deflector voltages can be adjusted until desired results are achieved.

3.7 Data Recording

The output of detector is fed into pre-amplifier than amplified output of pre-amplifier is fed to computer by BNC connectors 50 Ω resistance for optimal performance. This goes to Oscilloscope cards.

3.7.1 Pre-amplifier

Signals from anode of detector are amplified by pre-amplifier made locally by electronics workshop at Physics department. This consists of two NPN (2N5179) transistors and a PNP (NTE395) transistor with suitable combination of input and out put capacitors and resistors. Current from anode of detector is fed into input, and out put is resistance matched 50 Ω is fed into computer. This in a way provides a kind of safe mode because if for some odd reason current suddenly increases in detector PNP transistor can be destroyed . Nothing happens to transistors for long time in normal operation of TOFMS.

3.7.2 Gage scope

Two Gage scope cards (Gage CS82G) perform data capture. These cards were purchased from Gage Applied Inc. Data is acquired by two cards linked in master-slave configuration for each laser shot of laser system, which has a repetition rate of 1 kHz. Gage card is triggered by Pockels cell driver. Typically sampling rate is 500 MS/s. Data is acquired for a total of 1000 laser shots or data can be acquired in co-add mode. Data is taken back for analysis by external data storage device to save space on hard disc.

3.8 Laser System

Laser system in ultafast laboratory produces stable pulses of duration 100 fs. This laser system was used for irradiation of liquids and also was coupled to TOFMS for mass spectrometry. Laser system was developed in an earlier work by Steve Walker described in detail in his thesis [77] figure 3.13. This system uses two table top pump lasers and a infrared oscillator. One pump laser of wavelength 532 nm (Green Laser),

this laser is 20 W frequency doubled Nd:YLF (Quantronix Falcon, 527 nm, 20 mJ). This laser pumps regenerative amplifier. The other laser spectra-Physics Millennia, 532 nm, and 5 W Nd:YVO pumps oscillator. The Ti:sapphire oscillator (Femtolasers Femtosource Scientific Pro) is Kerr lens mode locked, this oscillator produces 800 nm , 5 nJ pulses, with a repetition rate of 75 MHz.

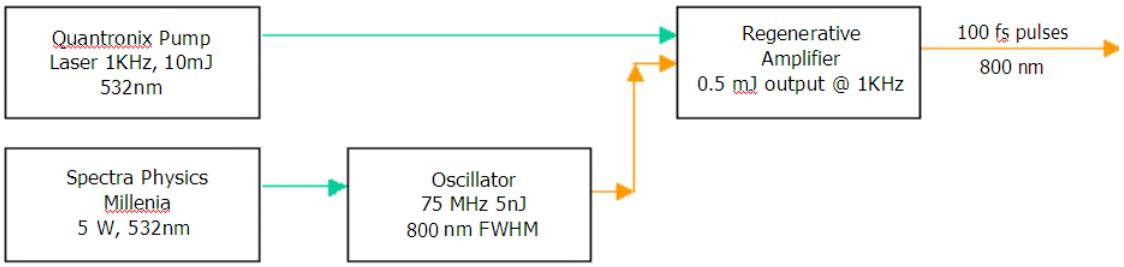

Figure 3.13: Components of laser system in ultrafast laser laboratory.

Oscillator pulses of 5 nJ were fed into regenerative amplifier which consists of a Brewster-cut Ti:sapphire crystal, two curved end mirrors, a polarizing beam splitter and a pockels cell operating as either a quarter or half wave plate. In usual operation pockels selects one seed pulse that keeps circulating through the amplifying medium (Cavity) for a set number of passes 16 in our case. When circulating seed pulse acquires about 450 μJ of energy it is switched out by the pockels cell. A double prism-pair is used to compress the amplified output and yields compressed pulses with 400 to 350 μJ of energy, a repetition rate of 1 kHz and a pulse duration of 90 to 110 fs is easily attainable and stable for a long period of time.

Chapter 4

Femtosecond laser irradiation of Acetone

Direct synthesis of polyyne molecules in acetone by dissociation using femtosecond laser irradiation

This chapter (in part) is adapted from an article that was published in C A R B ON 4 6 (2 0 0 8) 1 7 9 2 –1 8 2 8 , produced in collaboration with A. Hu, J. H. Sanderson, C. Wang, T. Zahang, Y. Zhou, W. W. Duley.

INTRODUCTION

Polyynes, linear carbon chains with alternating triple and single sp-hybridized C–C bonds terminated by atoms or groups (conventionally polyynes represent the class of molecules H(–C≡C–)$_m$H, with integer m), have attracted considerable interest in astrophysics and nanoscience [78, 79, 80]. These compounds have been detected in interstellar materials [78], and are important precursor molecular components in the formation of fullerenes and carbon nanotubes [79]. They have been investigated as prototypes of carbyne, a novel sp-bonded allotrope of carbon [79, 81]. Recently, hybrid nano-materials have been developed in which polyynes have been inserted into single wall carbon nanotubes [80] or bonded to silver nanoparticles [81]. Conventional syn-

thesis of polyynes involves reactions of acetylenic coupling [82]. However, due to the complex nature of these chemical reaction sequences, the generation of polyynes via laser ablation of suspended carbon solids [36, 37, 38, 35, 44] or by arc discharge [78] using carbon electrodes in organic solvents may constitute a more practical synthetic route. Polyynes have been generated by the laser ablation of suspended graphite [36, 37, 38, 44], C_{60} [35] and nanodiamond [44] particles in solution. In these experiments, polyyne molecules do not originate from decomposition of the solvent but by ablation of suspended particles. This is also true for the submerged arc, where the graphite electrode provides the precursor molecules required for the formation of polyynes [78]. It has also been shown that there is no direct formation of polyynes by pyrolysis at the focus of nanosecond laser pulses in hydrocarbon liquids even at pulse energies in excess of 300 mJ [36, 35]. It is expected, however, that pyrolysis would occur at the focus of femtosecond pulses because the high electric intensity generated leads to ionization and bond breaking [83][84]. It has been shown previously that fs irradiation of the surface of graphite produces liquid carbon as part of a non-equilibrium metastable high temperature phase containing polyynes [81]. This letter, reports the preparation of polyynes in solution by direct dissociation of acetone molecules with fs laser radiation followed by growth of polyynes from the dissociation products. Acetone was chosen because diamond- like carbon films have been successfully deposited using femtosecond laser ablation of frozen acetone [85]. It is found that a variety of carbon species are created by femtosecond laser ablation of hydrocarbons, however, since acetone contains a C=O bond the laser induced dissociation of this molecule is more complex than for alkane molecules [83, 84]. It is therefore of interest to elucidate the femtosecond laser induced dissociation of acetone.

Experimental system

The output beam of a regenerative amplified Ti:sapphire laser operating at 800 nm producing 90 fs pulses at a repetition frequency of 1 kHz was focused into an optical cell containing 20 ml of acetone with a 4 cm focal length lens. As the diameter at the beam focus was $\approx$ 10 mm, the resulting laser intensity was $\sim 10^{15}$ W/cm^2 at a pulse energy of 300 μJ. The molecular composition of the solution after irradiation for one

hour was obtained from surface enhanced Raman spectra (SERS) after mixing at a ratio of 5:1 with a 0.1 M solution of nanosilver particles. SERS spectra were recorded by focusing a 632 nm laser beam into the resulting solution with a × 50 objective at an excitation power of 0.3 mW.

Analysis

Figure 4.1 shows SERS spectra of irradiated and unirradiated acetone. It can be seen that four Raman bands appear in the 1800–2200 cm^{-1} range after irradiation. These features can be attributed to polyynes with different chain lengths [81, 44, 37]. An estimate of chain length can be obtained as the two primary SERS bands in polyynes have been characterized by Tabata et al. [44] using size-separated polyynes C_nH_2 in the range n = 8–16. They found that the high vibration frequency of the α mode is linearly dependent on chain length, with a lower frequency corresponding to an increase in chain length. Compagnini et al. [37] have used this correlation to show that C_6H_2 is produced as a result of the laser ablation of graphite in water. The inset to figure 4.1 shows the correlation derived by Tabata et al. [44] together with the high frequency band observed in fs-irradiated acetone. It is evident that the frequency of the present SERS mode lies on this curve indicating that the shortest chain produced after fs irradiation is also C_6H_2 . The possible presence of longer chains cannot be detected as the frequency of the β mode in SERS spectra of C_8H_2–$C_{14}H_2$ is not strongly correlated with chain length. In addition, there is considerable overlap between the β modes of short chains and the α mode of longer chains [44]. During irradiation of liquid acetone with fs pulses, bubbles were observed to evolve from the focal volume. This gas was collected and analyzed using gas-phase chromatography combined with ion trap mass spectroscopy (GC-MS). Irradiated acetone was colorless clear transparent liquid without solid suspension.

Molecular fragments due to fs irradiation were characterized by the Wiley–McLaren time-of-flight (TOF) mass spectrometer equipped with a double multichannel plate detector, which enables more than 10^7 gain. The pristine acetone was fed into the chamber through a high vacuum leak valve and the work pressure of the TOF mass spectroscopy was kept as 2×10^{-7} Torr. The laser was focused by a 5 cm focal length

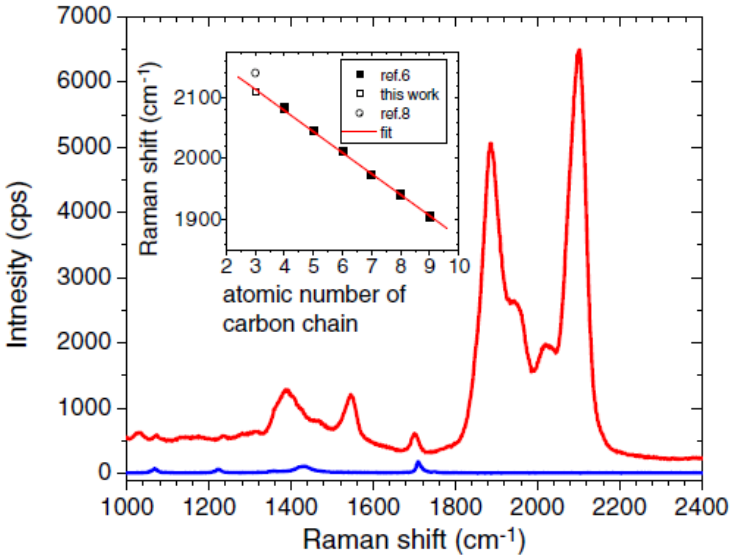

Figure 4.1: Surface enhanced Raman spectra of unirradiated acetone after irradiation with 120 fs pulses. Inset: Raman shift of the α mode of polyynes as a function of the number of carbon atoms in a polyyne chain [86].

spherical mirror. Figure 4.2 shows time-of-flight mass spectra of acetone vapor dissociated by fs pulses. The relationship between drift time and mass/charge ratio is given by t $\approx$ k $\sqrt{\frac{m}{q}}$, where k is a constant which depends on experimental configurations, t is the total drift time, m and q are the ion mass and charge. This relation is derived on the basis of the assumption that the initial ion velocity corresponds to that at 300 K (corresponding kinetic energy of 0.25 eV); and all ions experience the same extraction and acceleration voltages. All charged species in the TOF spectrum can be identified on the assumption that the first peak at 0.542 μs is that of H^+ while the last strong peak at 2.81 μs corresponds to singly-charged acetone. From fast species to low ones the analysis shows that these ions are H^+, H_2^+, C^{++}, C^+, CH_3^+, O^+, C_2^+, CO^+, O_2^+ , CH_3CO^+ and $(CH_3)_2CO^+$.

The inset to figure 4.2 shows all TOF peaks plotted vs. the root of m/q. The perfect linear correlation confirms that individual species have been correctly identified. It is apparent that carbon radicals and radical ions like C_2^+ , C^+ and C^{++}, are created in the dissociation of acetone molecules. These species are likely the primary building blocks in the growth of polyyne molecules. The growth of polyynes proceeds by the

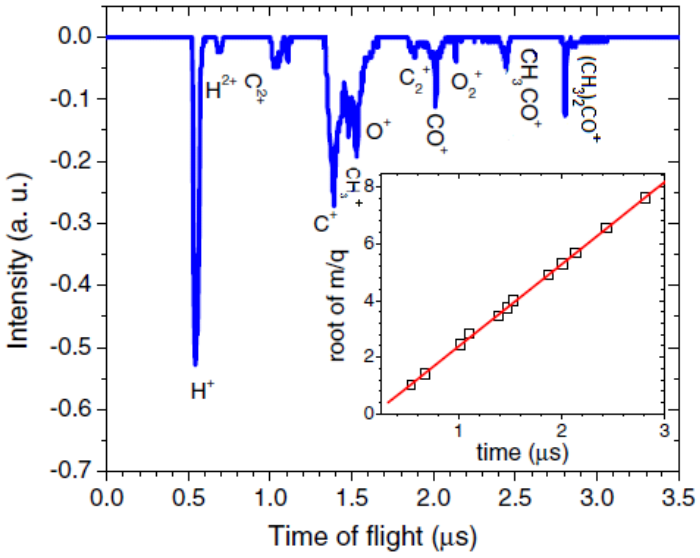

Figure 4.2: Time-of-flight mass spectra of molecular acetone after irradiation with 120 fs pulses from a 800 nm laser at a pulse energy of 300 μJ. Inset: drift time of identified atomic and molecular species plotted vs. mass/charge ratio.

addition of C, C_2 and H to acetylenic groups [36]. Hydrogen atoms required in the terminal or capping bonds can be extracted from the solvent. While C atoms require the breaking of all C–C and CH bonds the formation of polyyne molecules cannot proceed in the absence of this species. Previous experimental and theoretical work has shown that the dissociation of acetone with fs pulses is a stepwise procedure that occurs sequentially in increasing energy as C–C, C=O, C–H bonds are each dissociated [83, 84]. At intensities $< 10^{14}$ W/cm^2, the C–H bond does not break so that C atoms are not available for the growth of polyyne molecules. This result is consistent with the effects observed after irradiation with ns laser pulses where the intensity is in 10^8– 10^{12} W/cm^2 range [79]. In the present experiment, the laser intensity at the focus of the spherical mirror is 10^{15} W/cm^2, which is close to the threshold value for the production of a Coulomb explosion. At this intensity, all bonds in acetone can be easily broken resulting in the generation of C and C^+. The presence of the C^{++} ion may indicate that dissociation occurs via Coulomb explosion. A similar picture can also explain the femtosecond laser ablation of acetone solid, where the presence of C^+, C^{++} and C_2 are evident from emission spectra [85]. However, it is necessary to point out that the

use of acetone is not critical to the production of polyynes via fs laser irradiation of hydrocarbons. It is worth noting that polyynes are not stable at high temperature [86]. At temperatures in the range between 50 °C and 100 °C, polyynes form graphene-like species by cross-linking. This process cannot however occur during fs irradiation as the timescale for thermal heating is much longer than that of the pulse width. This is a manifestation of the highly non-equilibrium nature of fs laser processing and indicates that the local thermal effect (occurring over a nanoscale dimension) by fs irradiation can enhance the stability of the resulting polyyne composition [81].

Conclusion

In summary, polyynes have been successfully synthesized in a single-step process involving the dissociation of acetone molecules in a liquid. Time-of-flight mass spectroscopy confirms that the dissociation of acetone generates simple carbon species such as C^+ and C^+_2 ions and these ions act as the molecular building blocks of polyynes.

Chapter 5

Femtosecond laser irradiation of Alkanes

5.1 OVERVIEW

Polyynes were formed successfully first time by irradiating solid acetone by femtosecond laser [85]. In my experimentation with acetone described in chapter 4, irradiation of acetone was done at STP to see if polyynes form directly by irradiating liquid acetone. After seeing positive results on polyyne formation by liquid acetone irradiation, natural extension was to see if polyyne formation takes place using alkanes, because alkanes contain only C-H bonds and no double bond with oxygen is present.

Alkanes are single bonded linear chain hydrocarbons. Methane CH_4 is the smallest independent molecular unit in alkane group . At STP methane is a gas. In this class of linear chain organics first liquid is pantane C_5H_{12}. Generally the ionization potential of the group decreases as the carbon chain length increases implying that fewer number of photons are needed to ionize longer chain hydrocarbons. As chain length increases vibrational modes of the molecule increase as well therefore incident energy may be shared among different vibrating modes of the long chain molecules [87]. In the time of flight mass spectral study of alkanes, irradiation spectra of methane, butane and hexane has been studied to see ionization pattern in our laser conditions and the workings of TOFMS. Ionization potential of alkanes can be calculated by the formula (2.2) and the type of ionization process (MPI, TI or OBTI) can be predicted by

estimating keldysh parameter.

$$\gamma = \left(\frac{V_o}{1.87 \times 10^{-19} I \lambda^2} \right)^{1/2} \tag{5.1}$$

where 'I' is the intensity in W/cm^2; λ is the wavelength in 'nm' and V_o is the first ionization potential of the alkane molecule in electron volts [20].

5.2 TOF spectra of methane CH_4 and Butane C_4H_{10}.

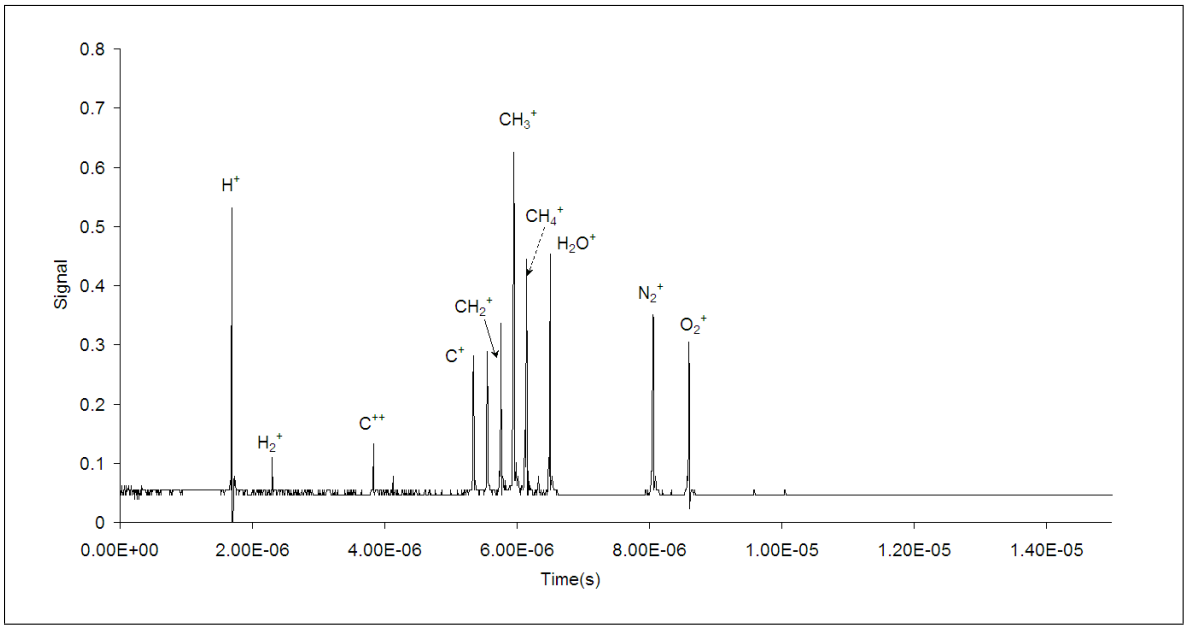

Figure 5.1: Methane spectrum at 800 nm, 300 μ J at intensity of $\sim 10^{15}$ W/cm^2.

Spectrum of methane contains parent ion peak CH_4^+, and all other associated peaks CH_3^+, CH_2^+, $CH^+$and C^+. This single carbon atom group is termed as C_1 group. As carbon chain increases in length, other C_2, C_3 and higher carbon groups will occur in the TOF spectrum at longer flight times. Looking at TOF spectrum of methane CH_4 figure 5.1 and butane C_4H_{10} figure 5.2, carbon groups appear from C_1 group for methane and C_1 to C_4 groups in butane spectrum. As length of carbon chain increases dissociation increases. Polyynes formed in the butane irradiation C_4H_2, C_2H_2 and C_2

due to breaking of C-H bonds in the laser focus fit well with other charged species on straight line plot of sqrt(m/q) as a function of time.

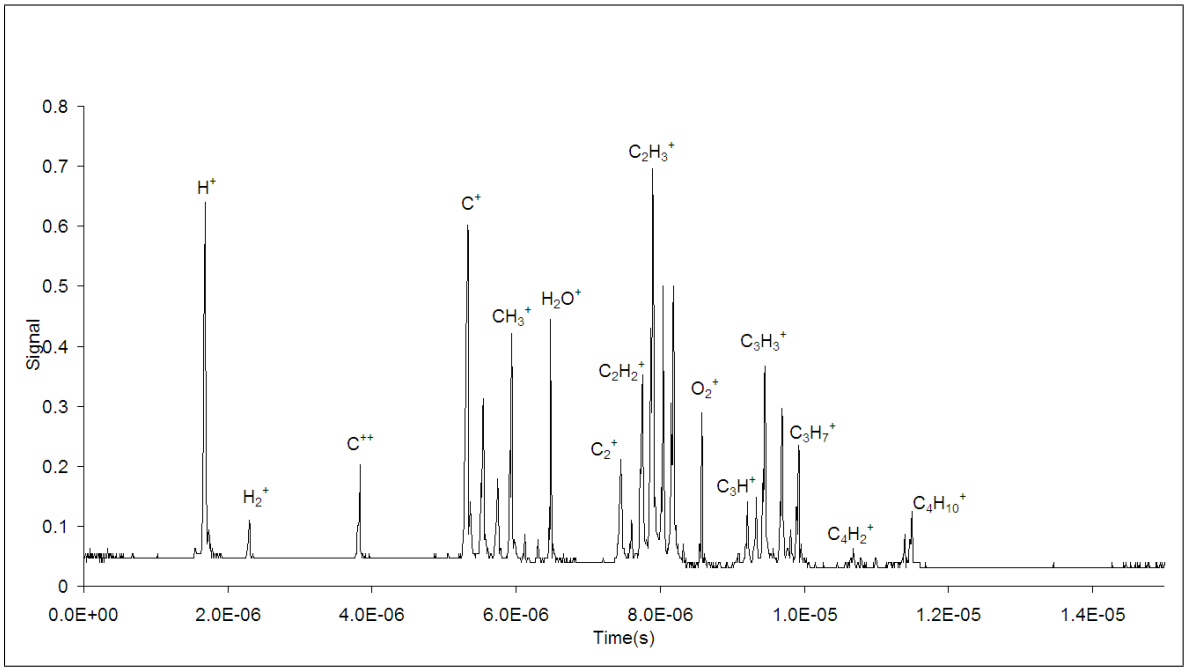

Figure 5.2: Butane mass spectrum at 800 nm, 300 μ J at the intensity of $\sim 10^{15}$ W/cm^2.

5.3 Irradiation of Hexane C_6H_{14}.

Hexane irradiation was carried out to study irradiated hexane spectrum and to compare it with the pure hexane spectrum at intensity 10^{15} W/cm^2 using the pulse width of 100 fs. One aspect of study was also to study polyyne formation by irradiation of pure hexane liquid. To irradiate pure hexane liquid laser was focused by a 4 cm focal length lens and the laser intensity measured just before entering liquid was $\sim 10^{15}$ W/cm^2. Laser intensity during irradiation was capped $\sim 10^{13}$ W/cm^2 in liquid due to filamentation [88] . This results in enlarged focal volume of lower intensity as compared with intensity in the gas phase. At this intensity and wavelength of 800 nm process governing ionization is MPI. Considering IP of hexane is 11.2 eV, equation (5.1) gives $\gamma \gg 1$ which is in MPI regime.

5.4 TOF Specra of pure and irradiated hexane.

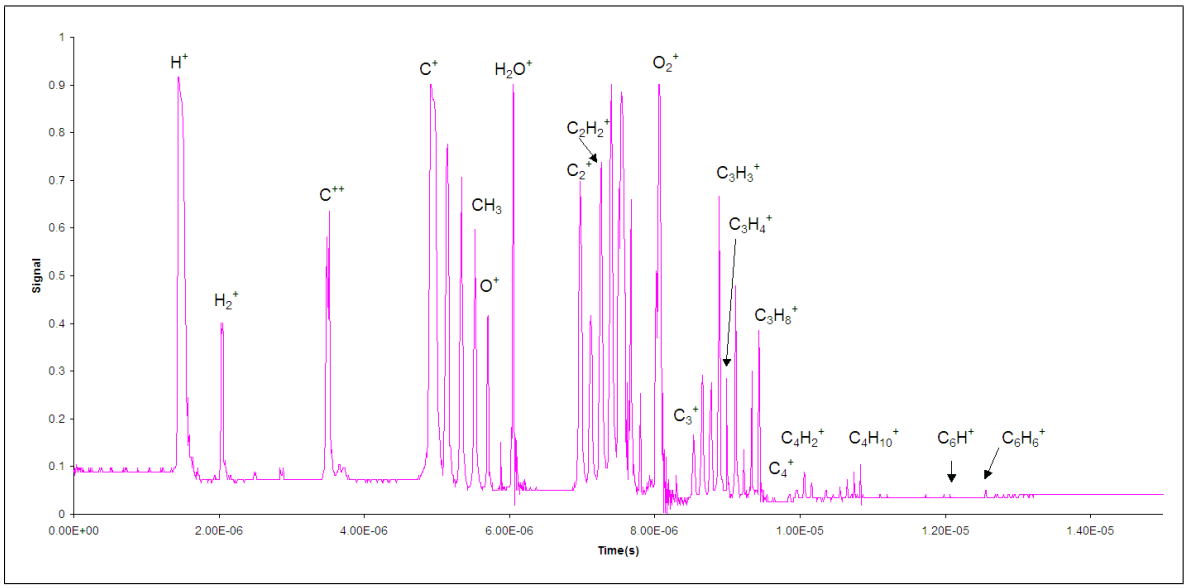

Figure 5.3: Mass spectrum of pure hexane leaked into TOF, mass spectrum shows carbon peaks from C_1 to C_6

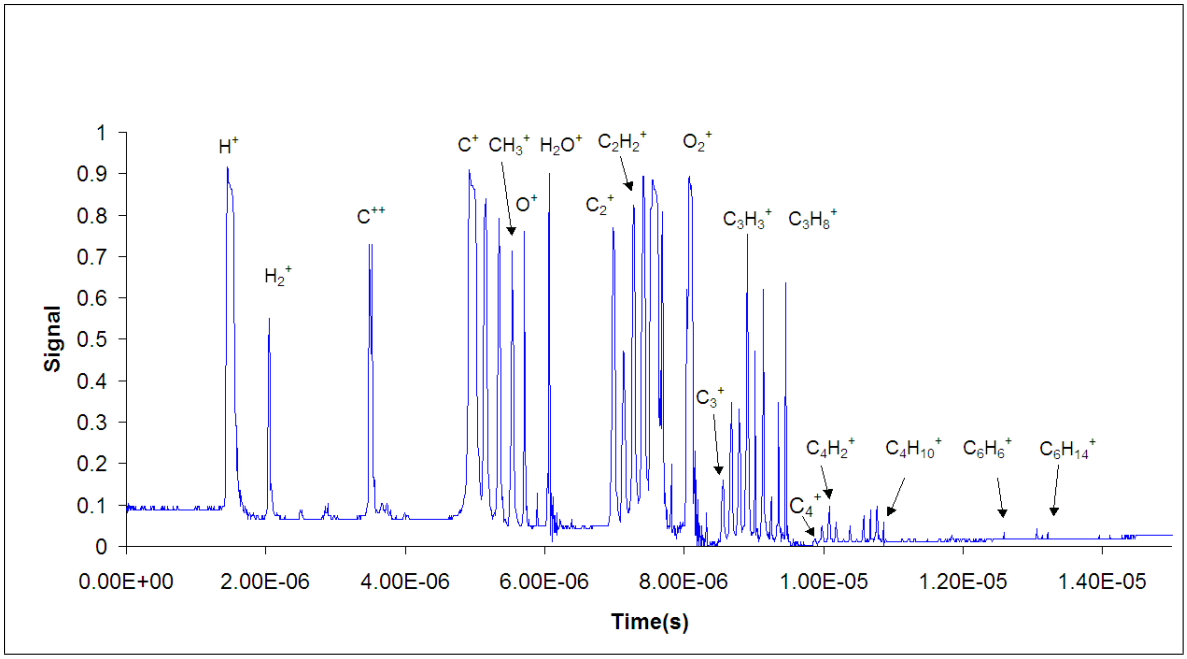

Figure 5.4: Mass spectrum of irradiated hexane leaked into TOF, mass spectrum shows carbon peaks from C_1 to C_6.

Polyynes and cumulenes detected in TOF spectrum

Species	Mass	Time (μs)
C_4 H_2^+	50	11.10
C_4^+	48	9.92
$C_2H_2^+$	26	7.28
C_2^+	24	6.98
$C_3H_4^+$	39	9.02
C_3^+	36	8.56

Table 5.1: Formation of Polyynes observed in TOFMS. Table indicates polyyne peaks (n $<$ 10) observed in TOF spectra of irradiated octane. Species containing double bond like C_3^+ (cumulene) are also present in TOF spectrum.

Mass spectral peaks of most dissociation species were found in the TOF spectrum of pure hexane figure 5.3, and irradiated hexane figure 5.4, as the groups of carbon chains C_1 to C_6. Polyyne formation detected in irradiated hexane leaked in the TOF is summarized in table (5.1), together with other double bonded species found in the

TOF spectrum. It can be seen from table (5.1) that all the polyynes detected in irradiated hexane spectrum the gas phase detection shows molecular mass lower than hexane. Higher polyynes were not detectable in our TOFMS because of the pulse duration of 100 fs. The pulse width is double of the required pulse width of 50 fs, ionization standard set by Glasgow group [70]. TOF spectra in our case causes much more dissociation; therefore longer chain polyynes are not detectable in our TOFMS.

Table (5.1) shows that cumulenes were also detected in TOFMS spectrum. Cumulenes are doubly bonded carbon chains, longer cumulenes are difficult to detect in our system because of ladder switching mechanism due to longer pulse duration in our experiment. A plot of $\sqrt{\frac{m}{q}}$ as a function of ion flight time figure 5.5 plotted for irradiated hexane indicates cumulene fit very well as polyynes detected in TOF spectrum.

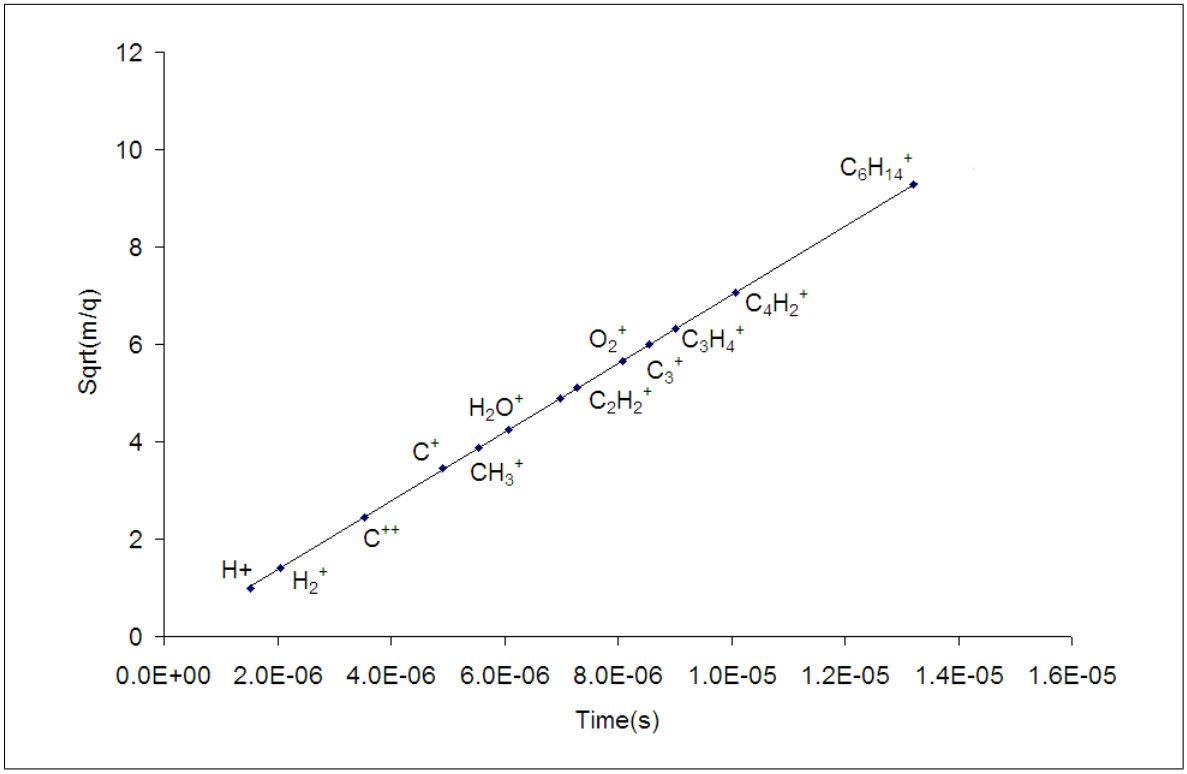

Figure 5.5: A plot of $\sqrt{\frac{m}{q}}$ as a function of ion flight time for irradiated hexane, both polyynes and cumulenes fit very well on a straight line.

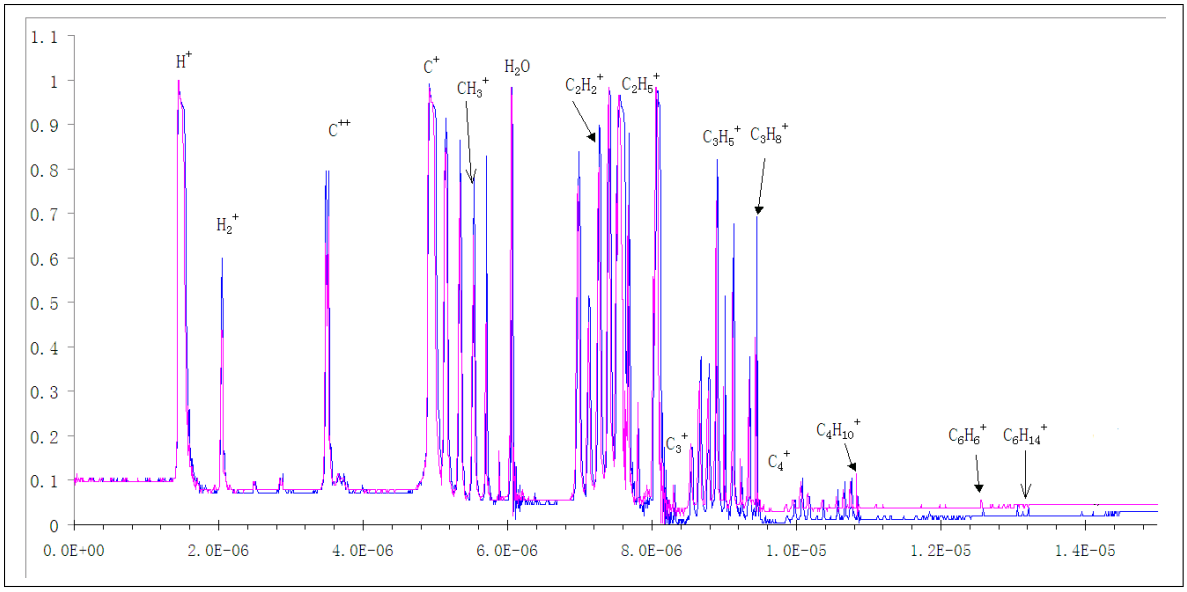

Figure 5.6: Normalized (w.r.t. H^+ ion) comparison spectra of pure and irradiated hexane. Blue is irradiated hexane it shows different features at higher mass side of spectrum.

Normalized TOF spectra (with respect to H^+ ion peak) of pure and irradiated hexane is shown in figure 5.6. Part of spectrum contains three carbon groups C_1 C_2 & C_3) figure 5.7. In general Irradiated hexane peaks are taller than pure hexane spectral peaks. Carbon groups C_1 and C_2 are more important dissociation products in liquid phase for higher polyyne formation because of their higher mobility and as a consequence ability to interact chemically. Charged C_1 and C_2 ions can attack higher electronic charge density regions in nearby molecules and can cause chemical change.

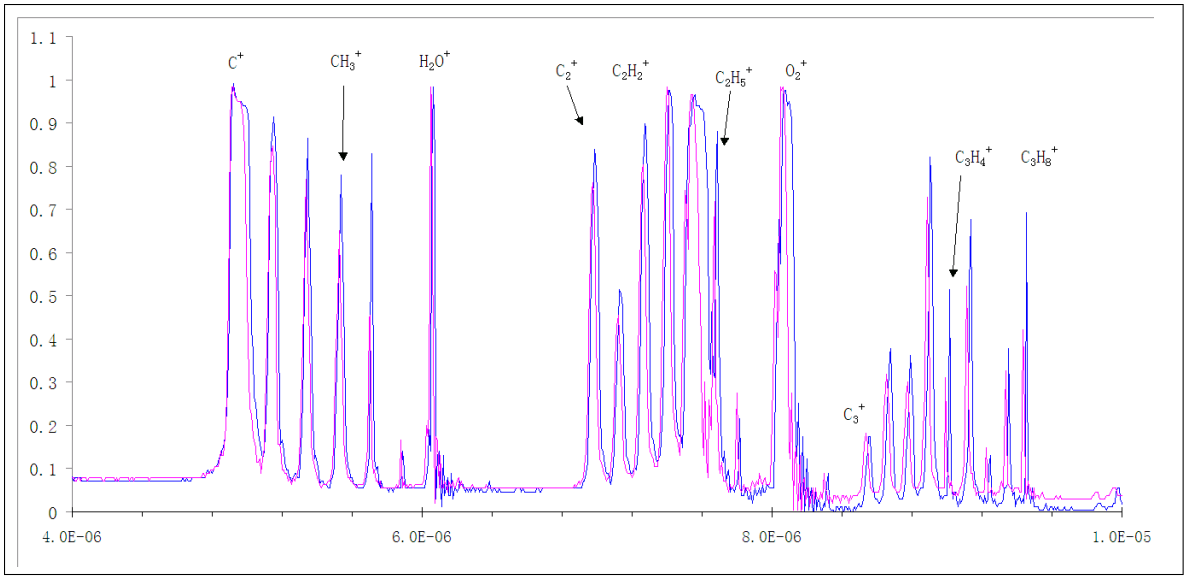

Figure 5.7: Normalized comparison spectrum of first three groups of pure and irradiated hexane.

A comparison of two normalized spectra plotted indicates irradiated hexane contains usually higher peaks of corresponding ions. This could be because the irradiated liquid contains more species than pure hexane such as linear chain single bonded, double bonded carbon chains (cumulenes) and polyynes. When these (irradiated hexane) are exposed to laser field in the gas phase, these species again go through ionization and dissociation process. Irradiated and non-irradiated hexane both contain polyynes of lower order than original molecular ion. Same is true for double bonded chains of carbon atoms cumulenes.

Considering three important carbon groups and comparing two spectra of pure and irradiated hexane yields some information about the irradiated liquid. Molecular ion peaks formed in irradiation process are sharp peaks like C_3H_8 and C_3H_4 figure 5.7. The first two carbon groups C_1 and C_2 are more important because ions of these groups are small and can move out of the laser focus in the surrounding liquid where these ions can cause addition reactions with other double or triple bonded carbon chains also produced by irradiation. The important ions for propagating addition reactions are C^+, CH^+, CH_2^+, CH_3^+, C_2^+, $C_2H^+$and C_3^+. Longer the carbon chain gets, it becomes less likely to be an initiator of addition reaction, instead it will be attacked by smaller ions.

Recently Sato *et al* 2010 published their work on hexane [42]. In their work they irradiated hexane liquid by 100 fs laser with repetition rate of 1 KHz and laser pulses of maximum energy 0.9 mJ/pulse. They indicate that polyyne formation is in very small quantity, they used high performance liquid chromatography (HPLC) to detect polyyne chains ranging from C_6H_2 to $C_{12}H_2$. In their work they also verified polyyne formation by resonance Raman spectroscopy by using nanosecond 227.0 nm laser pulses, tuned for the absorption band of C_8H_2. In my experimentation on hexane with 100 fs 800 nm pulses same range of polyyne formation has been detected by SERS experiment figure 5.8. Their conclusion that polyyne formation is unlikely to occur just by elimination of hydrogen directly, supports my view that polyyne formation occurs due to addition reactions just outside laser focus due to close proximity of reactants in liquid phase.

5.5 Surface enhanced Raman (SERS)

Comparison of SERS spectra of both pure and irradiated hexane shows in convincing manner that polyynes indeed form in irradiated hexane figure 5.8. Polyyne peaks exist in a range (1800-2200) cm^{-1} characterized by Tabata *et al* [44]. This polyyne formation is consistent in comparison with polyyne formation in acetone [40] and octane [41]. Therefore it is compelling to conclude that the addition of the carbon ions in double bonded carbon chains cause the lengthening of the carbon chain. This also causes elimination of attached hydrogen to form a polyyne molecule. Of course it will be very interesting to see if length of polyyne molecules can be controlled and instead of forming a mixture of polyynes, we could obtain selected polyynes by controlling the irradiation parameters in some way.

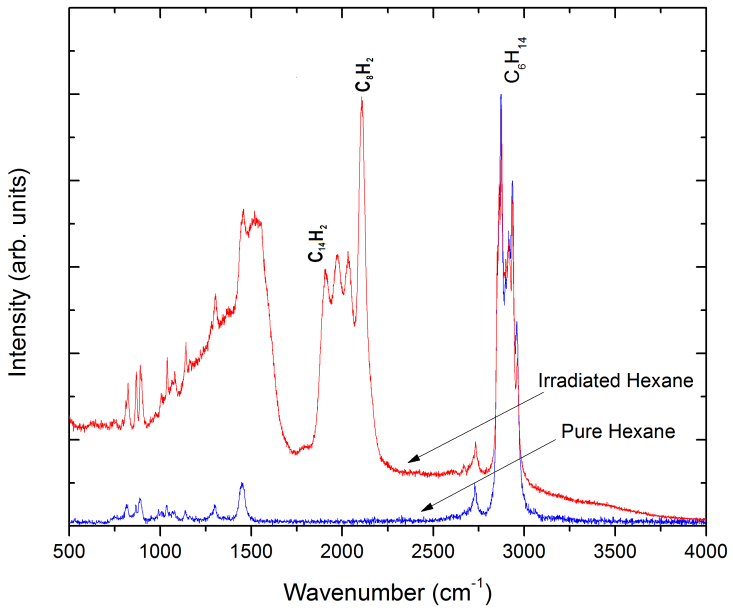

Figure 5.8: SERS spectra showing polyyne formation by 100 fs 800 nm laser irradiation of hexane. Polyyne band exists between 1800 to 2200 cm^{-1}.

Chapter 6

Time of flight mass spectrometry of polyyne formation in the irradiation of liquid alkanes with femtosecond laser pulses.

This chapter is adapted from an article that was published in C A R B ON 48 (2 0 1 0) 2517 – 2520, produced in collaboration with A. Hu, M. J. Wesolowski, X. Fu, J. H. Sanderson, Y. Zhou, W. W. Duley.

6.1 Introduction.

Recently polyynes, which are linear chain carbon molecules containing alternating single and triple bonds and capped at each end by one hydrogen atom, have been the subject of several studies. This is because of their importance as precursors in the formation of nano-structures [79] including nano-wires with controllable conductivity [89], and it is therefore of great interest to investigate novel methods for the tailored formation of these compounds. Studies have concentrated on production mechanisms such as nanosecond laser ablation of suspended graphite particles in water [36, 37], and in the laser ablation of graphite [81]. Very recently a method has been discovered for producing polyynes from pure liquid solvents acetone [40] and hexane [42] simply by

femtosecond laser irradiation. Here we study liquid octane as a source of polyyne chain production, after irradiation by femtosecond laser pulses. We investigate the length of the polyynes produced using Surface Enhanced Raman Spectroscopy (SERS) and we identify the precursor species using Time of Flight (TOF) mass spectrometry which allows us to comment on the mechanism for polyyne formation.

6.2 Experimental System Liquid irradiation.

Octane (99% purity) was irradiated by 800 nm 100 fs pulses of 300 µJ from a regeneratively amplified Ti: Sapphire tabletop laser with a repetition rate of 1 kHz. Octane was placed in a 20 ml rectangular quartz container and irradiated for two hours. The incident laser beam was focused with a 4 cm focal length lens to produce a visible white filament within the liquid; of a few millimeters in length. This has the effect of increasing the interaction volume by three orders of magnitude while capping the intensity at around $4x10^{13}$ W/cm^2 [88]. After irradiation, the liquid remained transparent with no evidence of suspended particles.

6.3 SERS of pure and irradiated octane.

In order to study the composition of the irradiated liquid we use the SERS technique employing a 488 nm laser (0.3 mW) and a solution of 0.1 M nano-silver particles in water added to the irradiated octane in a ratio of 1:5. In order to optimize the signal the laser was focused on the interface between the Ag solution and the irradiated octane. Figure 6.1 shows the SERS spectra of pure and irradiated octane, C_8H_{18}. SERS spectra of unirradiated octane show no evidence for the presence of polyynes in the fingerprint region 1800 - 2200 cm^{-1}. However, the spectrum of irradiated octane shows a complex of spectral features in this range that can be associated with the polyynes C_8H_2, $C_{10}H_2$, $C_{12}H_2$ and $C_{14}H_2$ [45]. Figure 6.2 shows a plot of the energy of the alpha mode in these polyynes versus the number of carbon atoms in the molecule. This dependence was also observed by Tabata et al. [45, 90]. It is apparent from these data, that a range of polyynes having different lengths are generated and are retained in the octane solution after irradiation by the fs pulses.

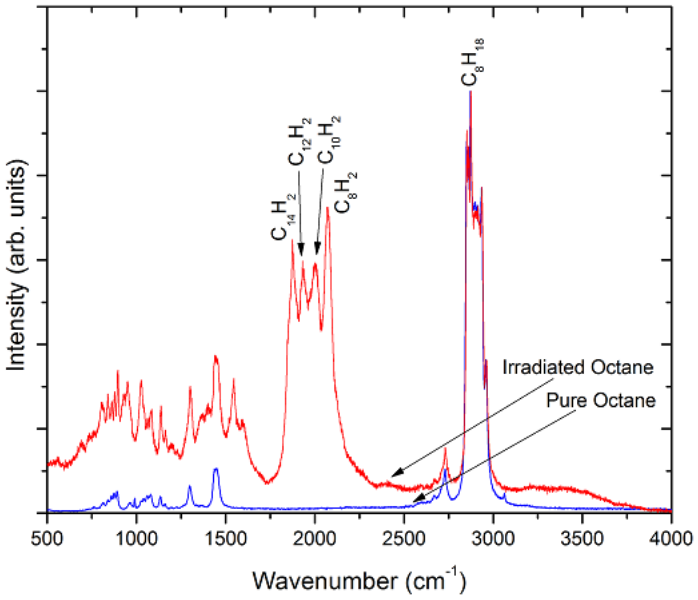

Figure 6.1: SERS spectra of octane before and after irradiation. The note-able difference in these spectra is the appearance of features arising from polyyne molecules between 1800 and 2200 cm^{-1} after irradiation.

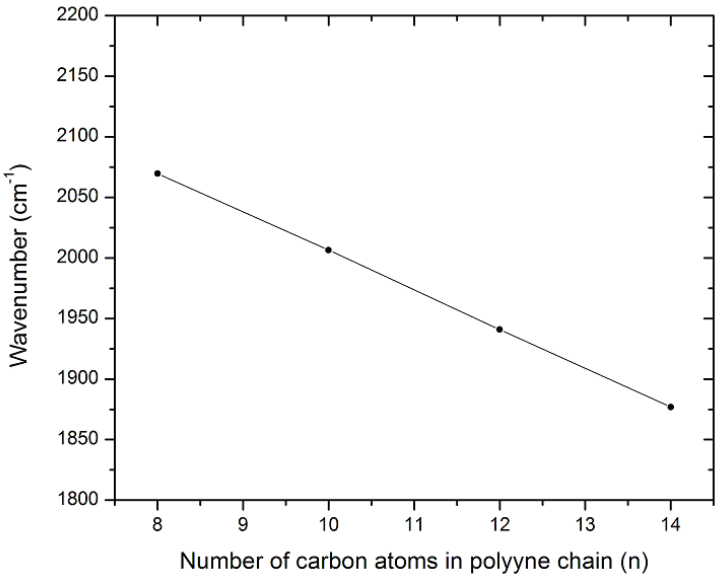

Figure 6.2: Wave number of Raman bands of polyynes detected in irradiated liquid octane plotted vs. number of carbon atoms.

6.4 Time of Flight Mass Spectrometry.

In order to start to understand the processes which lead to the observed polyynes we have studied the gas phase ionization and dissociation of octane using the same laser system and a time of flight mass spectrometer (TOFMS) of the dual-stage Wiley-McLaren type [75] with a drift region of 0.96 m. Using an on axis spherical mirror of focal length 5 cm, the laser beam in the source region was focused to produce a peak intensity of 10^{15} W/cm^2 and the pressure in the TOFMS during irradiation was maintained at 10^{-7} Torr, in order to prevent space charge effects. Although the peak intensity in the vacuum chamber is much higher than in the liquid, the largest focal volume in gas phase is responsible for producing the lowest intensity processes and so by monitoring the low charge state species produced in the vacuum experiment, we can effectively see the fragment ions which are produced in the liquid.

A TOF spectrum resulting from the irradiation of octane is shown in figure 6.3 while figure 6.4 shows a plot of $(m/q)^{1/2}$ for a selection of detected fragments. Usually for small molecules, one would expect to see a large parent ion peak but for larger molecules of this type and pulse length greater than 100 fs, so called ladder switching into a dissociative mode has been found to dominate [71, 70], so that for large molecules with many internal vibrational modes break up into smaller ions leading to the loss of all parent ions. Small amounts of C^{2+} C^{3+} from the high intensity region indicate that the majority of ions are formed in low intensity region of the focus. A variety of molecular ions together with H^+ and C^+ can be identified in this spectrum. Several groups of ions can be identified which include between one and four carbon ions, the C_2 group for instance shows the presence of $C_2H_2{}^+$, $C_2H_3{}^+$ and $C_2H_4{}^+$ which are common ions in the dissociation of alkanes. Most importantly, we see small polyynes from C_2H_2 to C_4H_2.

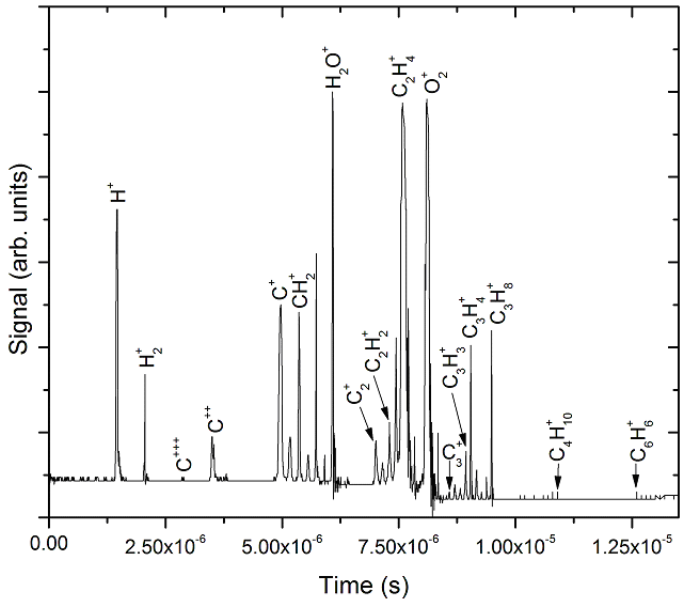

Figure 6.3: Normalized mass spectrum resulting from the irradiation of pure octane in the gas phase by 100 fs pulse at 800 nm and peak intensity of 10^{15} W/cm^2.

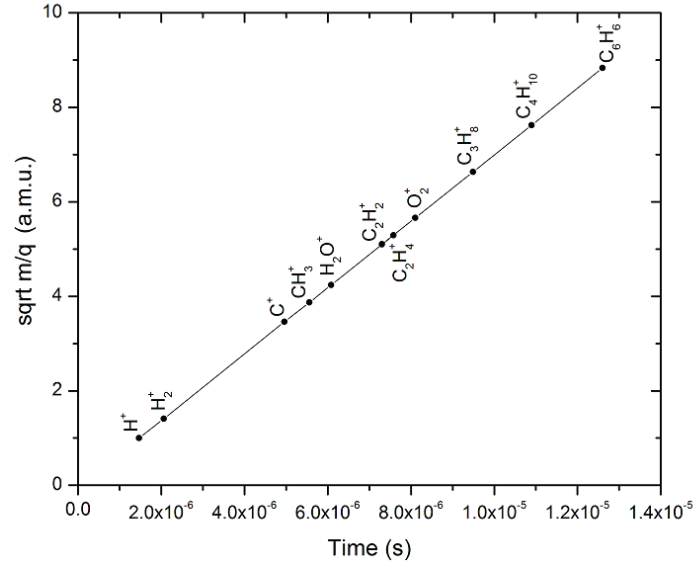

Figure 6.4: TOFMS plot of $(m/q)^{1/2}$ vs. time, t, in seconds. The largest molecule detected, $C_6H_6^+$ fits on this line well, but there is no evidence for polyynes larger than $C_4H_2^+$.

6.5 Discussion.

The TOF spectrum shows that the octane decomposition results in the formation of a wide variety of radical ions. When this process occurs in liquid octane, these radicals undergo secondary reactions with neutral octane molecules in the surrounding liquid. Recombination with electrons and negative ionic species is also expected. Despite the inherent complexity of the decomposition products, secondary reactions are likely dominated by reactions involving C, CH, C^+, CH^+, CH_2^+, C_2^+ , C_2H^+, etc. These species are traditionally the most significant species resulting from multi photon ionization (MPI) and multi-photon dissociation (MPD) of hydrocarbon molecules and all will react with octane to form secondary products. The reaction between octane and any of the species listed above will lead to a variety of branched hydrocarbons, with no single species dominating in the overall mixture. In solution then higher order polyynes can be observed since the concentration of each chain can build up by selected secondary reactions. These secondary reactions likely involve the insertion of C, C^+, C_2, etc. into smaller chains. Such reactions would take the general form.

$C + HC_nH \rightarrow HC_{n+1}H$

$C_2 + HC_nH \rightarrow HC_{n+2}H$

In this model, small polyynes and cumulenes such as HC_2H, HC_3H, HC_4H, etc. produced by laser-induced dissociation of octane are retained in solution and undergo subsequent insertion reactions with the fragments produced in the laser interaction. This leads to the formation and retention of longer polyyne molecules as indicated from the SERS measurements. Obviously, this mechanism is not possible when a gas phase octane molecule is dissociated by intense fs radiation since this occurs under collision free conditions.

Since 100 fs pulses result in the decomposition of octane into smaller fragments rather than the retention of the parent molecule, it is clear from our data that the HC_8H polyyne cannot then be produced directly from octane under the conditions of our experiments either in solution or in the gas phase. Furthermore it is clear that the produced polyynes can not survive laser irradiation if it results in ionization, otherwise they would be visible in the TOF spectrum. In the case of octane therefore we can say that an equilibrium in polyyne production and destruction must limit the ultimate concentration. It is of interest to see if this situation changes i.e. (HC_8H can be formed

directly from C_8H_{18}) when irradiation occurs with shorter pulses. This effect also gives a clue as to the reason for the observed maximum chain length in solution. In the very lowest intensity part of the focus, ionization will not be possible but multi photon dissociation MPD will be possible in fact a strong electronic absorption band moves to lower energy as the chain length increases [91]. This facilitates the absorption of incident laser radiation and enhances MPD once a critical length has been reached.

6.6 Study of irradiated octane spectra.

The normalized irradiated octane spectrum in figure 6.5 shows all carbon groups are present, but the molecular ion peak is not above background level. The spectrum shows a typical long pulse dissociation pattern but due to dissociation the lower mass species are present in sufficient quantity. Carbon chains indicative of polyyne formations are given in table 6.1.

Polyynes Detected in TOF Spectra

Species	Mass	Time (sec)
C_6^+	72	1.2630E-05
$C_4\ H_2^+$	50	1.0560E-05
C_4^+	48	1.0352E-05
$C_2H_2^+$	26	7.6480E-06
C_2^+	24	7.3600E-06
$C_3H_3^+$	39	9.3300E-06
C_3^+	36	8.9920E-06

Table 6.1: Formation of Polyynes observed in TOFMS. Table indicates polyyne peaks ($n < 8$) observed in TOF spectra of irradiated octane. Species containing double bond like C_3^+ (cumulene) are also present in TOF Spectra.

Mass spectral peaks of most dissociation species were found in the TOF spectra of irradiated octane fall into groups of carbon chains C_1 to C_8 figure 6.5. Polyyne formations detected in the gas phase is summarized in table (6.1), together with other double bonded species. It can be seen from table (6.1) that all the polyynes detected in the gas phase have molecular mass lower than octane. Higher polyynes and parent octane ion were not detectable in TOFMS.

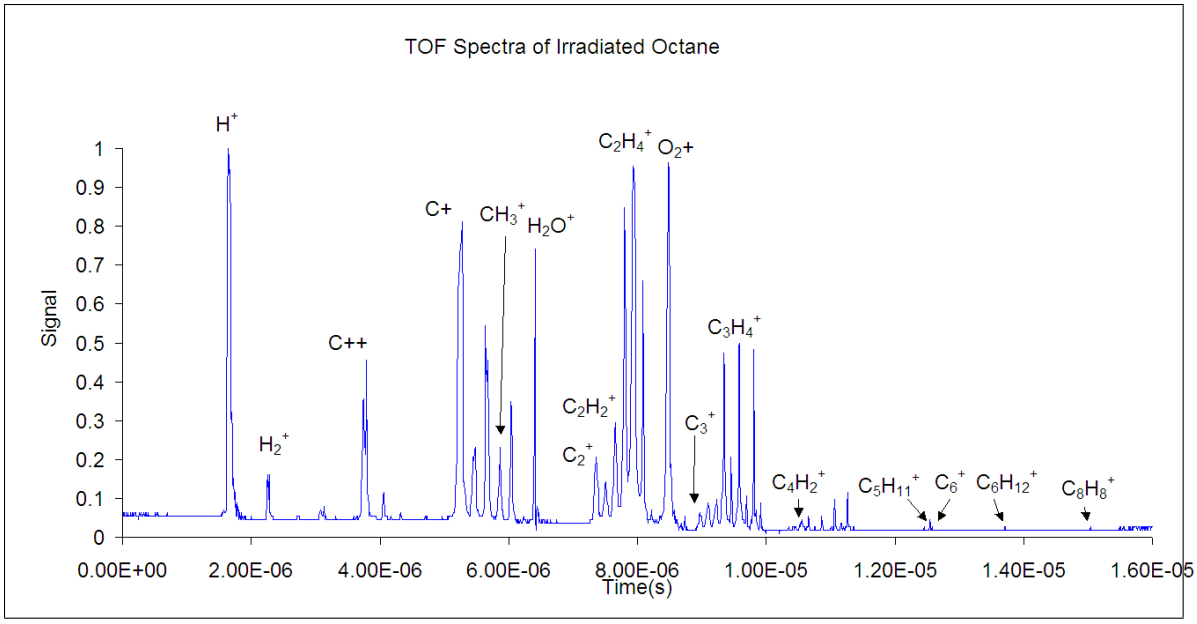

Figure 6.5: Mass spectra of irradiated octane with 100 fs 800 nm laser pulses. Mass peaks are separated by 1 amu difference, mass distribution also indicates there is more dissociation of octane irradiated with 800 nm, 100 fs width laser pulse.

6.7 Mechanism of Polyyne Formation in Liquid Octane.

Addition reactions of chemical nature in irradiated liquid [41] can be understood in chemical detail by considering ionization and dissociation of octane in larger part of focal volume capped by intensity of 10^{13} W/cm^2 due to filamentation in liquid octane [88]. This relatively lower intensity larger focal volume produces smaller ions which diffuse in surrounding liquid and cause addition reactions.

The TOF spectra of irradiated octane contains dissociation products of the laser field as shown in figure 6.5, H^+, C^{++}, C^+, CH^+, CH_3^+, C_2^+, C_2H^+, ..., $C_2H_6^+$, C_3^+, $C_3H_3^+$, including higher carbon chain species. The laser electric field can remove H atoms from octane and it can break C-C bonds at any location . The octane molecule can absorb several photons of 1.55 eV, it can ionize and subsequently dissociate depending on how many photons are absorbed. The ionization potential (accepted value) of octane is 8.6 eV, octane molecule needs to absorb 6 photons of 1.55 eV corresponding to incident laser wavelength of 800 nm to ionize, if more photons are absorbed, energy can go in electronic and vibrational excitation [87, 92] or can cause multiple ionization all these

processes lead to dissociation. For a long chain molecule like octane with much lower ionization potential than the hydrogen atom, all carbon positions are equally likely dissociation positions.

When liquid irradiation is being carried out the laser focus produces all above mentioned positive ions and electrons. These energetic positive ions and electrons move out of the laser focus and move into the surrounding liquid where they can interact with other long chain double or triple bonded species. This is facilitated by close proximity of molecules in the liquid state. Considering a small and more mobile charge carbon ion C^+ and a double bonded C_5H_4 formed in the laser focus,

$$C^+ + [H_2C = C = C = C = CH_2] \rightarrow [HC \equiv C - C \equiv C - C \equiv CH]^+ + H_2$$

C^+ is more mobile and positive it attacks a double bond which has a higher electron charge density and attaches itself resulting in bond redistribution in long chain molecule for the reasons of reaction energetics. This forms a polyyne and elimination of extra hydrogen occurs if it was attached to original C_5H_4 molecule. Newly formed $C_6H_2^+$ will absorb an electron and will form neutral polyyne molecule.

$$e^- + [HC \equiv C - C \equiv C - C \equiv CH]^+ \rightarrow HC \equiv C - C \equiv C - C \equiv CH$$

Similarly, C^+ can also attack and attaches to a laser formed nearby polyyne molecule,

$$C^+ + HC \equiv C - C \equiv C - C \equiv CH + H_2 \rightarrow$$

$$[H_2C = C = C = C = C = C = CH_2]^+$$

$$e^- + [H_2C = C = C = C = C = C = CH_2]^+ \rightarrow$$

$$H_2C = C = C = C = C = C = CH_2$$

This will cause bond redistribution and formation of C_7 which can further react with C^+ and can attach to it resulting in polyyne chain of C_8H_2,

$$C^+ + H_2C = C = C = C = C = C = CH_2 \rightarrow$$

$$[HC \equiv C - C \equiv C - C \equiv C - C \equiv CH]^+ + H_2$$

$$[HC \equiv C - C \equiv C - C \equiv C - C \equiv CH]^{+} + e^{-} \rightarrow$$

$$HC \equiv C - C \equiv C - C \equiv C - C \equiv CH$$

Above mentioned process can also lead to higher chain polyyne formations like $C_{10}H_2$ and $C_{12}H_2$ as has been detected in our SERS experiment figure 6.1. This reaction can also be initiated with other highly mobile charged ions present in the laser dissociation spectral distribution namely $C_2^+$and C_3^+. This laser initiated chemical reaction takes place few diffusion lengths away from laser focus. Polyynes formed during the process of irradiation and remaining octane are stable mixture at room temperature. Similar polyyne formation mechanism should hold for any alkane liquid irradiated with femtosecond laser.

Conclusions.

In this experimentation a combination of TOF mass spectroscopy and SERS measurements to investigate the mechanisms by which polyynes are formed in the irradiation of liquid octane with fs laser pulses. No evidence is found for the direct formation of HC_8H by elimination of H from C_8H_{18}. The primary mechanism for the generation of polyynes in solution appears to involve the laser-induced decomposition of octane to produce small chains including HC_2H, HC_3H, HC_4H, etc. These molecules then subsequently undergo addition reactions with C, C_2, etc., to form longer chains. Under the conditions of octane irradiation experiment, these reactions result in the formation of polyynes extending from (HC_8H to $HC_{14}H$). The maximum chain length appears to be determined by laser-induced photo-dissociation as a strong absorption band of the polyyne chain moves to longer wavelengths with increasing chain length.

Chapter 7

Summary

To study larger molecules, as compared to diatomics and triatomic molecules, a new TOF development was undertaken with resolution sufficient to detect the difference of one atomic mass unit for molecules of molecular mass ~ 100 amu. This was successfully achieved by developing a new TOFMS with 96 cm long flight tube and ion acceleration voltage of 3000 V. The basic design change involved development of both electrical and mechanical systems. The present TOFMS is a duel stage Wiley-McLaren design. It is possible to see clear resolution of 1 amu in a TOF spectrum. The TOF spectrum for hexane for instance detects ions from the carbon groups C_1 to C_6. New TOF has been tested using octane which has atomic mass of 114 amu.

The primary objective in this work was to study new ways to form polyyne molecules by organic liquid irradiation by using 100 fs and 300 μJ laser pulses, and to detect these molecules by TOFMS and surface enhanced Raman spectroscopy (SERS). This allowed a good balanced cross check system. The two detection systems combined together provided a good diagnostic of the presence of small and large polyynes. Analysis of the combined results indicated possible polyyne formation mechanism. In liquid irradiation, this fact is well known that the laser intensity is capped due to filamentation in a liquid at $\sim 10^{13}$ W/cm^2 [88]. Although the peak intensity in the vacuum chamber (TOF) is much higher than in the liquid, the largest focal volume in the gas phase is responsible for producing the lowest intensity processes and so by monitoring the low charge state species produced in the vacuum experiment, we can effectively see the fragment ions which are produced in the liquid.

First the irradiation of liquid acetone was carried out in an attempt to form polyynes. Acetone was chosen because diamond-like carbon films have been successfully deposited using femtosecond laser ablation of frozen acetone [85]. Experimentation with acetone showed in a convincing manner that polyynes form by acetone $(CH_3)_2CO$ irradiation. Precursors to polyynes C_2^+ and the polyyne monomer $C_2H_2^+$ were clearly detected in the TOF spectra while longer polyyne chains were detected and characterized by SERS experiments [40]. A plot of SERS spectra of both pure and irradiated acetone drawn on the same scale shows only irradiated liquid contains polyynes. Combining SERS and TOFMS results showed that all carbon chains forming polyynes are present from C_2 to C_{10}, as after irradiation in our experimentation Raman band appears in the 1800–2200 cm^{-1} range. The inset of figure 4.2 shows the correlation derived by Tabata et al. [45] together with the Raman band observed in fs-irradiated acetone. It is evident that the frequency of the present SERS mode lies on this curve indicating that the shortest chain produced after fs irradiation is C_6H_2. The possible presence of longer chains cannot be detected as the frequency of the β mode in SERS spectra of C_8H_2–$C_{14}H_2$ is not strongly correlated with chain length. In addition, there is considerable overlap between the β modes of short chains and the α mode of longer chains [45].

After successful work with acetone it was thought that linear chain hydrocarbon liquids may also be a good starting point for polyyne formation if direct liquid irradiation is carried out by 100 fs, 300 μJ laser pulses. Extensive experimentation was carried out both in the gas and the liquid phase for alkanes, alkenes and acetylene in order to observe ionization and dissociation patterns. Irradiation of molecules from methane to butane showed ionization and dissociation patterns in their TOF spectra, this indicated a basis to see how more complicated longer chain molecular TOF spectra would look like. As the butane C_4H_{10} spectrum contains all carbon groups from C_1 to C_4 and all peaks in a carbon group has a separation of 1 amu. However signal intensity decreases as one looks at the higher mass region; that is due to results by Glasgow group [71], for the wavelength of 800 nm, 50 fs pulse generates large parent ion peak and causes least dissociation.

The above considerations led to experiments with hexane and octane. Irradiation of hexane and octane both showed positive results with respect to polyyne formation. TOF spectra of pure and irradiated octane contained most polyynes or carbon chain

indicators lower in chain length than the original alkane molecule in both irradiated and the pure octane and the hexane spectra shows similar results. This indicated that smaller polyynes are formed directly in the laser focus. The small amounts of C^{2+} and C^{3+} present in the TOF spectrum show that the high intensity region of the laser focus is small indicating the majority of the ions are formed in the low intensity region of the laser focus. A variety of molecular ions together with H^+ and C^+ can be identified in TOF spectra. Several carbon groups have been identified in the spectrum of each irradiated molecule, depending on the carbon chain length in that molecule. The C_2 group of alkane for instance shows the presence of C_2^+, C_2H^+, $C_2H_2^+$, $C_2H_3^+$, $C_2H_4^+$, $C_2H_5^+$and $C_2H_6^+$ peaks which are common ions in the dissociation of alkanes. Most importantly, we see small polyynes from C_2H_2 to C_4H_2.

The SERS spectrum of irradiated octane shows a complex spectral features in the 1800–2200 cm^{-1} range that can be associated with the polyynes C_8H_2–$C_{14}H_2$. Figure 6.2 [41] shows a plot of the energy of the α mode in these polyynes versus the number of carbon atoms in the molecule. This dependence was established by Tabata et al [44, 90]. It is apparent from these data, that a range of polyynes having different lengths are generated and are retained in the octane solution after irradiation by the 100 fs, 800 nm laser pulses. Again combining both the TOFMS and SERS results show polyyne formation occurs for all ranges, from C_2 to C_{14}. Furthermore these results led to the conclusion that longer chain polyynes (compared with original molecule) were formed in the irradiated liquid by the addition of charged carbon species formed in the laser focus. During the liquid irradiation, the laser focus acts as a generator of charged species which interact with other generated molecules around the laser focus to generate longer polyynes via the following (symbolic) chemical addition reactions discussed in detail in section 6.8.

$$C + HC_nH \rightarrow HC_{n+1}H$$

$$C_2 + HC_nH \rightarrow HC_{n+2}H$$

It was also observed in the TOF spectra that the double bonded carbon chains (cumulene molecules) also form. A newly formed cumulene or polyyne molecules can add a C^+or a C_2^+ to form a longer carbon chain with equal probability. This model was made after careful study of both SERS spectra and the formation of carbon species

in TOF spectrum. Formed polyynes have finite probability to enter laser focus again during irradiation and can absorb two photons and dissociate, providing a reason why polyynes higher than $C_{14}H_2$were not seen in SERS spectra of hexane and octane.

It is likely that chemical addition reactions are the mechanism responsible for longer chain generation (for both polyynes and cumulene molecules) in irradiated alkane liquids. Similar results for hexane have recently been reported by Sato et al [42]. Based on these experimental results and looking at the nature of addition reactions, it is expected that similar chemical addition reactions will occur in other alkanes and cyclo-organic liquids when irradiated by 100 fs and 800 nm laser pulses.

7.1 Future work.

So far in this work a stable pulse of width of 100 fs has been used with alkanes, for both irradiation of alkane liquids and as a subsequent diagnostic. As 100 fs pulse is good for irradiation, but for TOF detection of ionized species stable 50 fs pulse with energy of at least 300 μJ is needed. At this moment 50 fs pulse is not stable and 100 fs at 300 μJ causes too much dissociation. This is apparent by seeing spectrum of hexane, parent ion peak is small. This situation can be improved by having stable 50 fs, 300 μJ pulses that will improve diagnostic very much by having large molecular ion peak and it will lift nearby peaks of polyyne as well.

To further test the proposed reaction mechanism experimentation with deccan $C_{10}H_{22}$ will be the next natural step, although intuitively same carbon addition reactions should occur in deccan irradiation. Intensity variation and irradiation with different time intervals may shed some more light on capping of chain length for polyyne formation at $C_{14}H_2$. To study capping of chain length at $C_{14}H_2$ an experiment can be designed in which alkane liquid flows once through laser focus. This can be done by selecting a small flow tube with diameter about five times the laser focal volume in liquid. It will be interesting to see how SERS spectrum of irradiated liquid appears in this experiment.

Cyclo-organics like benzene irradiation with 100 fs, 300 μJ laser pulses can be carried out to see if carbon addition reactions also take place in aromatic hydrocarbon irradiation, with similar chain building limitations as observed in the case of hexane

and octane.

Moreover studies can be expanded to see if polyyne formation of sufficiently longer chain with desired length can be generated (to be used as a nano-wire) in a more controlled fashion. This study initially can be done by intensity and wavelength variation of the irradiating laser, increasing irradiation time. For longer polyyne detection, it might be better to use longer wavelength of 1000 nm in combination with 10 fs pulses to obtain larger parent ion signal. At present such study can be carried out at advanced laser light source laboratory in Montreal.

Appendices

Appendix A

MATLAB code for Time of flight in TOFMS

```
clear;
clc
format long g;
%format compact;
s =1.5e-2;
s1 = (0.00001:.01:1.5)*1e-2; %[m]
%s1= 2.0e-2;
s2 = (0.53)*1e-2;
v1 = -300 ;
v2 = -3000;
T = 300;
k = (1.38)*1e-23;
d = 100e-2; % d= length
q = 1.602e-19;
%mass= m;
```

```
%v_inital= v0;
mass=[1 28 1000 1001].*1.67e-27;
%–m = 28*1.67e-27;
v_initial= sqrt((3*k*T)./mass);
for nn=1:3
v_matrix(1,:)=-v_initial;
v_matrix(2,:)=zeros(1,length(v_initial));
v_matrix(3,:)=v_initial;
end
%v01 = (1:1:1000);
%–v0= 0;
e1 = abs( v1 / s );
e2 = abs((v2 - v1) / s2);
for n=1:length(mass)
m=mass(n);
for nn=1:3
v0=v_matrix(nn,n);
t_1=(sqrt(v0^2 + 2*(q/m)*e1*s1) - v0)/e1;
t_2=sqrt(v0^2 + 2*(q/m)*(e1*s1 + e2*s2))/e2;
t_3=- sqrt(v0^2 + 2*(q/m)*e1*s1)/e2;
t_4=(q/m)*d./(sqrt(v0^2 + 2*(q/m)*(e1*s1 + e2*s2)));
t_sum=(m/q)*(t_1+t_2+t_3+t_4);
mn=(n-1)*3+nn;
t(:,mn)=t_sum';
end
end
```

```
dt_1=t(:,1)-t(:,3); % for mass=1;
dt_2=t(:,4)-t(:,6); % for mass=28;
dt_3=t(:,7)-t(:,9); % for mass=1000;
dt_4=t(:,10)-t(:,12); % for mass=1001;
s1 = (s1*100)';
%disp(' s1*100 t( -v0 ) t( v0 = 0) t( v0 ) dt
R=t(0)/dt');
%disp([s1 t(:,1) t(:,2) t(:,3) dt_1 t(:,2)./dt_1]) % for m=1
%disp([s1 t(:,4) t(:,5) t(:,6) dt_2 t(:,5)./dt_2]) % for m=28
%disp([s1 t(:,7) t(:,8) t(:,9) dt_3 t(:,8)./dt_3]) % for m=1000
%disp([s1 t(:,10) t(:,11) t(:,12) dt_4 t(:,11)./dt_4]) % for m=10001
%disp([t, s1]); % [s], [cm]
% aa=[1 5 10] i.e. it means you are plotting column i, j, k which correspond
% to m1 with -v0, m2 with v0=0, m4 with -v0
aa=[7 8 9];
plot(s1 ,t(:,aa));
title('TOF N2+')
xlabel('s1:Ion position: cm');ylabel ('t: Time: sec')
```

Appendix B

MATLAB code for Instrument Resolution.

```
clear;
clc
format long g;
%format compact;
%s =1.5e-2;
%s1 = (0.00001:.01:2.0)*1e-2; %[m]
s1 = 1.5e-2; % source length
s2 = 0.53e-2; % acc. length
T = 300;
k = (1.38)*1e-23;
q = 1.602e-19;
m = 28*1.67e-27;
v_initial= sqrt((3*k*T)/m);
v_matrix=zeros(1,3);
v_matrix(1)=-v_initial; % -v0
```

```
v_matrix(2)=zeros(1,length(v_initial)); % 0
v_matrix(3)=v_initial; % v0
v1= -10:-10:-600; % voltage on source
v2= -1000:-100:-5000; % acc. voltage
n_1=length(v1);
n_2=length(v2);
t = zeros(n_1*n_2,3);
D = zeros(n_1*n_2,1); %% for display output: d , v1 , v2
V1 = zeros(n_1*n_2,1);
V2 = repmat(v2',n_1,1);
for n=1:n_1
V1((n-1)*n_2+1:n*n_2,1)=v1(n);
end
for l=1:3
v0=v_matrix(l);
for n=1:n_1
for k=1:n_2
e1 = abs( v1(n)/s1 );
e2 = abs((v2(k) - v1(n))/s2);
sigma = s1+(e2/e1)*s2;
d_1=(sqrt(sigma)+sqrt(s1))^2;
d = 2*sigma^(3/2)*(1/sqrt(s1)-(s2/(sqrt(s1)*d_1)));
D((n-1)*n_2+k,1) = d;
%% calculate time t for different v1 , v2 and v0
t_1=(sqrt(v0^2 + 2*(q/m)*e1*s1) - v0)/e1;
t_2=sqrt(v0^2 + 2*(q/m)*(e1*s1 + e2*s2))/e2;
```

```
t_3=- sqrt(v0^2 + 2*(q/m)*e1*s1)/e2;
t_4=(q/m)*d/(sqrt(v0^2 + 2*(q/m)*(e1*s1 + e2*s2)));
t((n-1)*n_2+k,l)=(m/q)*(t_1+t_2+t_3+t_4);
end
end
end
dt=t(:,1)-t(:,3);
R=t(:,2)./dt;
Maximum_R=max(R);
%————————————————————————————
%% to find the corresponding d, v1 and v2 for maximum R.
[R_1 R_2]= find(R==Maximum_R);
v2_index = mod(R_1,n_2);
v1_index = (R_1-v2_index)/n_2+1;
%–v1_R_max = v1(v1_index); %% v1 value corresponding to maximum
    R
%–v2_R_max = v2(v2_index); %% v2 value corresponding to maximum
    R
%–d_R_max = D(R_1) ; %% d value coresonding to maximum R
%————————————————————————————-
% find R where d<1
AA=find(D<1);
Dd=D(AA);
Rd=R(AA);
Maximum_Rd = max(Rd)
% now find the corresponding v1 and v2 for Maximum_Rd
```

```
[r1 r2] = find(R==Maximum_Rd);
vv2_index = mod(r1,n_2);
vv1_index = (r1-vv2_index)/n_2+1;
if vv2_index==0
V2_R_max= v2(n_2)
V1_R_max = v1(vv1_index-1)
else
V1_R_max = v1(vv1_index)
V2_R_max = v2(vv2_index)
end
d_less = D(r1)
%-----------------------------------------------------------
%% output value.
disp(' v1 v2 d R ')
%disp([V1 V2 D R]); % table for all d
disp([V1(AA) V2(AA) Dd Rd]); % table for d<1
R_plot=zeros(n_2,n_1);
D_plot=zeros(n_2,n_1);
for n=1:n_1
R_plot(:,n)=R((n-1)*n_2+1:n*n_2,:);
D_plot(:,n)=D((n-1)*n_2+1:n*n_2,:);
end
[vv1,vv2]=meshgrid(v1,v2);
%figure(1)
%surf(vv1,vv2,R_plot) % 3D plot for R
% The following plots plot R and d vs v2
```

```
figure(1)
plot(-vv2(:,60),R_plot(:,60),'b',-vv2(:,60),R_plot(:,40),'g',-vv2(:,60),R_plot(:,30),'r',-
    vv2(:,60),R_plot(:,20),'k') % 2D plot for R
xlabel('V2'),ylabel('Resolution')
figure(2)
plot(-vv2(:,60),D_plot(:,60),'b',-vv2(:,60),D_plot(:,40),'g',-vv2(:,60),D_plot(:,30),'r',-
    vv2(:,60),D_plot(:,20),'k') % 2D plot for R
xlabel('V2'),ylabel('Distance')
%figure(4)
%surf(vv1,vv2,D_plot) % 3D plot for d
```

Appendix C

Source Circuit

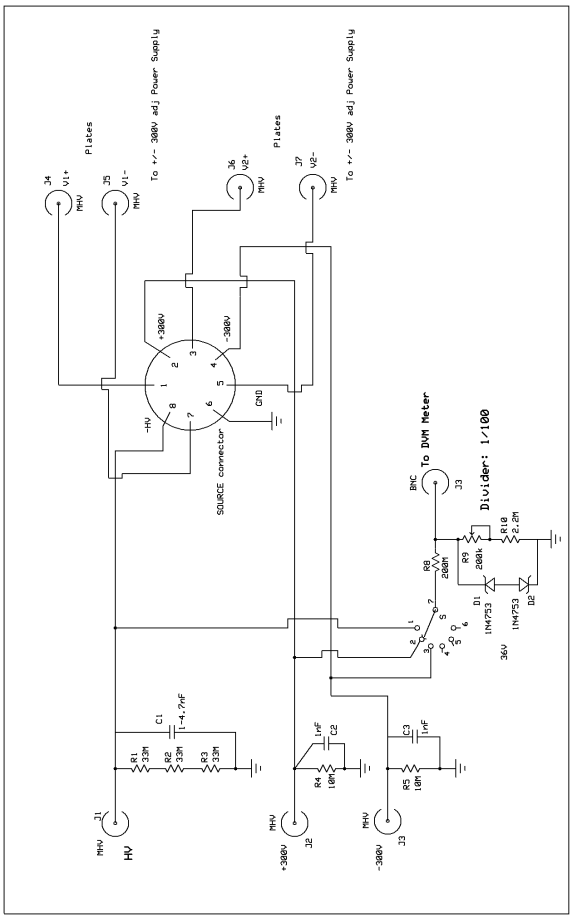

Figure C.1: Circuit diagram for the source region.

Appendix D

Detector Circuit

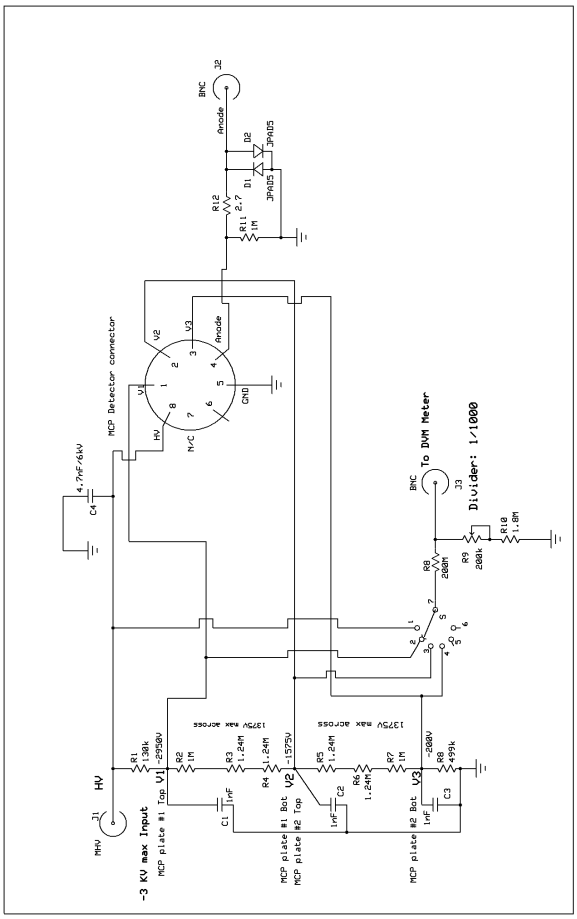

Figure D.1: Circuit diagram for the detector connections.

Appendix E

Basic Theory

E.0.1 Maxwell's Equations in SI units

$$\nabla.\mathbf{B} = 0 \tag{E.1}$$

$$\nabla \cdot \mathbf{D} = \rho \tag{E.2}$$

$$\nabla \times \mathbf{E} = -\frac{\partial \mathbf{B}}{\partial t} \tag{E.3}$$

$$\nabla \times \mathbf{H} = \frac{\partial \mathbf{D}}{\partial t} + \mathbf{J} \tag{E.4}$$

ρ: Charge density, and $\mathbf{J}$: Current density, $\mathbf{E}$ & $\mathbf{B}$ are electric and magnetic fields, $\mathbf{D}$: Displacement current.

In the case of light interacting with metals [12] the current density term $\mathbf{J} = \sigma\ \mathbf{E}$ is important in equation (1.4) and in a case when the medium is non-conducting, then the application of a light electric field causes displacement of the atomic or molecular electronic clouds. In non-conducting material media $\mathbf{D} = \epsilon_\mathbf{o}\mathbf{E} + \mathbf{P}$, where $\mathbf{P}$ is the media polarization and $\mathbf{P} \propto \mathbf{E}$. In a material medium $\mathbf{D} = \epsilon\mathbf{E}$ and $\mathbf{P} = \epsilon_o\chi\mathbf{E}$, this gives $\mathbf{P} = \epsilon_o(\frac{\epsilon}{\epsilon_o} - 1)\mathbf{E}$, therefore we set ($\frac{\epsilon}{\epsilon_o}$-1) = χ known as electric susceptibility constant of the medium and ϵ, ϵ_o are dielectric constants in the medium and free space respectively. $\mathbf{P} = \epsilon_o\chi\mathbf{E}$ determines the response of the medium to the electric

field. In the case of an isotropic medium, for example glass, the susceptibility is a scalar quantity and it has the same value in all directions of the applied field. For anisotropic media such as crystals, polarization depends on the direction of the applied field. This means that the polarization is not the same in all the directions and the electric susceptibility constant ' χ ' is not a scalar but a tensor. The domain of linear optics is characterized by the relation $\mathbf{P} = \epsilon_o \chi \mathbf{E}$.

Similarly for the magnetic induction '**B**' we have, $\mathbf{B} = \mu_o (\mathbf{H} + \mathbf{M})$, where **M** is the magnetization if $\mathbf{M} = 0$ (in non relativistic limit) so, $\mathbf{B} = \mu_o \mathbf{H}$. From Maxwell equations taking the cross product of equation (E.3) and using suitable vector identities, it is possible to derive wave equation as,

$$\nabla^2 \mathbf{E} - \frac{1}{c^2} \frac{\partial \mathbf{E}}{\partial t} = 0 \tag{E.5}$$

where $c_o = \frac{1}{\sqrt{\epsilon_0 \mu_0}} = 2.998 \times 10^8$ m/s is the speed of light in vacuum, and $n = \sqrt{\epsilon}$ refractive index, is the square root of the dielectric constant in the medium. The solution of the wave equation is,

$$\mathbf{E}(t) = \mathbf{E_o}(t) cos(\omega_o t + \phi) \tag{E.6}$$

ω_o: Angular frequency and ϕ: Phase of the wave

This represents a self propagating electromagnetic wave in the free space. This solution gives an oscillating electric field vector **E**(t) which changes with the associated magnetic field vector **B**(t) periodically with oscillating frequency ω_o. In light matter interactions strength of the electric field in equation (E.6) is used to determine the intensity of light.

E.1 Light Intensity

Materials are sensitive to the number of photons/unit time or classically the cycle average of the modulus of the poynting vector.

$$\mathbf{S} = (\mathbf{E} \times \mathbf{H})$$

For a plane waves in vacuum

$$|\mathbf{E}| = |\mathbf{H}| \sqrt{\frac{\mu_0}{\epsilon_0}}$$

$$\mathbf{S} = |\mathbf{S}| = \sqrt{\frac{\epsilon_0}{\mu_0}} |\mathbf{E}|^2$$

Since $\mathbf{E}(t) = \mathbf{E}_o cos(\omega_o t + \phi)$: The cycle average $\langle \mathbf{E}(t) \rangle = \frac{1}{2}\mathbf{E}_o^2; \langle cos^2(\omega_o t + \phi) \rangle = \frac{1}{2}$

$$I = \langle \mathbf{S} \rangle = \frac{1}{2} \sqrt{\frac{\epsilon_0}{\mu_0}} \mathbf{E}_o^2 \tag{E.7}$$

E.1.1 Laser focal volume and Power

To attain the high power densities at which strong field effects become dominant requires focusing of the laser beam. The peak intensity can be estimated from the ratio of the peak power of the laser to the cross section of the focus. Considering Gaussian beam and the TEM_{oo} mode, from equation (E.6) for a Gaussian beam,

$$E_o(t) = E_o exp - \left(\frac{t}{t_o}\right) \tag{E.8}$$

$$\mathbf{E}(t) = E_o e^{-\left(\frac{t}{t_o}\right)} cos(\omega_o t + \phi) \tag{E.9}$$

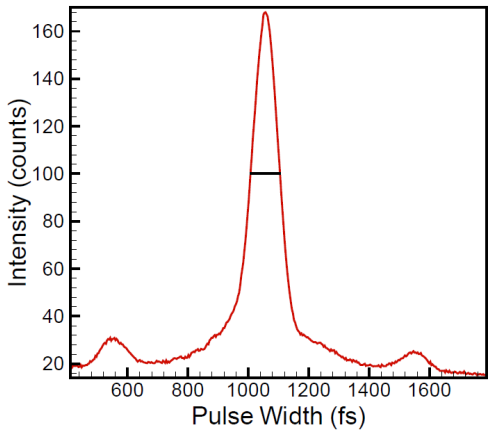

Figure E.1: Computer screen snap shot of a 100 fs laser pulse in an autocorelator pulse measurement in our laboratory.

Considering a Gaussian beam's TEM_{oo} mode the beam radius [14] is given by,

$$I\left(r\right) = I_{max} e^{-\frac{2r^2}{\omega^2}}$$

where 'r' is the radial distance from the beam axis, focusing with a concave mirror of focal length 'f' yields a beam waist radius, ω_o as,

$$\omega_o = \frac{\lambda f}{\pi \omega}$$

The laser focus presents a difficulty, it is not uniform in intensity, there is a spatial variation of laser intensity around the center of the focus (Iso-intensity shells). This results in occurrences of different processes in different intensity zones, and the signal from a zone is proportional to the intensity dependent probability and the focal volume of the region. Considering 'z' as the axial coordinate, for the Gaussian beam

$$I(r,z) = \frac{I_{max}}{1 + \left(z/z_R\right)^2} exp\left(-\frac{2r^2}{\omega_o^2\left(1 + \left(z/z_R\right)^2\right)}\right) \tag{E.10}$$

The Rayleigh range z_R is defined as the distance along the beam axis at which the intensity reduces to 50%. The radial range of a shell at z = 0 is beam waist ω_o.

$$z_R = \frac{\pi \omega_o^2}{\lambda}$$

Intensity I(r,z) in equation (E.10) is spatially Gaussian along 'r' and Lorentian along 'z'. Inverting this equation for 'r' values gives the equation that generates iso-intensity curves for laser focal volume.

$$r_i = \frac{\omega_o^2}{2}[1 + \left(z/z_R\right)^2]\left[ln\left(\frac{I_{max}/I_i}{1 + \left(z/z_R\right)^2}\right)\right]^{1/2} \tag{E.11}$$

In our ultafast laboratory, a Ti:sapphire laser beam figure 1.2 of wavelength 800 nm and ω = 0.5 cm, is focused by concave mirror of focal length of 5 cm, this gives w_o= 2.5 μm, for pulse width τ intensity is given by,

$$I = \frac{E}{A\tau} \tag{E.12}$$

For E = 300 μJ and $\tau \sim 100$ fs laser intensity is $\sim 10^{16}$ W/cm^2. Experiments show that at this intensity the hydrogen atom ionizes efficiently.

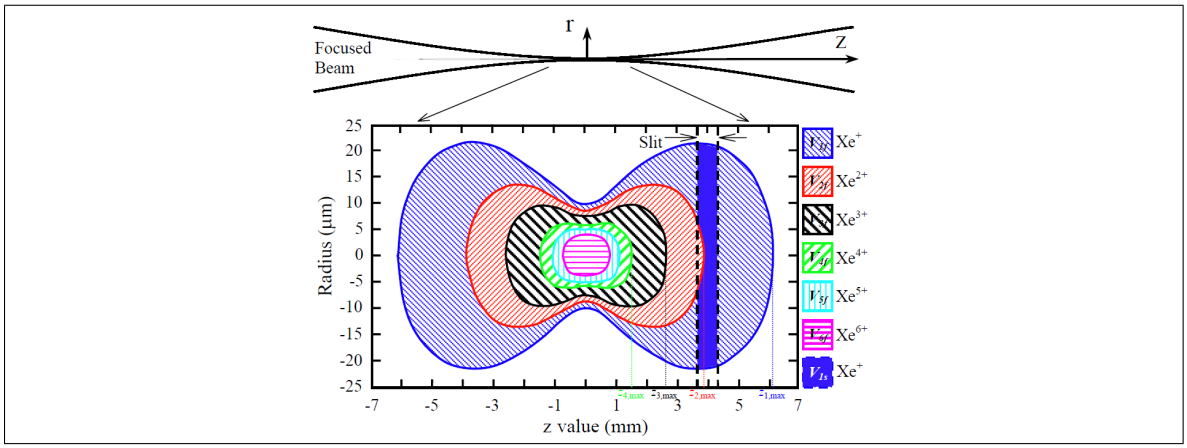

Figure E.2: Iso-intensity curves generated by equation (E.11) indicates variation of intensity in different regions of laser focus for Gaussian beam TEM$_{oo}$. Degree of Xe ionization serves as an indicator of the intensity in different zones. Above diagram has been adopted from the Ph.D. thesis [15] of Ali-ElZein 2001.

E.2 The Structure of Matter.

The simplest atomic structure is one of the hydrogen atom. An electron bounded by proton in a Coulomb potential.

$$V(r) = -\left(\frac{1}{4\pi\epsilon_o}\right)\frac{Ze^2}{r} \tag{E.13}$$

r: electron-proton distance; e : charge on electron; ϵ_o: permittivity of free space; Z: atomic number

In Bohr's Picture, discrete energy levels exist around proton. These electronic levels can be obtained by Schrodinger equation of wave mechanics, treating this as a one body problem using reduced mass.

$$\left[-\frac{\hbar^2}{2m}\nabla^2 - \frac{Ze^2}{(4\pi\epsilon_o)\,r}\right]\psi(\mathbf{r}) = E\psi(\mathbf{r}) \tag{E.14}$$

For the central Coulomb potential, this equation can be solved in spherical polar coordinates and has solutions [16]

$$\psi(r,\theta,\phi) = R_{nl}(r)Y_{lm}(\theta,\phi) \tag{E.15}$$

.

Solution of the radical part of the Schrodinger equation gives values of atomic energy levels as,

$$E_n = -\frac{1}{2}\left(\frac{1}{4\pi\epsilon_o}\right)\frac{Ze^2}{a_o}\left(\frac{1}{n^2}\right) \tag{E.16}$$

n = 1, 2, 3,—-

For hydrogen atom Z = 1, a_o: Bohr's radius,

$$E_n = -\left(\frac{13.6}{n^2}\right)eV \tag{E.17}$$

n = The principle quantum number, the lower the "n" the more deeply lying is the energy state. These energy levels depend only on the value of "n". This system has an infinite number of energy levels with $E < 0$, known as bound states.

As $V(r) \to 0$ for large "r" solutions of the radical equation for $E > 0$ will have oscillatory behavior at infinity and will be an acceptable eigenfunction for any $E > 0$. Therefore we have continuous spectrum for $E > 0$. Energy levels are degenerate with respect to quantum numbers "l" and "m", degeneration is n^2 fold, where $l = n - 1$. Hydrogen wave functions [16] obtained from solution of wave equation are,

$$\psi_{n.l,m}(r,\theta,\phi) = R_{nl}(r)Y_{lm}(\theta,\phi) \tag{E.18}$$

.

Plot of the energy as a function of the principle quantum number generates a potential well with electronic states.

where,

$$R_{nl} = -\left[\left(\frac{2Z}{na_o}\right)^3 \frac{(n-l-1)}{2n\left[(n+1)\,1\right]^3}\right]^{\frac{1}{2}} e^{-\frac{\rho}{2}}\rho^l L_{n+l}^{2l+1}(\rho)$$

$L_{n+1}^{2l+1}(\rho)$: Laguerre Polynomials

$Y_{lm}(\theta,\phi)$: Spherical harmonics.

$$Y_{lm}(\theta,\phi) = (-1)^m\left[\frac{(2l+1)!}{4\pi(l+m)!}\right]P_l^m(cos\theta)^{l^{im\phi}}$$

$m \geq 0$

The ground state hydrogen atom wave function is given by $n = 1$, $l = 0$, $m = 0$.

$$\psi_{1,o,o}(r,\theta,\phi) = \psi_{1oo} = \frac{1}{\sqrt{\pi}}\left(\frac{Z}{a_o}\right)^{\frac{3}{2}} exp\left(-\frac{Zr}{a_o}\right) \tag{E.19}$$

The charge distribution of ψ_{1oo} is spherically symmetrical, but the charge distribution of "p" levels is dumbbell shaped. When an atom is under an external electric field, electronic energy levels get shifted, this is known as a Stark Shift [16]. Similarly, under the influence of a magnetic field, energy shift occurs because degeneracy of Coulomb potential is lifted. At this stage, since problem is non-relativistic, therefore Stark shift plays an important role in the laser-matter interactions.

E.3 Molecular Structure

Atoms combine in various ways to form molecules mainly by electron sharing (covalent bond) or by complete electron transfer (ionic bond). As two different elements combine and share electrons, the resulting pull on shared electrons is usually different, this gives rise to polar molecules like HCl or H_2O. In situations where homo-nuclear molecules combine they form non-polar bonds such as H_2 and N_2. Molecules have vibrational and rotational degrees of freedom, so they have rotational and vibrational spectra. Long complex molecules have many more degrees of freedom and can vibrate in many modes. For simplicity we can consider a diatomic molecule to study the rotational and vibrational impact on molecular spectra.

E.3.1 Energy levels

Molecules exhibit rotational and vibrational motion, from basic consideration of rotational motion and quantum restrictions rotational energy levels are given by

$$E_{rot} = \frac{1}{2}\frac{\hbar^2}{I} l(l+1) \tag{E.20}$$

$l = 0,\ 1,\ 2,\ 3,$——

Transitions in rotational levels belonging to the same electronic and vibrational level give rise to a pure rotational spectrum. Rotational band spectra are observed in far infrared and microwave region. Level splitting for rotational spectrum $\sim 10^{-3}$ eV.

Vibrational motion of bounded atoms generates vibrational energy levels. The vibration of a diatomic molecule is analogues to two masses connected by a spring of spring constant k, this system can be represented by the differential equation again applying quantum conditions gives vibrational energy levels as,

$$E_{vib} = \hbar\sqrt{\frac{k}{\mu}}\left(v + \frac{1}{2}\right) \tag{E.21}$$

where $k/m = \omega^2$, and μ: is the reduced mass and $\nu = 0, 1, 2, 3 - --$, is vibrational quantum number.

The vibrational spectra of diatoms is in the infrared range, this causes first order of level splitting of electronic levels ~ 0.1 eV. Considering diatomic molecule for simplicity vibrational levels exist in between electronic levels, and in between two vibrational levels rotational levels exist. Therefore rotational and vibrational spectra [17] of a molecule can be understood with selection rules $\triangle v = \pm 1$ and $l = 0, 1, 2, ...$ $v = 0, 1, 2, ...$

$$E_{rot,Vib} = \frac{\hbar^2}{2I} l(l+1) + \hbar\sqrt{\frac{k}{\mu}}(v + \frac{1}{2}) \tag{E.22}$$

Basic molecular structure can be thought of as electronic levels and corresponding associated vibrational and rotational levels. Allowed transitions between these levels gives rise to molecular spectra, depending on nature of molecule i.e. molecule is polar

or non-polar. As homo-nuclear molecules are non-polar such as H_2, N_2, these molecules do not have dipole moment and as a consequence no infrared absorption spectra. The interaction with the laser field is considered to be due to the electron in the outer most region of the molecule which is bonded with the molecule with binding potential V_o.

E.3.2 Atomic Structure and Coupling to Light

If a system has only one level it will remain in that state forever in case if it is undisturbed. For a system with two or more than two allowed states, some probability exists that system is in one of the allowed states [18]. Considering a simple system of an isolated hydrogen atom, the electronic wave function $\psi_1(\mathbf{r},t)$, is a solution of the wave equation representing state 1, and the wave function $\psi_2(\mathbf{r},t)$ representing state 2.

The total wave function $\Psi(\mathbf{r},t)$,

$$\Psi(\mathbf{r},t) = a_1\psi_1(\mathbf{r},t) + a_2\psi_1(\mathbf{r},t) + ... \tag{E.23}$$

Considering the two states $\psi_1(\mathbf{r},t)$ & $\psi_2(\mathbf{r},t)$. The probability that that system is in state 1 or 2,

$$|\Psi(\mathbf{r},t)|^2 = |a_1\psi_1(\mathbf{r},t) + a_2\psi_1(\mathbf{r},t)|^2$$

Charge density corresponding to system is given by

$$\rho(\mathbf{r},t) = -e\,|\Psi(\mathbf{r},t)|^2$$

Considering two atomic states

$$\rho(\mathbf{r},t) = -e\left|a_1(t)e^{-\frac{iE_1t}{\hbar}}\psi_1(\mathbf{r}) + a_2(t)e^{-\frac{iE_2t}{\hbar}}\psi_2(\mathbf{r})\right|^2$$

$$= |a_1(t)\psi_1(\mathbf{r})|^2 + |a_2(t)\psi_2(\mathbf{r})|^2 + a_1(t)a_2^\star(t)\psi_1(\mathbf{r})\,\psi_2^\star(\mathbf{r})\,e^{\frac{i(E_2-E_1)t}{\hbar}}$$

$$+ a_1^{\star}(t)a_2(t)\psi_1^{\star}(\mathbf{r})\,\psi_2(\mathbf{r})\,e^{-\frac{i(E_2-E_1)t}{\hbar}} \tag{E.24}$$

In equation (1.28) the first two terms of charge density are constant. The contributing term to the radiation field is the cross term. It represents an oscillating charge density with oscillation frequency $\omega_{21} = (E_2 - E_1)/\hbar$. This represents a natural oscillating dipole, a result of the occupation probability of quantum states. The magnitude of the oscillating component is proportional to cross term amplitudes.

E.3.3 Dipole Approximation

Atomic and molecular dimensions are of the order of Bohr's radius i.e about .05 nm, but wavelength of the incident laser radiation is 800 nm in our experiments. Even the long octane molecule of length 1 nm is short enough. So it is reasonable to say wavelength $\lambda \gg a$, the atomic dimensions, this implies $ka \ll 1$ and for many cases of practical interest it is possible to approximate associated exponential,

$$exp(i\mathbf{k}.\mathbf{r}) = 1 + (i\mathbf{k}.\mathbf{r}) + \frac{1}{2}(i\mathbf{k}.\mathbf{r})^2 + - - - - -$$

as

$$exp(i\mathbf{k}.\mathbf{r}) = 1$$

This means it is possible to neglect the spatial variation of the field over atomic dimensions, or the laser electric field can be treated as constant over atomic and molecular dimensions. Since $\lambda \gg a$ this is also known as the long wave length approximation. Dipole approximation becomes less accurate if the wavelength of the radiation decreases. The dipole approximation is valid over the range of this study.

References

[1] D. C. Lindberg. “The Greeks and the Cosmos.” *The Beginnings of Western Science*. Chicago: University of Chicago Press, 2007. 1

[2] A. L. Basham. *Cultural History of India*. Oxford University Press, 1999. 1

[3] N. Melchert. *The Great Conversation: A Historical Introduction to Philosophy*. McGraw Hill, 2002. 1

[4] J. Dalton. *New System of Chemical Philosophy*. 1808. 1

[5] E. Rutherford. *Philos. Mag.*, 6(21):669-688, 1911. 1

[6] N. Bohr. *Philos. Mag.*, 6(26):1-25, 1913. 1

[7] G. N. Lewis. *J. Am. Chem. Soc.*, 38:762, 1916. 2

[8] L. Boltzmann. *Lectures on Gas Theory*. Berkeley: University of California Press, 1964. 2

[9] M. Planck. *The theory of heat radiation*. Philadelphia: Blackiston’s Son & Co, second edition, 1914. 2

[10] E. Schrödinger. "Quantisierung als Eigenwert problem; von Erwin Schrödinger". *Annalen der Physik*, (Leipzig):361–377, 1926. 5

[11] J. C. Maxwell. *A dynamical theory of the electromagnetic field*. 1865. 3

[12] G. R. Fowlers. *Introduction to modern optics*. Dover, second edition, 1989. 3, 119

[13] M. Wegener. *Extreme nonlinear optics*. Springer, 2005. 4, 8, 9

[14] J. H. Posthumus. *The dynamics of small molecules in intense laser fields*. 2003. 122

[15] A. A. A. El-Zain. Electron and photon interactions with molecules. PhD thesis, University College London, UK, 2001. 123

[16] B. H. Bransden, C. J. Joachain. *Physics of atoms and molecules*. Prentice Hall, England, 2003. 5, 7, 124, 125

[17] G. Herzberg. Molecular Spectra and Molecular Structure: *Electronic Spectra and Electronic Structure of Polyatomic Molecules*. Krieger Publishing, 1991. 126

[18] A. E. Segman. *Laser physics*. University Science Books, 1986. 127

[19] M. Frasca. Strong-field approximation for the Schrödinger equation. *Phys. Rev. A*, 45:43–46, 1992. 6

[20] L. Keldysh. *Sov. Phys. JETP,* 20:1307, 1965. 7, 33, 38, 84

[21] W. Bryns. Ultrafast processes in small molecules. PhD thesis, University College London, UK, 2001. x, 11, 13, 15, 71

[22] M. V. Ammosov, N. B. Delone, V. P. Krainov. Tunnel ionization of complex atoms and atomic ions in a varying electromagnetic field. *Zh. Eksp. Teor. Fiz.*, 91:2008-2013, 1986. 12, 13, 36

[23] A. Saenz. On the influence of vibrational motion on strong-field ionization rates in molecules. *J. Phys. B*: *At. Mol.Opt. Phys.* 33:4365, 2000. 14

[24] X. M. Tong. *Phys. Rev. A*, 66:033402, 2002. 14, 36

[25] R. W. Boyed. *Nonlinear Optics*. Academic Press, third edition, 2007. 14, 31

[26] W. Kaiser, C. G. B. Garrett. *Phys. Rev. Lett.*, 7, 229-231, 1961. 16

[27] J. H. Posthumus, L. J. Frasinski, A. J. Giles, K. Codling. *J. Phys. B: At. Mol. Opt. Phys.*, 28:L349-L353, 1995. 17, 18, 36, 50

[28] J. H. Posthumus, L. J. Frasinski, A. J. Giles, K. Codling. Field-ionization, Coulomb explosion of diatomic molecules in intense laser fields. *J. Phys. B: At. Mol. Opt. Phys.*, 29 5811–5829, 1996. 19

[29] W. A. Chalifoux, R. R. Tykwinski. Synthesis of polyynes to model the sp-carbon allotrope carbyne. *Nature chemistry,* 2010. x, 21

[30] N. Oku, S. Matsugana, N. Shishijimicins Fusetani. *Novel enediyne antitumor antibiotics from the Ascidian Didemnum proliferum. J. Am. Chem. Soc.*, 125:2044-2045, 2003. 21

[31] W. W. Duely, D. A. Williams. Interstellar polyynes from disruption of carbon grains. *Mon. Not. R. astr. Soc.*, 211, 97-103, 1984. 21

[32] H. Wang, M. Chhowalla, N. Sano, S. Jia, G. Amaratunga. Large-scale synthesis of single-walled carbon nanohorns by submerged electric arc. *Nanotechnology*, 15:546, 2004. 21

[33] D. Nishide et al. Single-wall carbon nanotubes encaging linear chain $C_{10}H_2$ polyyne molecules inside. *Chem Phys Lett.*, 428:356–360, 2006. x, 21, 22

[34] L. Itzhaki, E. Altus, H. Basch, S. Hoz. Harder than Diamond. Determining the Cross-Sectional Area and Youngs Modulus of Molecular Rods. *Angew. Chem.*, 117:7598 –7601, 2005. 21

[35] M. Tsuji, S. Kuboyama, T. Matsuzaki, T. Tsuji. Formation of hydrogen-capped polyynes by laser ablation of C_{60} particles suspended in solution. *Carbon*, 41:2141–8, 2003. 22, 78

[36] M. Tsuji, T. Tsuji, S. Kuboyama, S. H. Yoon, Y. Korai, T. Tsujimoto, et al. Formation of hydrogen-capped polyynes by laser ablation of graphite particles suspended in solution. *Chem Phys Lett.*, 355:101–8, 2002. 22, 78, 81, 93

[37] G. Compagnini, V. Mita, R. S. Cataliotti, L. D'Urso, O. Puglisi. Short polyyne chains produced by pulsed laser ablation of graphite in water. *Carbon*, 45:2445–58, 2007. 22, 78, 79, 93

[38] R. Matsutani, T. Kakimoto, K. Wada, T. Sanada, H. Tanaka, K. Kojima. Preparation of long-chain polyynes by laser ablation of pellets of graphite and perylene. *Carbon*, 46:1091–9, 2008. 78

[39] M. Tsuji, T. Tsuji, S. Kuboyama, S. H. Yoon, Y. Korai, T. Tsujimoto, K. Kubo, A. Mori, I. Mochida. *Chem. Phys. Lett.*, 355, 101–108, 2002. x, 23

[40] A. Hu, J. H. Sanderson, A. A. Zaidi, T. Zhang, Y. Zhou, W. W. Duley. Direct synthesis of polyynes in acetone by dissociation using femtosecond laser radiation. *Carbon*, 48:1823–5, 2008. 23, 92, 93, 104

[41] A. A. Zaidi, A. Hu, M. J. Wesolowski, X. Fu, J. H. Sanderson, Y. Zhou, W. W. Duley. Time of flight mass spectrometry of polyyne formation in the irradiation of liquid alkanes with femtosecond laser pulses. *Carbon*, 48:2517–2520, 2010. 23, 92, 100, 105

[42] Y. Sato, T. Kodama, H. Shiromaru, J. H. Sanderson, T. Fujino, Y. Wada, et al. Synthesis of polyyne molecules from hexane by irradiation of intense femtosecond laser pulses. *Carbon*, 48:1673–6, 2010. 23, 91, 93, 106

[43] J. Kürti, C. Magyar, A. Kürti, C. Hungarian, A. Balázs, P. Balazs, Fri Rajczy. Vibrational analysis for short carbon chains with alternating and cumulenic structure. *Synthetic Metals*, 71:1865-1866, 1995. 24

[44] H. Tabata, M. Fujii, S. Hayashi. Laser ablation of diamond nanoparticles suspended in solvent: synthesis of polyynes. *Chem. Phys. Lett.*, 395:138–42, 2004. 22, 78, 79, 92, 105

[45] H. Tabata, M. Fujii, S. Hayashi, T. Dio, T. Wakabayashi. Raman and surface-enhanced Raman scattering of a series of size separated polyynes. *Carbon*, 44:3168–76, 2006. 24, 94, 104

[46] J. R. Ferraro. *Introductory Raman spectroscopy*. Second edition. 1967. 29, 30

[47] A. L'Huillier, L. E. Lompre, G. Mainfray, C. Manus. *Phys. Rev. A*, 27:2503, 1983. 34

[48] K. Codling, L. J. Frasinski, P. A. Hatherly, J. R. M. Barr. *J. Phys. B: At. Mol. Phys.*, 20:L525, 1987. xi, 34, 35

[49] P. Lambropoulos. *Phys. Rev. Lett.*, 51:2141, 1985. 34

[50] S. Augst, D. Strickland, D. D. Meyerhofer, S. L. Chin, J. H. Eberly. *Phys. Rev. Lett.*, 63:2212-2215, 1989. 34

[51] L. J. Frasinski, K. Codling, P. A. Hatherly, J. Barr, I. N. Ross, W. T. Toner. *Phys. Rev. Lett.*, 58:2424, 1987. 35

[52] S. Larochelle, A. Talebpour and S.L. Chin. *J. Phys. B: At. Mol. Opt. Phys.*, 31:1201, 1998. 36

[53] J. McKenna et al. Ultrafast ionization study of N_2 in intense linearly and circularly polarized laser fields. *Phys. Rev. A*, 73:043401, 2006. 36

[54] T. Seideman, M. Y. Ivanov, P. B. Corkum. *Phys. Rev. Lett.*, 75:2819, 1995. 36

[55] J. Muth-Bohm, A. Becker, F. H. M. Faisal. *Phys. Rev. Lett.*, 85:2280, 2000. 36

[56] B. Gaire, J. McKenna, N. G. Johnson, A. M. Sayler, E. Parke, K. D. Carnes, I. Ben-Itzhak. *Phys. Rev. A*, 79(6), 063414, 2009. 36

[57] Z. Wu, C. Wu, X. Liu, Y. Liu, Y. Deng, Q. Gong. *Optics Express*, Vol. 18, No. 10 / 10395, 2010. 37

[58] D. J. Smith et al. Rapid communications in mass spectrometry. *Rapid Commun. Mass Spectrom.* 12, 813–820, 1998. 38

[59] K. W. D. Ledingham et al. Behavior of Polyatomic Molecules in Intense Infrared Laser Beams. *J. Phys. Chem. A*, 102 (18), 3002–3005, 1998. 46

[60] M. Castillejo, S. Couris, E. Koudomas, M. Martin, *Chem. Phys. Lett.* 289, 303–310, 1998. xi, 38, 41, 42

[61] R. Itakura, J. Watanabe, A. Hishikawa, and K. Yamanouchia. *J. Chem. Phys.*, 114, 13, 2001. 38, 45

[62] F. A. llkov, J.E. Decker, S.L. Chin. *J. Phys. B: At. Mol. Opt. Phys.*, 25:4005, 1992. 38

[63] Y. K. Codling, L. J. Frasinski. Dissociative ionization of small molecules in intense laser fields. *J. Phys. B: At. Mol. Opt. Phys.*, 26:783-809, 1993. 39

[64] L. Zandee, R.B. Bernstein. *J. Chem. Phys.*, 71:1359, 1979. 39

[65] J. J. Yang, D. A. Gobeli, M. A. E1-Sayed. *J. Phys. Chem.*, 89:3426, 1985. 39

[66] K.W.D. Ledingham. High intensity laser mass spectrometry - a review. *International Journal of Mass Spectrometry and Ion Processes*, 163:149-168, 1997. xi, 40, 41

[67] D. J. Smith et al. *Rapid Communications in Mass Spectrometry.* 13, 1366-1373, 1999. 38, 41

[68] M. J. DeWitt, R. J. Levis. *J. Chem. Phys.*, 108:7739-1998. 41, 43

[69] D. J. Smith et al. *Rapid Communications in Mass Spectrometry.* 12, 813-820, 1998. 43, 44

[70] X. Fang et al. *Rapid Commun. Mass Spectrom.* 13:1390–1397, 1999. xi, 44, 45, 46, 88, 96

[71] A. Hollingsworth. Near infrared femtosecond photoionisation of large molecules. Annual report, 112-113, 1997. 47, 48, 96, 104

[72] M. Lezius et al. Nonadiabatic Multielectron Dynamics in Strong Field Molecular Ionization. *Phys. Rev. Lett.*, 86, 1, 2001. 48, 49

[73] J. H. Sanderson, T. R. J. Goodworth, A. El-Zein, W. A. Bryan, W. R. Newell, A. J. Langley, P. F. Taday. Coulombic and pre-Coulombic geometry evolution of carbonyl sulde in an intense femtosecond laser pulse, determined by momentum imaging. *Phys. Rev. A*, 65:043403, 2002. 50

[74] J. P. Brichta, W-K Liu, A. A. Zaidi, A. Trottier, J. H. Sanderson. Comparison of ADK ionization rates as a diagnostic for selective vibrational level population measurement. *J. Phys. B: At. Mol. Opt. Phys.*, 39:3769-3779, 2006. 50, 62

[75] W. C. Wiley, I. H. McLaren. Time of flight mass spectrometer with improved resolution. *Rev. Sci. Instr.*, 26:1150-1157, 1955. xi, 53, 58, 64, 96

[76] R. J. Cotter. *Time-of-Flight Mass Spectrometry - Instrumentation and Applications in Biological Research*. American Chemical Society, Washington, DC, 1997. 55, 58, 63, 67

[77] S. J. Walker. Development and characterization of a regeneratively amplified ultrafast laser system with an all-glass stretcher and compressor. Master's thesis, University of Waterloo, Waterloo, Ontario, Canada, 2006. 75

[78] F. Cataldo. *Polyynes: synthesis, properties and applications*. Boca Raton: CRC Tayor & Francis, 2006. 77, 78

[79] A. Hu, Q. B. Lu, W. W. Duley , M. Rybachuk. Spectroscopic characterization of carbon chains in nanostructured tetrahedral carbon films synthesized by femtosecond pulsed laser deposition. *J. Chem Phys.*, 126:154705-1–5, 2007. 77, 81, 93

[80] D. Nishide, T. Wakabayashi, T. Sugai, R. Kitaura, H. Achiba, et al. Raman spectroscopy of size-selected linear polyyne molecules $C_{2n}H_2$ (n = 4–6) encapsulated in single-wall carbon nanotubes. *J. Phys. Chem. C*, 111(13):5178–83, 2007. 77

[81] A. Hu, M. Rybachuk, Q. B. Lu, W. W. Duley. Direct synthesis of sp-bonded carbon chains on graphite surface by femtosecond laser irradiation. *Appl. Phys. Lett.*, 91:13906-1–3, 2007. 77, 78, 79, 82, 93

[82] R. Estmond, T. R. Jonson, D. R. M. Walton. Silylation as a protective method for terminal alkynes in oxidative couplings. *Tetrahedron*, 28:4601–16, 1972. 78

[83] S. A. Buzza, E. M. Snyder, A. W. Castleman Jr. Further direct evidence for stepwise dissociation of acetone and acetone clusters. *J. Chem. Phys.*, 104(13):5040–7, 1996. 78, 81

[84] S. Wang, X. Tang, L. Gao, M. E. Elshakre, F. Kong. Dissociation of methane in intense laser fields. *J. Phys. Chem. A*, 107(32):6123–9, 2003. 78, 81

[85] M. Okoshi, S. Higuchi, M. Hanabusa. Femtosecond laser ablation of frozen acetone for deposition of diamond-like carbon films. *J. Appl. Phys.*, 86(13):1768–70, 1999. 78, 81, 83, 104

[86] C. S. Casari, A. L. Bassi, L. Ravagnan, F. Siviero, C. Lenardi, P. Piseri, et al. *Phys. Rev. B*, 69:075422-1–7, 2004. 80, 82

[87] C. F. Matta, N. Castillo, R. J. Boyd. *J. Chem. Phys.*, 125:204-103, 2006. 83, 100

[88] V. P. Kandidov, O. G. Kosareva, W. Liu, A. Becker, N. Akozbek, C. M. Bowden, et al. Self-transformation of a powerful femtosecond laser pulse into a white light laser pulse in bulk optical media (or supercontinuum generation). *Appl. Phys. B*, 77:149–165, 2003. 86, 94, 100, 103

[89] T. Wakabayashi, T. Murakami, H. Nagayama, D. Nishide, H. Kataura, Y. Achiba, et al. Raman spectral features of longer polyynes $HC_{2n}H$ (n = 4–8) in SWNTs. *Eur. Phys. J. D*, 52:79–82, 2009. 93

[90] A. Lucotti, M. Tommasini, M. Del Zoppo, C. Castiglioni, G. Zerbi, F. Cataldo, et al. *Chem. Phys. Lett.*, 417:78–82, 2006. 94, 105

[91] T. Wakabayashi, H. Nagayama, K. Daigoku, Y. Kiyooka, K. Hasimoto. Laser induced emission spectra of polyyne molecules $C_{2n}H_2$ (n = 5–8). *Chem. Phys. Lett.*, 446:65–70, 2007. 99

[92] D. M. Lubman, R. Naaman, and R. N. Zare, "Multiphoton Ionization of Azulene and Naphthalene," *J. Chem. Phys.* 72, 3034-3040 (1980). 100

[.]